Applying Mixed-Integer Quadratically Constrained Programming to Reduce Fuel Cell Degradation Onboard a Hybrid Ship

P. C. Degeling

Delft University of Technology

TU Delft

Thesis for the degree of MSc in Marine Technology in the specialisation of *Marine Engineering*

Applying Mixed-Integer Quadratically Constrained Programming to Reduce Fuel Cell Degradation Onboard a Hybrid Ship

by

P. C. Degeling

Performed at

Delft University of Technology

This thesis (MT.23/24.017.M) is classified as confidential in accordance with the general conditions for projects performed by the TUDelft.

February 7, 2024

Daily supervisors
Responsible supervisor: Dr. ir. L. van Biert
E-mail: L.vanBiert@tudelft.nl
Supervisor: Dr. ir. A. Coraddu

Thesis exam committee
Chair/Responsible professor: Dr. ir. L. van Biert
Staff member: Dr. ir. A. Coraddu
Staff member: Dr. ir. H. Polinder

Author details
Study number: 4565827

An electronic version of this thesis is available at `http://repository.tudelft.nl/`.

Cover: Image of the MV Ankie by Marcel Coster (Modified)

TU Delft

Preface

This thesis has been written to fulfil the requirements of the master's program in Marine Technology and represents the end of my time as a student at the TU Delft. I have been interested in the challenges associated with climate change throughout my study, which led me to follow my minor in Wageningen. During this semester I decided that I wanted to continue to increase my knowledge of renewable technologies, both in a general sense as well as directly applied to maritime problems. A specific interest in fuel cell technology led me to the research presented in this thesis, which provides an approach to tackle one of the challenges to effective fuel cell application.

I want to thank my supervisors, Lindert van Biert and Andrea Coraddu, without whom I would not have been able to deliver this thesis. Thank you, Lindert, for guiding this project from start to finish. I could always reach you with my questions, and the resulting discussions on fuel cell systems were very interesting. Thank you, Andrea, for your valuable feedback during our meetings throughout this project, guiding me in the right direction when I missed some focus.

Additionally, the support from and discussions with Marijn Postma and Foivos Mylonopoulos helped me gain additional insight into the modelling of hybrid systems, for which I am very thankful. I would also like to thank Wouter Balk, test engineer at Nedstack, for his support in modelling the fuel cell system and for the interesting tour at the company.

Finally, I want to thank my friends and family for being there for me. I am grateful for the full support my parents have given me throughout my years studying in Delft. I want to thank my friends who joined me at Pulse when I was busy studying there and, equally, those whose time I enjoyed outside of the academic context. Finally, I want to thank my girlfriend, Kitty, for her unconditional support.

As I write the final sentence of my report, I look forward to the changes to come.

P. C. Degeling
Delft, February 2024

Abstract

New methods of ship propulsion are required to meet the targets for reducing global emissions of greenhouse gases. Hydrogen-powered fuel cells can be used to greatly reduce emissions, facilitating renewable shipping. Fuel cell durability is recognised as a large barrier to widespread fuel cell application. The goal of this graduation project is to develop a model which can be used to examine the trade-off between hydrogen consumption and degradation in the operation of a fuel cell/battery hybrid ship. The main research question is defined as follows:

"How does incorporating fuel cell degradation in the energy management system of a hybrid marine propulsion system affect the resulting fuel consumption and degradation?"

An optimisation approach is used to develop an energy management system. A quadratic mathematical model is constructed using the fuel cell's polarisation curve as its basis. Linear relations for a fuel cell's current-voltage relation are used to describe the fuel cell power as a quadratic current-power relation. Fuel cell degradation is included in the model by defining various operating conditions and relating them to degradation rates reported in the literature. In turn, the degradation influences the polarisation curve, thereby limiting the fuel cell's performance. This quadratic approach to modelling the interplay between fuel cell degradation and the fuel cell's performance is the main contribution to the literature.

The proposed energy management system is used to determine a vessel's optimal operation, depending on the objective function applied. Two objectives are defined: minimisation of fuel consumption and minimisation of fuel cell degradation. Besides testing these single objectives, a weighted-sum approach to multi-objective optimisation is carried out using hydrogen and fuel cell system costs.

The optimal operation of the vessel is analysed based on key performance indicators such as fuel consumption, fuel cell degradation and operating costs. Incorporating fuel cell degradation in the energy management system leads to a reduction in degradation of up to 33% for the long-term simulation of the case study applied in this thesis when compared to the results for the minimisation of fuel consumption. A large increase (50%) in fuel cell lifetime can be accomplished with a very limited increase in hydrogen consumption (0.5%).

This research contributes an intuitive modelling method for the interplay between fuel cell degradation and the fuel cell's performance. It provides insight into the considerations between fuel cell degradation and hydrogen consumption while operating a hybrid vessel, addressing a small part of a technical solution to mitigating emissions.

Contents

List of Figures

List of Tables

Nomenclature

Abbreviations

Abbreviation	Definition
AC	Alternating Current
ASR	Area-Specific Resistance
BoL	Beginning-of-life
BoP	Balance of Plant
CO_2	Carbon Dioxide
DC	Direct Current
DoD	Depth of Discharge
DP	Dynamic Programming
DWT	Deadweight Tonnage
ECM	Equivalent Circuit Model
ECSA	Electrochemical Surface Area
EMS	Energy Management System
EoL	End-of-Life
ESS	Energy Storage Systems
EU	European Union
HOR	Hydrogen Oxidation Reaction
GDL	Gas Diffusion Layer
GHG	Greenhouse Gas
IMO	International Maritime Organization
NO_x	Nitrogen Oxides
LHV	Lower Heating Value
MAPE	Mean Absolute Percentage Error
MILP	Mixed-Integer Linear Programming
MIQCP	Mixed-Integer Quadratically Constrained Programming
MIQP	Mixed-Integer Quadratic Programming
OCV	Open-Circuit Voltage
ORR	Oxygen Reduction Reaction
PEM FC	Proton Exchange Membrane Fuel Cell
PM	Particulate Matter
PMP	Pontryagin's Minimum Principle
RHS	Right-Hand Side
SoE	State-of-Energy
SoH	State-of-Health

Symbols

Symbol	Definition	Unit
A	Tafel slope	[V]
ASR_{ohm}	Area Specific Resistance	[$\Omega \cdot \text{cm}^2$]
E^0	Standard-state reversible voltage	[V]
E_{N}	Non-standard reversible voltage	[V]
$E_{\text{N}}(T)$	Reversible voltage that varies with both temperature and pressure	[V]

Symbol	Definition	Unit
F	Faraday constant	[C/mol]
I	Current	[A]
I_0	Exchange current	[A]
J	Current density	[A/cm^2]
J_0	Exchange current density	[A/cm^2]
J_{cross}	Hydrogen crossover current density	[A/cm^2]
J_{L}	Limiting current density	[A/cm^2]
J_{leak}	Leakage current density	[A/cm^2]
K_{C}	Rated voltage constant	[-]
n	Number of cells in fuel cell stack	[-]
N	Number of stacks in fuel cell system	[-]
P	Power	[W]
p_{i}	Partial pressure of species i	[bar]
R	Ideal gas constant	[J/mol/K]
R_{ohm}	Ohmic resistance	[Ω]
s	Laplace variable	[1/s]
T	Temperature	[K]
T_{d}	Response time	[s]
V	Voltage	[V]
V_{OC}	Open-Circuit voltage	[V]
z	Number of electrons transferred in reaction	[-]
α	Charge transfer coefficient	[-]
α_{j}	Activity of species j	[-]
$\Delta\hat{s}$	Entropy change	[mol/K]
η_{act}	Activation overpotential	[V]
η_{con}	Concentration overpotential	[V]
η_{loss}	Open-circuit loss	[V]
η_{ohm}	Ohmic overpotential	[V]
ν	Molar Hydrogen Consumption [mol/s]	

Notation for the mathematical model

Sets and indices		
T	Set for the time steps	$t \in T$
F	Set for the fuel cell systems	$f \in F$
Parameters		
c	Coefficient translating fuel cell current to grams of hydrogen	[g/A]
$deg_{0,f}$	Degradation status of fuel cell f at start of optimisation	[V]
E_{bat}	Energy capacity of the battery	[kWh]
I_{high}	Start of the fuel cell's high-current region	[A]
I_{lb}	Minimum operating current	[A]
I_{low}	End of the fuel cell's low-current region	[A]
I_{ub}	Maximum operating current	[A]
M	Big M, used to model on/off status and presence in operating regions	[-]
n	Number of cells in a stack	[-]
N_{s}	Number of series-connected stacks in fuel cell system	[-]
N_{p}	Number of parallel-connected stacks in fuel cell system	[-]
$P_{\text{dem}}(t)$	Power demand at time step t	[kW]
P_{max}	Maximum battery power	[kW]
P_{rated}	Rated power of the fuel cell system	[kW]
R_{ohm}	Ohmic resistance of fuel cell, used for linear $I-V$ curve	[Ω]
SoE_0	Battery's initial state-of-energy	[-]
SoE_{lb}	Lower bound for the battery's state-of-energy	[-]
SoE_{ub}	Upper bound for the battery's state-of-energy	[-]
V_{OC}	Open-circuit voltage of fuel cell, used for linear $I-V$ curve	[V]
ΔV_{base}	Base hourly degradation rate	[V/h]
ΔV_{dP}	Degradation per cycle from 0 W to P_{rated}	[V]
ΔV_{high}	Increase in hourly degradation when operating at high-current region	[V/h]
ΔV_{low}	Increase in hourly degradation when operating at low-current region	[V/h]
ΔV_{start}	Degradation rate per start cycle	[V]
η_{aux}	Efficiency related to auxiliary losses in fuel cell system	[-]
η_{c}	Charge efficiency	[-]
η_{d}	Discharge efficiency	[-]
Variables		
$dE(t)$	Change in energy content due to battery power at time step t	[kWh]
$deg_f(t)$	Actual degradation status of the fuel cell at time step t	[V]
$diff_f(t)$	Normalised power change of fuel cell f at time step t	[kW]
$dP_f(t)$	Normalised absolute power change	[kW]
$E(t)$	Energy content of battery at time step t	[kWh]
$P_{\text{c}}(t)$	Charging power at time step t	[kW]
$P_{\text{d}}(t)$	Discharge power at time step t	[kW]
$I_f(t)$	Current at time step t of fuel cell f	[A]
$P_f(t)$	Power at time step t of fuel cell f	[kW]
$V_f(t)$	Voltage at time step t of fuel cell f	[V]
$z_{\text{low}\,f}(t)$	Binary variable indicating if current is below I_{low}	[-]
$z_{\text{high}\,f}(t)$	Binary variable indicating if current is above I_{high}	[-]
$z_{\text{start}\,f}(t)$	Binary variable which indicates if a starting procedure is initiated	[-]
$\Delta deg_f(t)$	Increase in degradation	[V]
$\delta_{\text{c}}(t)$	Binary variable for the battery's charging status at time step t	[-]
$\delta_{\text{d}}(t)$	Binary variable for the battery's discharging status at time step t	[-]
$\delta_f(t)$	Binary variable for on/off status at time step t of fuel cell f	[-]

1 Introduction

The International Maritime Organization (IMO) set targets for the reduction of greenhouse gas (GHG) emissions in the maritime sector in the coming decades. The development of IMO objectives during this graduation project illustrates the urgency of climate change. At the start of this thesis, IMO's GHG strategy set goals for a reduction of total GHG emissions by 50% in 2050, while the carbon intensity should be reduced by 40% and 70% in 2030 and 2050, respectively [1]. These goals could theoretically be reached while still using fossil fuels, for example, by applying wind-assisted propulsion and lowering ship speeds [2]. In the meantime, the 2023 IMO Strategy on Reduction of GHG Emissions from Ships has been adopted, which states that the emissions from international shipping should reach net zero around the year 2050 [3], a radical change in objectives. In addition, the 2023 strategy includes goals to support the uptake of near-zero GHG emission technology, which should represent at least 5% of all energy used in 2030 [3]. Similarly, the recent FuelEU maritime proposal of the European Union creates goals for the reduction of GHG intensity of maritime fuels [4]. The proposed regulation defines the GHG intensity as "CO_2-equivalent (emissions) established on a well-to-wake basis, per MJ of energy used on-board" [5]. Critically, this is per unit of fuel consumed. The regulation should lead to the use of cleaner types of energy. The maximum GHG intensity of a ship will slowly decrease every five years, beginning with a reduction of 2% in 2025 and ending with a 75% decrease in 2050, compared to the 2020 fleet average [5]. A growing demand for cleaner fuels and more efficient propulsion methods can be expected in the coming years due to the IMO and EU regulations.

The GHG intensity can be drastically reduced by applying fuel cells with renewably produced hydrogen, as there are no tank-to-wake GHG emissions, and well-to-tank GHG emissions are very limited [6]. Besides, no SO_x and PM emissions are generated when using hydrogen as a fuel, and no NO_x emissions are formed in fuel cells [7]. It is clear that the operation of hydrogen-fuelled fuel cells leads to a negligible amount of emissions and may become more relevant in the coming years. However, more research into the application of fuel cells is necessary, as they are not yet widely applied in the maritime industry [7].

One of the barriers to increased fuel cell application is their durability and reliability [8]. The stack lifetime of fuel cells is often very limited [7], which is caused by a wide array of degradation mechanisms, dependent on the operating conditions of the fuel cell [9]. Experience with fuel cells in the automotive industry led to the conclusion that "complex automotive operating conditions significantly accelerate fuel cell aging" [10]. Stationary fuel cell stacks have been designed with a realised lifetime of 23,000 hours and a projected lifetime of 40,000 hours [11]. Some applications of fuel cells in buses have reached a lifetime of 20,000 hours without maintenance [12]. The difference in lifetime between stationary applications and applications in fuel cell vehicles is likely caused by the harsher operating conditions [10]. According to a report by the EU's public-private partnership, Clean Hydrogen Joint Undertaking, the lifetime of state-of-the-art maritime fuel cell systems was 20,000 hours in 2020, with a lifetime objective of 80,000 hours in 2030. This lifetime definition includes stack replacements. In order to increase the lifetime of fuel cell systems in maritime applications, their degradation has to be limited.

An energy storage system (ESS) can be used to avoid harmful operating conditions of the fuel cells, for example, by using the fuel cell only for base load and using the ESS for the load transients [13].

Besides that, the ESS may enable peak shaving and load levelling, and it can supply a backup load [14]. In the context of fuel cell systems, energy storage systems may be used to generate stable power at complex operating conditions to compensate for the limited dynamic response of fuel cells [15], [16]. In the case of a fuel cell/battery hybrid, an energy management system (EMS) can be used to determine the power allocation between each fuel cell stack and battery pack. Various types of EMS modelling exist, and they can have several goals, mostly focused on efficiency in the power allocation [17]. As a large barrier to increased fuel cell application is their durability, this thesis is focused on limiting the degradation of fuel cell systems using the EMS.

The main objective of this study is to investigate the effects of incorporating fuel cell degradation in the energy management system of a fuel cell/battery hybrid vessel. The system will consist of proton exchange membrane fuel cells (PEM FCs) and lithium-ion batteries. The research question is as follows:

"How does incorporating fuel cell degradation in the energy management system of a hybrid marine propulsion system affect the resulting fuel consumption and degradation?"

The following sub-questions are defined to help answer the main research question.

- Is there a gap between state-of-the-art fuel cell (degradation) modelling and fuel cell (degradation) models applied in energy management systems?
- Can an energy management system for the hybrid system be constructed which is suitable for incorporating fuel cell degradation?
- How can the operational characteristics of the fuel cell and battery be described in a way suitable for this thesis?

The first sub-question is answered in the two chapters comprising the literature review: chapters 2 and 3. A mathematical model for a fuel cell/battery hybrid energy system, incorporating fuel cell degradation, is proposed in chapter 4, answering the second sub-question. The vessel used in the case study is introduced in chapter 5, after which the selection and modelling of the fuel cell system are described, answering the third sub-question. The verification of the mathematical model is presented in chapter 6. Finally, the results, discussion and conclusion are presented in chapters 7, 8 and 9.

2

Fuel cell modelling

The results of the literature review on fuel cell modelling are discussed in this chapter. The modelling of fuel cell voltage is reviewed in section 2.1. The theoretical models are discussed first, after which various methods of fuel cell modelling applied in relevant literature are compared. A review of auxiliary power modelling is given in section 2.2, and the necessity of including auxiliary components in a fuel cell model is explained. Finally, a detailed overview of fuel cell models applied for simulation purposes is given in section 2.3.

2.1. Fuel cell modelling

The hydrogen combustion reaction is split into two half-reactions in a proton exchange membrane (PEM) fuel cell. The hydrogen oxidation reaction (HOR) occurs at the anode, while the oxygen reduction reaction (ORR) occurs at the cathode. Whereas the energy from electron configuration in the hydrogen combustion is recovered as heat in a combustion engine, a fuel cell directly harnesses the energy in the electrons by physically separating the half-reactions and designing an external path for the current to be used to power a load [18]. The power generated by a fuel cell is thus one that is generated by the product of its voltage and its current. The voltage generated by a fuel cell can be modelled in various ways.

In the first subsection, the theoretical modelling of fuel cell power from the perspective of electrochemical engineers is discussed. The models found here are used as a benchmark for the models used for simulation purposes. In the second subsection, various fuel cell models used in relevant literature are discussed. In the third subsection, a comparison is made between the theory and the models applied in literature, and differences are discussed.

2.1.1. Fuel cell theory

The text in this paragraph is based on the book of O'Hayre et al. [18].

The theoretical potential of a fuel cell under standard conditions (E^0) can be found by using the standard electrode potentials for each of the half-reactions, from which a standard-state potential of 1.23 V follows for the HOR and ORR half-reactions in the PEM fuel cell. The theoretical potential of a PEM fuel cell (Nernst voltage E_{N}) under non-standard conditions can be described using the Nernst equation as given in equation 2.1.

$$E_{\mathsf{N}} = E^0 - \frac{RT}{zF} \ln \frac{p_{H_2O}}{p_{H_2} p_{O_2}^{\frac{1}{2}}} \tag{2.1}$$

Note that while equation 2.1 does account for the influence of the operating temperature on the chemical activity, it does not yet account for the influence of the operating temperature on the reversible voltage. The temperature-dependent Nernst voltage $E_{\mathsf{N}}(T)$ for a PEM fuel cell is defined as in equation 2.2, which for the PEM fuel cell with water vapour as a product can be written as equation 2.3.

$$E_{\mathsf{N}}(T) = E^0 + \frac{\Delta \hat{s}}{zF}(T - T_0) - \frac{RT}{2F} \ln \frac{p_{H_2O}}{p_{H_2} p_{O_2}^{\frac{1}{2}}} \tag{2.2}$$

$$E_{\mathrm{N}}(T) = E^0 + \frac{-44.34}{2 \cdot 96485}(T - T_0) - \frac{RT}{2F} \ln \frac{p_{H_2O}}{p_{H_2} p_{O_2}^{\frac{1}{2}}} \tag{2.3}$$

While the theoretical potential of a fuel cell can be found by using the Nernst equation, losses occur when the fuel cell is operated. The decrease in potential as a function of current density is depicted in the polarisation curve in figure 2.1, adapted from [18].

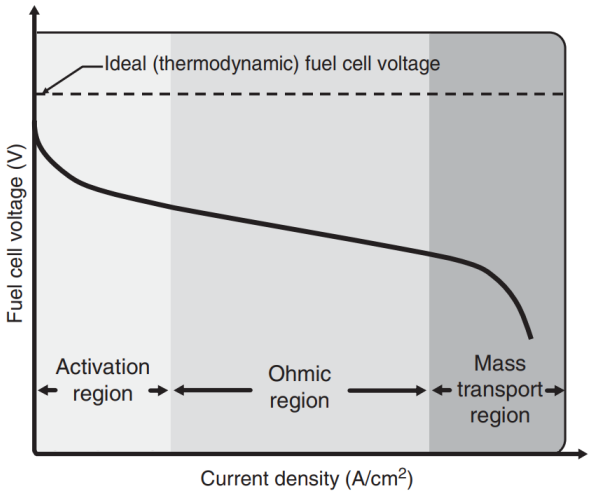

Figure 2.1: Voltage decrease as a function of current density, adapted from [18]

The decrease in voltage can be represented by three distinct types of losses. These include activation losses, ohmic losses and mass transport losses. The generated voltage can be described as follows:

$$V = E_{\mathrm{N}} - \eta_{\mathrm{act}} - \eta_{\mathrm{ohm}} - \eta_{\mathrm{con}} \tag{2.4}$$

In a basic voltage model proposed by O'Hayre et al. [18] the losses can be written by the following three equations. This model is based on current densities, but note that the same model can also be described using current instead of current density.

$$\eta_{\mathrm{act}} = (a_{\mathrm{A}} + b_{\mathrm{A}} \ln(J)) + (a_{\mathrm{C}} + b_{\mathrm{C}} \ln(J)) \tag{2.5}$$

$$\eta_{\mathrm{ohm}} = J \cdot ASR_{\mathrm{ohm}} \tag{2.6}$$

$$\eta_{\mathrm{con}} = c \ln(\frac{J_{\mathrm{L}}}{J_{\mathrm{L}} - J}) \tag{2.7}$$

The activation losses represent the voltage that is expended to overcome the activation energy of an electrochemical reaction. It mostly affects the low-current region. The Butler-Volmer equation is used to describe the relation between the generated current and the required activation potential. The definition of η_{act} follows from this equation. In the Butler-Volmer equation, the generated current increases exponentially with the activation overpotential. The activation losses are given separately for the anode and cathode and are modelled with a constant value dependent on the exchange current density J_0 (a_{A} and a_{C} respectively) and a value that is logarithmically dependent on the operating current density J. The activation losses can be reduced by increasing the reactant concentration, temperature or the number of reaction sites, or by decreasing the activation barrier with the use of catalysts. These factors all influence the exchange current density, and thus the activation losses, at a given operating current.

Ohmic losses are the sum of all losses due to resistance to charge transfer in the fuel cell and increase linearly with the current (density). It is mainly responsible for the linear voltage drop in the ohmic region. The losses are dominantly caused by the ionic resistance, caused by charge transport of ions in the fuel cell. It can be modelled using the area-specific resistance (ASR). This term represents the ASR of all components in the fuel cell that generate an ohmic resistance, such as the electrolyte and the electrodes. It is found by multiplying the area of the fuel cell by its normal ohmic resistance.

The ohmic losses can be reduced by either increasing conductivity or reducing the length (or thickness) of the conductor. Conductivity is related to the number of charge carriers available for charge transport (number of available vacancies in the electrolyte) and the mobility of those carriers (ion diffusivity). For polymer electrolytes, water content is of great influence on the conductivity of the electrolyte.

Concentration losses, or mass transport losses, are related to poor transport of uncharged species, specifically the resulting concentration of reactants and products in the catalyst layer. It dominates losses in the high-current region. Mass transport in fuel cell flow structures is driven by fluid flow and convection while gas transport in electrodes is driven by diffusion. The porosity of electrodes shelters the gas from the convective forces and allows diffusion to take place. This occurs in the gas diffusion layer (GDL), where gas molecules are transported to the membrane via diffusion. The concentration losses are related to a drop in the Nernst voltage, and increased activation losses. The Nernst voltage, defined in equation 2.1, is dependent on the partial pressures of reactants (hydrogen and oxygen gas) and product (water). These relate to the partial pressures at the reaction site (catalyst), not the partial pressures of the product as it enters the fuel cell. As the reactant concentration at the catalyst decreases and product concentration increases, the ideal Nernst voltage decreases. On top of that, the reactant concentration also influences the reaction kinetics, and activation losses increase as the reactant concentration decreases. These effects are both encapsulated by equation 2.7.

Besides the voltage drops due to the three different losses discussed above, extra losses in the form of electrical shorting and fuel crossover may occur. This may be caused by electrolytes that are too thin, which may be a design choice or a result of degradation or manufacturing mistakes. These losses can be represented by an additional leakage current density J_{leak}; the fuel cell has to produce extra current to compensate for this leakage. The $J - V$ curve gets shifted to the left. This effect can be included in the model by adding the leakage current to the actual current for the J terms in η_{act} and η_{con}. Only the operating current is actually passing through the fuel cell, and thus, the ohmic losses are based on J instead of $J + J_{\text{leak}}$.

When the operating voltage V is multiplied by the current I at which the fuel cell operates, the power P can be found. This follows the well-known relation described in equation 2.8.

$$P = VI \tag{2.8}$$

The current directly follows from the speed of the electrochemical reaction and thus the fuel consumption rates.

The efficiency of a fuel cell is, just like the efficiency of an internal combustion engine, inherently limited. This limit, the thermodynamic efficiency, can be used to calculate the theoretical maximum efficiency of the fuel cell. The actual fuel cell efficiency is lower because of voltage losses and fuel utilisation losses and can be described as the product of thermodynamic efficiency, voltage efficiency, and fuel utilisation efficiency.

2.1.2. Fuel cell models in literature

Because most of the work regarding fuel cells is limited to research, it is important to compare the various methods of modelling the fuel cell. The linear current-voltage relation suggested in [7], discussed below, sparked the initial interest in the various ways of modelling fuel cells. A review that includes modelling methods for ship energy systems [19] is used as a starting point for finding various articles where fuel cells are modelled.

Van Biert and Visser [7] suggest that activation and transport losses may be neglected in specific parts of the operating window, and a linear relation between the cell voltage and the current density can be found by using the area-specific resistance. Equation 2.9 is adapted from [7].

$$V_{\text{cell}} = V_{\text{OC}} - J \cdot ASR_{\text{ohm}} = V_{\text{OC}} - I \cdot R_{\text{ohm}} \tag{2.9}$$

In this model, the open-circuit voltage gives the voltage at 0 A and are seen as a value that includes the initial activation voltage losses. However, current-dependent activation losses are not included. Besides the initial activation voltage loss, the ohmic losses are modelled using the ASR and mass transport losses are not included.

In contrast, Yousfi-Steiner et al. [20] suggest that the difference between the open-circuit voltage and the theoretical Nernst potential may be caused by a partial pressure drop of reactants due to hydrogen crossover through the membrane, or by reactions between the platinum surface and oxygen or impurity

oxidation resulting in a mixed cathode potential. In this case, the activation losses are not represented in the open-circuit voltage and a different schematic overview of the losses is proposed, which can be seen in figure 2.2.

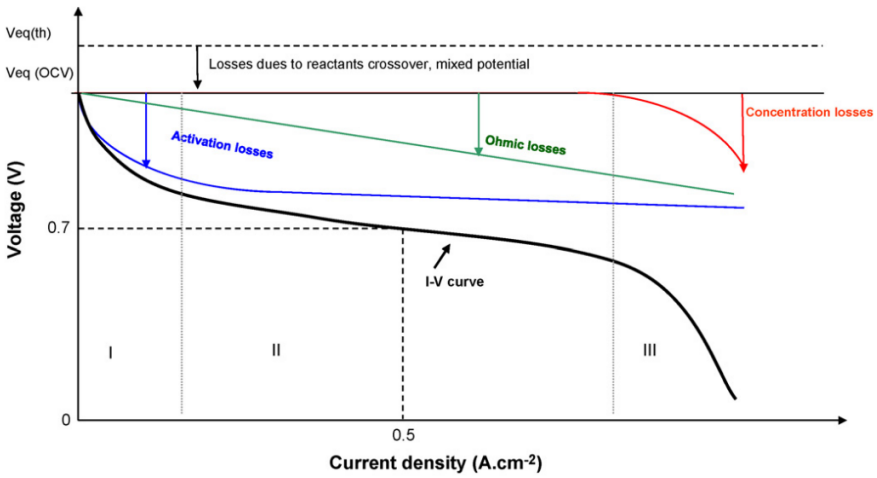

Figure 2.2: Polarisation curve showing a possible origin of the difference between E_{N} and V_{OC}, from [20]

A similar way of defining the difference between the Nernst voltage and the open-circuit voltage is proposed by Ren et al. [10], who define an additional voltage drop η_{loss}, the open-circuit loss. This term is related to the sum of current densities due to gas crossover and electrical shorting and can be described with equation 2.10. Here J_{leak} is again the loss in effective current density due to gas crossover and electrical shorting.

$$\eta_{\mathrm{loss}} = \frac{RT}{\alpha z F} \ln\left(\frac{J_{\mathrm{leak}}}{J_0}\right) \tag{2.10}$$

Note that the authors of [10] use i for current density and n for the number of electrons transferred, as seen in the figure. The equation and variables are edited in equation 2.10 for continuity in this review. When looking at figure 2.3 it is unclear if the activation at OCV conditions does indeed include the η_{loss} term, and this does not become clear in the paper.

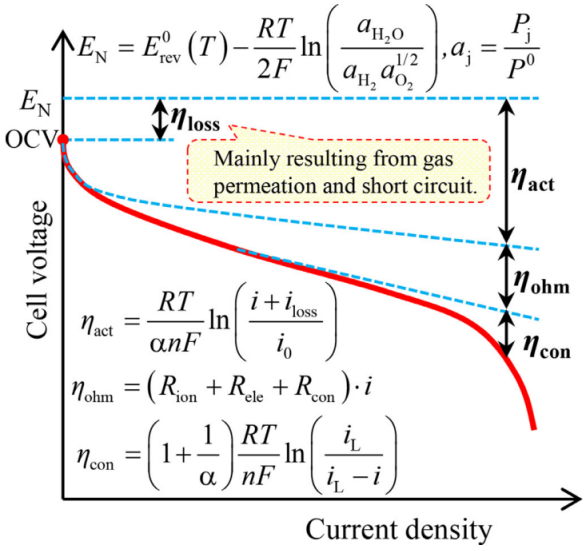

Figure 2.3: Polarisation curve, from [10]

Chakraborty [21] notes that this additional current J_{leak} should only be applied to the concentration and activation losses. She writes about this as useful current and useless current in the paper where

she discusses this frequently made mistake in fuel cell modelling. The loss in current due to hydrogen fuel crossover and current leakage through the fuel cell is considered useless, while useful current relates to the transfer of protons through the electrolyte and electrons through the electrodes. The ohmic drop is only related to the useful current, and there is no ohmic drop η_{ohm} under open-circuit conditions, even though there may be a current loss due to internal leakage and fuel crossover. It can be seen in figure 2.3 that the current leakage term is only included in the activation losses and not the concentration losses, which may be a mistake as Chakraborty suggests.

Bagherabadi et al. [22] made a fuel stack model that uses equation 2.4 to model the stack voltage. In the model, the activation losses are modelled by using the Tafel equation and are dependent on the stack temperature, cell current, and partial pressures in the system. Ohmic resistance is modelled with a temperature-dependent area-specific resistance, multiplied by the current density. Concentration losses are dependent on the current, stack temperature, and partial pressures in the system. The model was used for the simulation and sizing of marine power systems, especially the influence of component sizing and configuration on the dynamic response of the system. It was not used for long-term modelling.

Several sources use a variant of the generic fuel cell model proposed by [23] to develop and simulate hybrid fuel cell/battery ships [24], [25], [26]. Two generic fuel cell models were proposed, a simplified and a detailed one, which both can be constructed using data from fuel cell data sheets as input [23]. The simplified model subtracts the current-dependent activation losses and ohmic losses from the open-circuit voltage. Only the polarisation curve of the fuel cell is required to develop this model. It can be used to simulate fuel cell stacks operating at nominal temperature and pressure and does not include mass transport losses. The model is described by only one equation, given in equation 2.11, adapted from [23] to be consistent with variable names. The final component of the equation is a transfer function that is used to model the delay in the activation losses. The simplified model can be seen in figure 2.4.

$$V_{cell} = V_{\text{OC}} - R_{\text{ohm}} \cdot I - nA \ln\left(\frac{I}{I_0}\right) \cdot \frac{1}{s \cdot T_{\text{d}}/3 + 1} \tag{2.11}$$

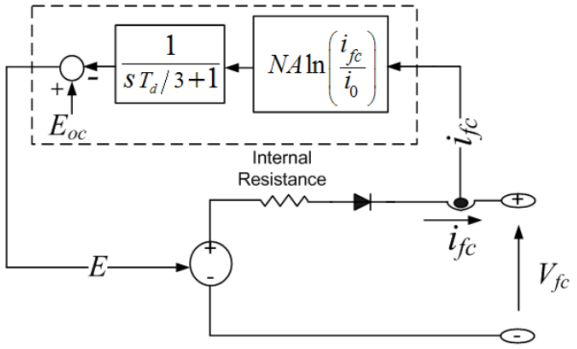

Figure 2.4: Simplified generic FC model, from [23]

The detailed model developed in [23] may include pressure and temperature variations, as well as changes in the composition and flow rate of reactants. The model also excludes concentration losses. Additional fuel cell data is required to generate this model, including knowledge about the dynamic behaviour of the stack. The model can be seen in figure 2.5. In this model, the open-circuit voltage, exchange current, and Tafel slope (A) are affected by each of the possible variations in the model. Further details can be found in [23].

Another possible way of developing a fuel cell model is by using a parametrised model and finding the parameters using optimisation methods. Priya et al. [27] wrote a review of parameter estimation techniques. Fuel cell voltage is determined as in equation 2.4, and the three voltage losses are modelled using nine parameters in total, that all depend on the operating conditions of the fuel cell. An overview of optimisation methods used to determine these parameters is given, and includes a wide array of metaheuristics and algorithms.

Lastly, Boettner et al. [28] adjusted an existing PEM FC model for the simulation of automotive vehicles. The model is expanded to include auxiliary components. Boettner et al. suggest that a stand-

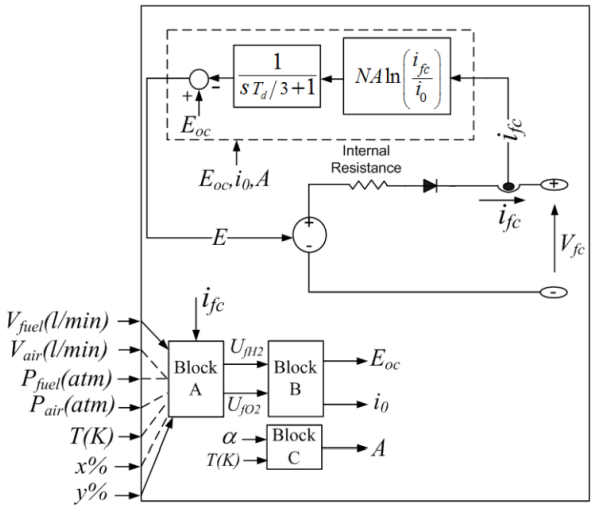

Figure 2.5: Detailed generic FC model, from [23]

alone fuel cell stack model is insufficient to analyse fuel cell performance in automotive applications. The influence of auxiliary components on the simulation of hybrid vehicles will be discussed in the next section.

2.1.3. Discussion

The formula proposed by van Biert and Visser [7] may be used to accurately portray the ohmic region of a fuel cell, but this means that the operating conditions of the fuel cell must be limited to ensure the validity of the equation. It is unclear to what extent the current leakage losses are included in the open-circuit voltage. Yousfi-Steiner et al. [20] show this loss as a constant reduction, independent of current density, and the three other losses are modelled as an additional reduction. Ren et al. [10] give a schematic polarisation curve and suggest the loss is constant as well in the figure, but the term is formulated as being dependent of the current loss, which may change with the operating current.

Bagherabadi et al. [22] developed a model suitable for detailed modelling, but modelling of the stack temperature and partial pressures in the fuel cell may be too complex for longer fuel cell simulation.

The simplified model developed in [23] requires significantly less input from the fuel cell compared to the detailed model, and is simple to construct. It is unclear how well the simplified model correlates to the actual product, as only the detailed model was validated. The detailed model is reported to simulate the stack voltage with an error of $\pm 1\%$ if the humidity level in the fuel cell is controlled.

The overview of parameter estimation techniques given by Priya et al. [27] gives a new insight in the possibilities of fuel cell modelling. A large variation in computational complexity and accuracy can be observed for the various estimation methods. The methods may generate an accurate model in standard test conditions, but the parameters vary a lot in operating conditions; ”the models must be tested for all operating conditions” [27].

2.2. Fuel cell auxiliary systems

Fuel cells require additional subsystems to operate. By only modelling the fuel cell itself, these auxiliary systems are ignored while their impact on the fuel cell output may not be negligible. In the first subsection, the theory behind the auxiliary systems is discussed, while in the second subsection the inclusion of auxiliary systems in simulations is discussed.

2.2.1. Role of auxiliary systems in theory

Fuel cells require auxiliary systems, for example, to manage the temperature in the fuel cell, to deliver reactants at the right pressure and to control the power electronics [18].

Large low-temperature PEM fuel cells may require active cooling, while passive cooling may be enough for small systems [18]. Active cooling may be done by an increased cathode air flow, separate air flow, or liquid cooling [29]. Two applications of separate air flow cooling [30], [31] are discussed

in [29]. They reported a power consumption by the cooling system of 3 and 2% of the stack power respectively.

The process of delivering hydrogen to the fuel cell is highly dependent on the storage mechanism. When pure hydrogen is stored on the vessel, it can be used directly in the fuel cell and the fuel cell system is simplified [18]. However, system energy density may be limited, and energy is expended to store the hydrogen. For compressed hydrogen, it is stated that ”approximately 10% of the energy content of H_2 gas must be expended to pressurise it to 300 bars” [18]. The same principle applies to liquefied hydrogen, where up to 30% of the energy stored may be expended during the liquefaction process. Conversely, using a hydrogen carrier fuel may lead to higher system energy densities, but reforming is required to extract the hydrogen which then can be used in PEM fuel cells. The reforming system may consume some energy, and depending on the fuel, the hydrogen may contain some impurities, lowering the performance of the fuel cell [18]. The hydrogen and air need to be delivered to the electrodes and may need to be pressurised. This is done using pumps and compressors, and these consume parasitic power. When hydrogen is stored in compressed form, only a compressor is required for the air. At low currents, all power generated by the fuel cell is consumed to keep the compressor running, and the total system efficiency is extremely low. O'Hayre et al. suggest that the parasitic power may be represented by a linear equation, where there is a fixed parasitic power even at 0 W fuel cell power, and an increase in parasitic power as the fuel cell power increases [18]. A schematic overview of this effect can be seen in figure 2.6.

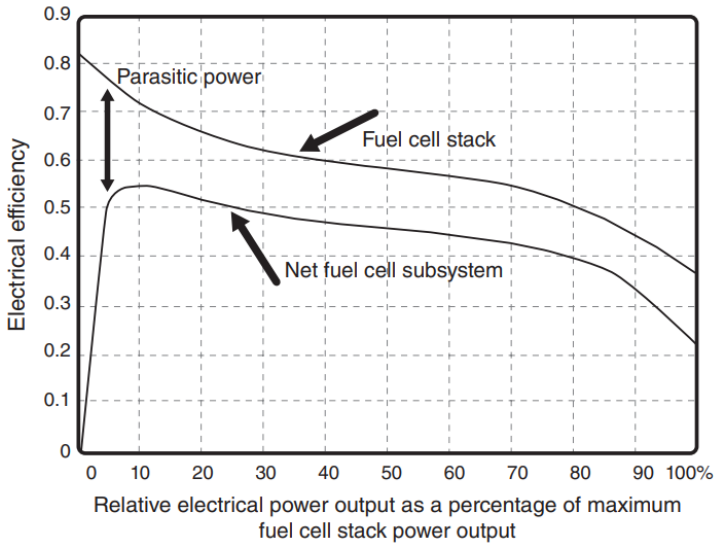

Figure 2.6: Electrical efficiency of stack and total system, from [18]

Power regulation is essential for almost all fuel cell applications, and in case AC power is required, inversion must also be applied. The generated fuel cell power must be delivered at the right voltage. DC-DC converters used for power regulation may lead to somewhere between 2 and 15% of extra losses, whereas DC-AC inverters may lead to between 3 and 15% extra losses [18].

2.2.2. Inclusion of auxiliary systems in literature

To start, the generic detailed model developed in [23] is validated using both a 6 kW from NedStack and a 500 W stack from Hpower, and shows accurate results for both fuel cell stacks. It is not reported what the auxiliary power is, nor is there any word on the efficiencies of converters or inverters. Balestra and Schjølberg [24] use the generic model by [23] to model and simulate a hybrid ferry. The power values used in the operational profile represent the combination of propulsion load, auxiliaries, and hotel load, and do not specifically speak of a compressor load. The converters are modelled with ideal switches, just like the compressor is modelled as being ideal [24].

Bassam et al. [25] use data from the fuel cell vessel FCS Alsterwasser, and note that the required auxiliary power is included in the load profile of the vessel. No auxiliary systems are included in the model by Bassam et al., but by generating enough power to meet the load profile this should indirectly

include the auxiliary power demand. [25] uses [26] as a source, where the same data is used to develop an EMS for the FCS Alsterwasser. In contrast to Bassam et al. [25], Han et al. [26] do not consider the auxiliary power included in the load profile data from the FCS Alsterwasser. Instead, they show that the compressor has a large effect on the effectively produced power and that the compressor power constitutes most of the auxiliary power (up to 93.5% [28]) and is estimated to be up to 30% of the stack power [26]. The effect of compressor power on system power and efficiency can be seen in figure 2.7 [26]. The compressor power has an extreme impact on system efficiency at low-load operation, and increasing effect at higher operating currents.

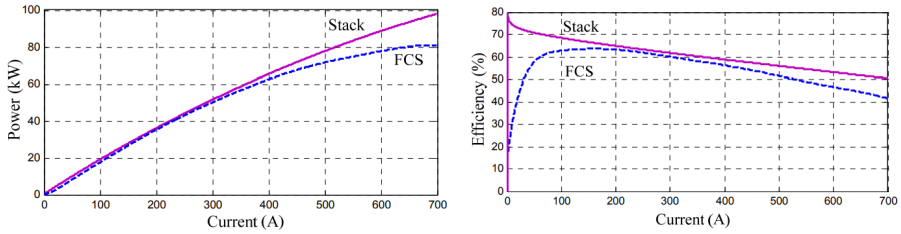

Figure 2.7: Power and efficiency including and excluding compressor, from [26]

Boettner et al. [28] extended an existing vehicle performance simulator to include a PEM FC model with auxiliary components. In their simulation, the compressor power constituted up to 93.5% of the auxiliary power. Besides that, the cooling fan made up 5% of auxiliary power, followed by the cooling water pump (1%) and the hydrogen recirculation pump (0.5%). When simulating the fuel cell vehicle, ”typical values for both motor and power converter efficiencies were used”. The extended model by Boettner et al. [28] was used to define power management strategies for hybrid vehicles [32], [33]. Their findings regarding the power consumed by the compressor were used in a wide array of studies to support the inclusion of compressor power in fuel cell models, among which the study by Han et al. [26].

2.2.3. Discussion

Balestra and Schjølberg [24] state that auxiliary power is included in the load profile of the vessel, while the paper which it is based on states that auxiliary power is not included [23]. This is a controversial deviation. An EMS is developed in [24] and it is stated that the hybrid powerplant will be suitable for low-power operation, because the efficiency is higher than at rated load. This is contrary to the findings in [26], where the efficiency of the system, including the compressor, is very low at part load conditions, due to the inclusion of the compressor in the fuel cell system.

Boettner et al. [28] found that the compressor consumes up to 93.5% of the auxiliary power, and Han et al. [26] report that compressor power can reach up to 30% of the total fuel cell stack power. It can be concluded that the inclusion of compressor power in the modelling of a fuel cell system is an important consideration.

2.3. Simulations of energy management systems

In this section, an overview of the various models applied in energy management systems will be given. Research from various sectors such as the automotive and maritime sector is used to determine the level of detail of fuel cell models used in state-of-the-art energy management systems. While researching the various methods of modelling the fuel cell systems, a split in modelling methods has been observed. Two terms are proposed to characterise the difference in the methods: voltage models and reduced models. This distinction has been made to differentiate between simulations where the fuel cell voltage is calculated at each time step in the simulation of the energy system (voltage models) versus simulations where the fuel cell system is modelled using its output characteristic (reduced models). An overview of voltage models applied in relevant literature is shown in table 2.1. Note that the term ”simulation time” refers to the virtual time, the time that is simulated by the researchers. This does not relate to the computational time required to run the simulation.

The overview in the table entails some of the voltage models that were found in simulations in the maritime field, as well as one source that was used to model a hybrid tramway. Two sources [24], [25] apply the simple and detailed generic fuel cell models by [23], respectively. In both studies, only the

Table 2.1: Voltage models applied in relevant literature

	Voltage model				Auxiliary components			Modelling method	Simulation time
Ships	Voltage	η_{act}	η_{ohm}	η_{con}	Compressor	Converter	BoP		
[24]	V_{OC}	✓	✓	✗	✗	✓	✗	ECM, Simulink	1 hour
[25]	V_{OC}	✓	✓	✗	✗	✓	✗	ECM, Simulink	8 hours
[26]	$E_N(T) \cdot K_C$	✓	✓	✗	✓	✓	✗	Analytical model, Simulink	5 minutes
[34]	V_{OC}	✓	✓	✓	✓	✓	✓	Optimisation, Deterministic DP	1 hour
Rail									
[35]	$E_N(T) \cdot K_C$	✓	✓	✗	✓	✓	✓	ECM, Simulink	5 minutes

converter is modelled, the mass concentration region is not included in the model and equivalent circuit models (ECMs) are applied. Han et al. [26] apply a very short drive cycle of only five minutes. During this drive cycle, the ship operates in cruising mode for 92 seconds, docks in 46 seconds, stops for 24 seconds and then accelerates to its cruising speed in 35 seconds. It is interesting to note that Bassam et al. [25] simulate the fuel cell system for way longer, while using data from the same vessel, the FCS Alsterwasser. The fuel cell model included in the paper by Wu and Bucknall [34] is defined by several PEM FC governing equations, that take a similar shape to the equations in subsection 2.1.1. In the model, it seems like the open-circuit potential V_{OC} was defined as the temperature-dependent Nernst potential, but it is not completely clear if this is the case or if a rated voltage constant K_C has been applied.

It can be seen that most of the reduced fuel cell models are applied in the automotive industry, while most of the voltage models that were found were applied in the maritime research sector. It seems that more reduced models are applied in the automotive research sector because of the more widespread application of fuel cells in the industry; there is simply more data available on which to base your study. On the other hand, most research on fuel cell applications for maritime purposes remains related to voltage models, due to the fact that there is a limited number of pilot projects available for data purposes.

Two studies from the same maritime research group did use a reduced fuel cell in optimisation methods. Pivetta et al. [13] describe the fuel cell by a linear relation between fuel consumption and power output. They use this reduced fuel cell model in a multi-objective optimisation which is used to determine the optimal design (number of fuel cells, total installed battery capacity) and operation while also reducing degradation. The degradation does not influence the performance of the system in their model. Dall'Armi et al. [17] use a similar reduced fuel cell model to simulate the long-term performance of the hybrid system. They use two linear relations to describe the characteristics of the fuel cell: the relation between power and current and between hydrogen consumption and current. Fuel cell degradation does influence the performance of the system through the angular coefficient in the linear relation between power and current.

The research by Dall'Armi et al. [17] was the inspiration for the idea of long-term modelling of the fuel cell system. No similar long-term simulations of hybrid fuel cell/battery systems were found for maritime purposes. Of the long-term models that were found, two studies [41], [42] were optimisations of standalone hybrid energy systems for distribution and generation of electricity, and included degradation and lifetime considerations. A daily power load was determined in [41], which was extrapolated to 25 years of service of the hybrid energy system. Both a simulation of one year of running and 25 years of running were described, as well as short-term simulations used to evaluate the control strategy.

Table 2.2: Reduced fuel cell models found in literature

	Reduced fuel cell model	Auxiliary components			Modelling method	Simulation time
Ships		Compressor	Converter	BoP		
[13]	Model FC with linear curve for fuel consumption as a function of power, from various data sheets	✗	✓	✗	Optimisation, MILP	24 hours
[17]	Linear power-current & fuel consumption-current relations to describe fuel cell characteristics	✗	✗	✗	Optimisation, MILP	Until end-of-life
Automotive						
[36]	Find voltage, hydrogen consumption and degradation from FC power based on manufacturer data	✗	✓	✗	Optimisation, stochastic DP	1 hour
[37]	Normalised efficiency-power curve based on test data	✗	✓	✗	Optimisation, direct algorithm	25 minutes
[38]	Defines FC characteristics with nonlinear relationships defined from own experimental data	✗	✓	✓	Simulink simulation, control strategy applied in real time testing	20 minute tests
[39]	Quadratic relations for current as function of FC power and aux power as function of current	✓	✓	✗	Model applied in FC bus simulator, PMP controller	20 to 40 minutes
[40]	Define curves for net power and hydrogen consumption as function of current	✓	✓	✗	PMP controller, simulations	10 to 20 minutes

Three separate optimisation-based EMSs were applied in [42]. They also simulated a time frame of up to 25 years, and found, among others, the total fuel cell power generated over time as well as life degradation of the components in the hybrid energy storage system. A third research paper discussing the long-term modelling of a fuel cell system is the study by Wang et al. [43]. They modelled the system lifetime of a fuel cell battery hybrid vehicle. Consecutive optimisations were carried out using dynamic programming; the fuel cell power profile is modelled at several time steps throughout its lifetime. The polarisation curve of the fuel cell is updated after each dynamic programming simulation. They show that the optimal control strategy shifts over the lifetime of the system's lifetime. Lastly, they found that assigning different cost factors to the fuel cell has a large effect on the optimal operation of the fuel cell.

It is clear that there are various ways of modelling the fuel cell system. Mixed-integer linear programming (MILP) has been used to find the optimal operation of a fuel cell/battery hybrid ship [13], [17]. This requires the use of reduced fuel cell models to represent the fuel cell with linear equations. Voltage models may reflect the internal operating conditions of the fuel cell more accurately than the reduced models. The polarisation curve of a fuel cell is regarded as an important characteristic describing the fuel cell by the author of this thesis. Modelling the power output of a fuel cell by using its polarisation curve turns the model into a problem described by non-linear equations: power is the product of voltage and current (equation 2.8). If the voltage can be described as a linear function of current, as suggested by van Biert and Visser [7], then the problem becomes quadratic.

An alternative to the use of mixed-integer linear programming is the use of mixed-integer quadratic programming (MIQP), which would allow the modelling of a fuel cell system using its polarisation curve. The downside of mixed-integer quadratic programming is its increased computational complexity compared to mixed-integer linear programming [17].

An MIQP approach has been used to model quadratic aspects in various energy management systems. Examples are a quadratic cost function for battery degradation [44], [45], quadratic constraints describing the performance of a diesel generator [46], [47] and a quadratic cost function of an electrolyser on an offshore platform [48].

To the best of the author's knowledge, an MIQP approach has not yet been used to model the fuel cell using its polarisation curve in an energy management system for a fuel cell/battery hybrid ship.

3

Fuel cell degradation

As mentioned in the introduction, low durability and reliability of fuel cell technology are aspects that obstruct large-scale commercialisation of fuel cells [8]. In this chapter, various degradation mechanisms will be discussed and the relation to the fuel cell modelling will be analysed. It is important to consider how degradation of a fuel cell is related to its performance.

First, the relevant definitions are given in section 3.1. Next, the various degradation modes are discussed in section 3.2. Degradation rates are quantified in section 3.3 and the findings are discussed in section 3.4.

3.1. Degradation definition

In the review of PEM fuel cell degradation mechanisms by Wu et al. [49], three terms related to the lifetime of the fuel cell are defined: reliability, durability, and stability. Reliability is related to the functionality of the fuel cell at this moment or the near future; can the fuel cell start, or is failure expected in the short-term [50]. Durability concerns the resistance to irreversible decay of the fuel cell performance, and stability refers to the reversible decay of the fuel cell [49].

This research is related to the durability aspect of the fuel cell: how does irreversible degradation influence the performance of the fuel cell during its lifetime. The lifetime of the fuel cell can be defined in several ways. Several sources [49], [51] define the end of life (EoL) as a 10% voltage, efficiency, or power reduction. Pei et al. [51] define the EoL as a 10% voltage reduction under constant current operation (so also a 10% power reduction), which is reported as being the same lifetime target as set out by the Department of Energy in the US. Wu et al. [49] report that normal degradation targets are a 10% loss in efficiency. The lifetime can also be defined as time before critical failure, as is done in a durability study on PEM FCs under severe operating conditions [52]. This definition is then more closely related to the reliability aspect of fuel cell degradation. As a final option, Chen et al. [53] propose an EoL definition that takes into account the profitability of the system. At the economic lifetime of the system, the average cost reaches its lowest point, and the system should be replaced.

While degradation and its effects on the performance of the fuel cell might be modelled in a fuel cell system, the point of critical failure may best be determined using real-life testing, as this point may not be represented well in models. The definition used by Chen et al. is certainly interesting, but requires extensive knowledge about the cost of operating the system, and this may not always be clear. Initially, the 10% voltage reduction may be a suitable EoL definition for modelling purposes. The EoL definition of 10% voltage reduction is not necessarily the only suitable EoL definition for maritime purposes. It may be more economical to install more fuel cell stacks than necessary and keep using them even after a 10% voltage reduction has occurred. In that case, using the 10% voltage reduction as an EoL criterion may be considered arbitrary. However, as the fuel cell degradation increases, so does the chance of critical failure, and thus the 10% voltage reduction may be suitable when critical failure is not considered.

As discussed in subsection 2.1.1, the losses in the fuel cell consist of activation, ohmic and transport losses, as well as electrical shorting and fuel crossover. The various causes of degradation will be related to one of these types of losses.

Activation losses are determined by the speed of the electrochemical reaction, and can be reduced by increasing the reactant concentration, temperature or the number of reaction sites, or by decreasing the activation barrier with the use of catalysts, influencing the modelling parameter I_0, the exchange current [18]. The influence of the activation losses is the highest at low-current operation of the fuel cell. The main part of the activation losses occur at the cathode, due to the slower reaction of the ORR. The losses increase as the catalyst or ionomer degrade [20].

Ohmic losses are related to the internal resistance of the fuel cell. They can be reduced by either increasing conductivity (charge carrier availability, mobility of carriers, water content), or reducing length of the conductor [18]. Ohmic losses may increase due to membrane drying or degradation, and bipolar plate corrosion [20].

Concentration losses are a result of insufficient mass transport. Convective mass transport losses can be reduced by designing good flow channels [18]. The porosity of the electrode is important for the diffusion that takes place in the gas diffusion layer [18]. These characteristics are represented in the modelling parameter I_L, the limiting current, referred to before in section 2.1.

Fuel crossover may be caused by reduced electrolyte thickness, and leads to a reduction in generated current; the same goes for current leakage due to shorting, which may also be caused by thin electrolytes [18].

3.2. Degradation modes and effects

De Bruijn et al. [9] wrote an extensive review on durability aspects of the fuel cell system. They discussed the irreversible degradation of the membrane, electrodes, bipolar plates and seals.

Membrane degradation can be caused by low relative humidity, high temperature, high cell voltage, relative humidity cycling and manufacturing damages. This can result in chemical and mechanical degradation mechanisms, as well as ion contamination and structural changes of the membrane. These degradation mechanisms may then lead to membrane pinholes and cracks and membrane thinning, resulting in increased fuel crossover and related voltage reduction [9].

Electrode degradation, or specifically the degradation of platinum catalysts and its carbon support structures, is considered as one of the most important factors that decrease the operation life of PEM fuel cells [54]. The number of active platinum sites is related to the electrochemical surface area (ECSA), and thus the performance of the fuel cell [54]. According to de Bruijn et al. [9], electrode degradation may be caused by OCV conditions, fuel starvation, load cycling, air starvation, dry conditions, and freeze/thaw cycles. These operating conditions may lead to degradation of the catalyst by platinum dissolution or particle growth on the platinum structures and by corrosion of the carbon structures [9]. Platinum dissolution may cause ion contamination in the membrane, decreasing conductivity [49]. Platinum dissolution and particle agglomeration may also lead to a loss of platinum surface area and thus a loss of electrochemical surface area [49]. Carbon corrosion, or carbon oxidation, may enhance platinum dissolution and particle formation as this weakens the bond between the platinum particles and the carbon support structure [55]. Carbon corrosion also leads to reduced porosity of the electrode [56]. It may be prevented with a sufficient water management system unless the current becomes too high [49]. The degradation of the electrode increases both the activation and mass transport losses due to decreased ECSA and porosity, respectively. Additionally, water management becomes increasingly more complex as the catalyst layer becomes hydrophilic due to carbon corrosion [56]. Electrode degradation may be worsened by high voltage operation, fuel starvation during start-stop operations, or oxygen crossover [54]. Besides, it is noted that potential cycling has a larger effect on ECSA losses compared to time at a high potential [54].

The gas diffusion layer is in contact with the electrode. Its functions are conducting current, transporting reactants and draining water from catalyst layers [57]. The layer consists of carbon fibres, and sometimes a hydrophobic coating [9], [57]. Carbon corrosion of the GDL may occur to a lesser extent compared to carbon corrosion of the electrodes, as electrochemical corrosion does not occur [9]. Decomposition of the coating may also occur [49]. This may lead to reduced hydrophobicity and different pore structures, leading to increased water content in pores that were previously available for gas transport, and thus leads to increased mass transport losses [9].

Bipolar plates are used to separate cells with various functions: they separate the gases inside the fuel cell, conduct current and distribute reactant and coolant flows. Degradation of the plates may lead to poisoning of the membrane and catalysts caused by the corrosion of metal particles [9], [49]. The

formation of oxide layers on the plate may lead to losses due to increased electrical resistance between the plate and the gas diffusion layer [49].

Seals are used to prevent gas leakage and electrical shorting. According to de Bruijn et al., ”degradation phenomena on seals are in general poorly understood” [9]. Only a small selection of authors have published papers on seal degradation. Wu et al. [49] report one possible degradation mechanism that is proposed by an author but also show that their conclusions are in conflict with other findings. Seal degradation may cause increased gas crossover and electrical shorting as well as compression loss and coolant leaks [49]. Seal degradation may accelerate performance degradation of the fuel cell as a whole [49]. It may be prevented by appropriate material selection [9], [49].

3.3. Quantifying degradation

Fuel cell degradation can be tested in two ways: by doing long-term observation of fuel cell performance, or by applying accelerated stress test [9], [49]. The tests can be performed in steady-state operating conditions or by applying load cycling. Tests can be done in situ, or ex situ. Yuan et al. [58] give an overview of testing protocols for both testing of single components and testing of fuel cell stacks. While long-term steady-state testing may be representative of stationary applications, different testing methods are applied for transportation applications. In addition to steady-state tests, several other tests can be run to simulate the dynamic load of automotive applications, such as potential cycling tests or startup/shutdown tests [58].

Various definitions of operating conditions can be used to determine condition-dependent degradation rates. In the paper from Ren et al. [10], the differences between operating conditions between fuel cell buses and lightweight vehicles are discussed. Pei et al. [51] defined four different operating conditions for a fuel cell bus, namely start-stop cycling, idling, load changing, dynamic loading and high power operation. They found that there were, on average, 56 load-changing cycles, 0.99 start-stop procedures, 13 minutes of idling and 14 minutes of high power per hour of operation, representing respectively 56.5%, 33.0%, 4.7%, and 5.8% of the performance degradation. In the same paper by Ren et al. [10], the paper from Jouin et al. [59] is discussed, where the operating conditions for a light vehicle are defined the same, except for leaving out the high voltage operation. This was based on the work of Shimoi et al. [60], where they predicted that the degradation due to start-stop cycling would represent 44% of the degradation, while load cycling and idling would both represent 28% of the total degradation of a light vehicle. Even though degradation rates in the proposed operating conditions may be higher than the ones reported for the steady-state conditions, many ships sail for long times at the same power. For this reason, it seems logical to add the constant load operation to the four conditions proposed by Pei et al. [51]. Five operating conditions will be used to try to effectively predict the degradation of the fuel cell during operation: startup/shutdown, open-circuit/idling, dynamic loading, constant load conditions and high power operation.

3.3.1. Startup/shutdown degradation

Pei et al. [51] defined the stop/start cycle as one minute running in idle conditions, stop and purge with nitrogen and wait until stack voltage is back to 0 V. Idle conditions are defined as a cell voltage no higher than 0.9 V and a current density of 10 $\mathrm{mA}/\mathrm{cm}^2$. The degradation rate was found to be 0.00196% per cycle. If an initial stack voltage of 0.7 V is used, which is reported in the study, the degradation rate can be calculated to be 13.72 $\mu\mathrm{V}/\mathrm{cycle}$. The authors report that the voltage remains in OCV conditions after shutdown (5 minutes above 0.8 V, 25 minutes until 0 V), and postulate that the degradation in start-stop cycling is caused by this lingering effects: by directly reducing the voltage after shutdown the degradation rate can be reduced by approximately a factor 100. It is unclear if this effect is actually realised by the authors and what the effect of this after-treatment process is on the auxiliary power requirements.

Chen et al. [53] used the same data from the fuel cell bus research of Pei et al. [51] to determine the economic lifetime of a fuel cell. Contrary to the report by Pei et al., Chen et al. give more information about the fuel cell system: the rated power was 10 kW, with a rated current of 100 A [53]. The fuel cell stack consists of 100 cells with an effective area of 274 cm^2 per cell. The start/stop condition is described with a degradation of 13.79 $\mu\mathrm{V}/\mathrm{cycle}$, similar to what was inferred from the study by Pei et al.

Gas purging is confirmed to mitigate degradation during start/stop procedures [61]. Another possible mitigation strategy could be the addition of an auxiliary load to consume residual oxygen and hydrogen

from the cathode and anode respectively [61]. Yang et al. [62] report that the generation of reverse current, which usually occurs during start/stop procedures, is prevented when applying an auxiliary load. They reported a reduction in degradation from 1882 µV/cycle to 119 µV/cycle after applying an auxiliary load but noted that the effect of the load on a single cell may not accurately reflect the possible impact on a fuel cell stack [62]. The start-stop procedure defined by Yang et al. includes the vehicle starting process with 20 seconds at OCV, 10 seconds of increasing the current to 5 A, 100 seconds at 5 A, and 10 seconds of decreasing current followed by the shutdown process.

Fletcher et al. [36] determined degradation rates based on literature and manufacturer information and found a start/stop degradation rate of 23.91 µV/cycle. They acknowledge the relatively high degradation rate for this operating condition in comparison with the findings reported by Chen et al. and suggest this difference may be explained by the fact that the fuel cell used by Chen et al is more recent. However, they may not have realised that the paper from Chen et al. from 2015 is based on the study from Pei et al. from 2008, preceding the study from Fletcher et al., so this may not be the reason for the deviating values.

Takei et al. [63] performed research on fuel cell degradation in various load cycling conditions with OCV conditions. Each load cycle has been performed 10,000 times. The results show that long-term idling (10,000 times 60s OCV) leads to very limited ECSA reduction (12-13%) and no clear performance reduction. The 'normal' operating conditions, at a high current density load of 3s OCV/3s load and 3s idling/60s load, led to a decrease in ECSA of 20% and no noticeable performance loss. In contrast, the load cycle of 60s OCV/3s load led to the most ECSA loss (60%) and significant voltage reduction. Long idling with load cycling in between leads to high voltage reduction. The voltage reduction is a function of current density, but the average reduction can be estimated to be 0.1 V, which relates to about 10 µV/cycle. The conclusions of the study at this point are that long-term idling, short-term idling between longer load times and frequent OCV/load changes lead to way smaller losses than long idling with infrequent loads in between.

The degradation has been reduced by first testing with 60s OCV/3s low current load, and next by lowering the relative humidity in this condition. These steps significantly reduced the ECSA loss and related performance loss, especially in high-current density operation. Again, the voltage reduction is current-dependent, but it can be estimated to be, on average, about 0.4 V, or 4 µV/cycle. The authors conclude that the high degradation for 60s OCV/3s high load is not caused by either the high load time period or the long OCV duration but rather the combination of high load and long OCV duration, which leads to short load cycles between long-term OCV. The degradation can be suppressed by switching to a lower load and reducing relative humidity. The conclusions of this study are important to take into consideration when looking at degradation rates from the automotive industry. Generally speaking, start/stop procedures in cars must be achieved quicker than in maritime applications. By slowly increasing load from OCV conditions under optimal relative humidity, degradation during start/stop procedures may be suppressed.

3.3.2. Idling

When operating in idling conditions, the fuel cell system must deliver power to keep some components running [10]. Pei et al. [51] defined the idling condition as running at 10 mA/cm^2, and got a voltage reduction rate of 0.00126% per hour, which can be calculated to be 8.82 µV/hr. The study by Chen et al. [53] gives the actual degradation rate as 8.662 µV/hr. Fletcher et al. [36] reported a degradation rate of 10.17 µV/hr in low-power operation but did not define this condition.

An accelerated stress test in near OCV conditions by Wu et al. [64] resulted in an average degradation rate of 128 µV/hr over a duration of 1200 hours. The fuel cell was operated at a constant current of 0.5 A (10 mA/cm^2), with some unexpected interruptions in the testing due to problems in the lab. The average hydrogen crossover current density J_{cross} increased from 1.84 mA/cm^2 at the beginning, to 2.15 mA/cm^2 after 800 hours, to 9.54 mA/cm^2 at 1000 hours and 20.71 mA/cm^2 after 1200 hours. The resistance of the cell R_{ohm} slightly increased from 31.3 to 35.5 mΩ in 1200 hours.

Franck-Lacaze et al. [65] investigated PEM fuel cell degradation at low current densities. Operation cycles between low (20 or 120 mA/cm^2 and nominal (540 mA/cm^2) current densities were repeated. The degradation rate of the load cycle with 20 and 540 mA/cm^2 was compared to the cycle with 120 and 540 mA/cm^2. The degradation rate at nominal conditions was eight times larger for the 20 mA/cm^2 low-current condition (400 µV/hr) than for the 120 mA/cm^2 low-current condition (50 µV/hr) [65]. This large difference in degradation rates indicates the relevance of degradation during low-current operation.

3.3.3. Transient loading

Pei et al. [51] tested load changing by varying between idling and rated power conditions. The results were edited to isolate the effects of the loading cycle and showed a voltage reduction of 0.0000593% per cycle, or 0.415 μV/cycle. It is unclear what the characteristics of the rated power conditions are, as neither the current density nor the voltage are reported for this condition. The idling condition is running at 10 mA/cm^2, as discussed above. Again, Chen et al. [53] report the degradation rate as 0.419 μV/cycle, and from their paper, the rated power condition of 10 kW with 100 cells at 100 A can be found.

The degradation rate due to transient loading was given as a function of the change in generated power in the paper by Fletcher et al., with a value of 0.0441 μV/ΔkW [36]. Interestingly, this value gives the degradation per power load change, not per cycle of load change. However, it is not explained how this value was found.

Pivetta et al. [13] use the value of Fletcher et al. [36] while citing both Fletcher et al. and Chen et al., even though the two papers report different values and ways of reporting those values: a voltage drop per power change by [36] versus a voltage drop per cycle in [53].

Lin et al. [66] determined the degradation rate of dynamic loading using a comprehensive 20-minute load cycle, which includes several start/stop procedures and idle running, full power running and overload running, simulating real engine running for an automotive vehicle. The degradation rates were rather constant for the first 280 hours, after which the rates sharply increased for the next 70 hours. The degradation rates were found for 0, 200, 500 and 700 mA/cm^2 current densities, and it was found that the effect of voltage reduction was significantly worse at higher current densities. The degradation rates for the first 280 hours are 104, 188, 270 and 276 μV/hour respectively, while for the 70 hours after that, the rates of 1100, 1300, 1500 and 2300 μV/hour were found. Because of the inclusion of start/stop conditions and several up and down ramps in the load cycle, it is hard to isolate the effect of transient loading.

3.3.4. Constant load degradation

Both Wu et al. [49] and de Bruijn et al. [9] wrote a review paper on degradation mechanisms in 2008. Of the eleven long-term steady-state lifetime tests that were cited by Wu et al., only four sources were also cited by de Bruijn et al., and together, they reviewed seventeen unique long-term steady-state lifetime tests. An analysis of the results from the two studies shows that the fuel cells that were tested at high relative humidity and temperatures around 75 °C showed a degradation rate between 1 and 6 μV/hr.

The manufacturer of the fuel cell used by Fletcher et al. [36] reportedly expects essentially no degradation at constant load degradation below 80% of full load, excluding the low-load regions.

While the conditions of constant load were not included by the two important papers on fuel cell degradation from the automotive industry [51], [53], it seems important to consider this for maritime purposes, as long operation at constant load may be applicable.

3.3.5. High power operation

Pei et al. [51] reported the degradation rate of high power operation as 0.00147% per hour, which can be calculated to be 10.29 μV/hr. They report that the condition was set with the limited voltage of 0.7 V, but it is unclear at what current (density) the fuel cell is initially operated. From the study by Chen et al. [53] it becomes clear that the fuel cell stack consisting of 100 cells is operated at a current of 100 A in rated condition of 10 kW power. A degradation rate of 10 μV/hr was given [53].

Fletcher et al. [36] determined a degradation rate of 11.74 μV/hr at full load, but it is unclear what the exact specifications of the fuel cell are. The manufacturer reportedly expected a degradation rate of 11.6 μV/hr at full load conditions [36].

3.4. Discussion

In the first section, the various definitions of fuel cell lifetime have been discussed. There are several options, and for durability purposes, it would make sense to consider the 10% voltage reduction as a guideline, as increased degradation may eventually lead to unexpected critical failure of the fuel cell. No end-of-life definition was found that was suggested specifically for maritime purposes.

Several components have been discussed that can experience degradation. Membrane degrada-

tion may lead to pinholes, cracks and membrane thinning, resulting in increased fuel crossover and voltage losses related to it [9]. Electrode degradation has one of the largest impacts on a PEM fuel cell's lifetime, according to Shao et al. [54], and degradation may occur due to, among others, OCV conditions, start/stop operations and load cycling [9]. Platinum dissolution may lead to membrane contamination and corresponding conductivity loss of the membrane (increased η_{ohm}), while the ECSA is also reduced due to both platinum dissolution and particle agglomeration [49] (increased η_{act}). Carbon corrosion leads to increased platinum dissolution [55] and reduced porosity of the electrode. The porosity reduction leads to increased transport losses (η_{con}) as the diffusivity decreases [18]. Degradation of the GDL may lead to reduced hydrophobicity and different pore structures, and the related increase in mass transport losses (η_{con}) [9]. Degradation of bipolar plates may lead to increased resistance caused by the formation of oxygen layers, while poisoning of the membrane and catalysts may also occur [49]. Seal degradation may lead to gas leakage and electrical shorting [9].

To determine condition-dependent degradation rates, the steady-state operating condition has been added to the four operating conditions recognised for a fuel cell bus by Pei et al. [51]. Limited information can be found on in-situ experiments that lead to condition-dependent degradation rates: the research of a fuel cell bus by Pei et al. [51] and Chen et al. [53] form the basis of the results as they report a complete analysis of condition-dependent degradation rates during the operation of a fuel cell bus. In general, the comparison of the degradation rates in the various studies is complicated by both the variations in fuel cell characteristics and the absence of clear definitions of testing conditions.

The degradation rates found in the fuel cell bus studies [51], [53] are based on the principle of applying complex load cycles and adjusting for occurrences of other conditions in this load cycle. First, the degradation rate of the start-stop procedure is found by cycling between startup, one minute at idling conditions and shutdown. The results are then used to compensate for start/stop conditions that occur in the following load cycles. The value for idling conditions is then found by applying one start/stop procedure per 5 hours, and having the fuel cell at idling conditions for 15 minutes. After every 15 minutes, the fuel cell performance is recorded at nominal voltage and thus the voltage of the fuel cell has to increase, however the value for idling conditions is only compensated for the start-stop procedure. The degradation rates for load changing and high power operation are found in a similar manner. This method leads to isolated values for degradation per condition, but it is unclear how accurate this method is, as idling occurs during the start-stop procedure yet it is not compensated for. One of the strengths of this study is the fact that is entirely based on actual data of the fuel cell applied in the fuel cell bus.

The degradation rates found by Fletcher et al. [36] are reportedly based on a combination of literature by Chen et al. [53] and information supplied by the manufacturer of the fuel cell applied in their case study. It is unclear how the information from Chen et al. and the data from the manufacturer are combined to find the degradation rates, and to what extent which source is used.

In general, several authors agree on the effects of the start-stop procedure and possible mitigation strategies. Pei et al. [51] suggest that the degradation is caused by lingering OCV conditions, and the degradation can be reduced by approximately a factor of 100 by applying an after-treatment process that directly reduces the voltage. It is unclear if this procedure is realistic and what the consequences would be. Besides that, the authors also report that a nitrogen purge is already applied, seemingly contrasting their conclusion that the degradation rate they reported can further be reduced by after-treatment processes. Zhao et al. [61] confirm that both gas purging and applying an auxiliary load are possible mitigation strategies. Yang et al. [62] reported a degradation reduction of approximately 93% by applying an auxiliary load for a single cell. It is unclear how this would translate to a fuel cell stack. For start/stop testing in automotive applications, fuel cell power may be required faster after starting compared to maritime applications. Takei et al. [63] found that the degradation of long-term idling cycled with short times at nominal load leads to way higher degradation than frequent cycling between OCV and high load or even short idling and long times at high load. Start/stop procedures may be optimised to reduce degradation, by initially increasing to low-load and applying the correct relative humidity [63]. Complex control mechanisms may be more suitable for maritime applications than for automotive applications, so these mitigation measures may be highly suitable for ship applications.

Increased degradation at low-current density (OCV/idling) is confirmed by the fuel cell bus studies by Pei et al. [51] and Chen et al. [53] with a degradation rate of 8.662 $\mu V/hr$, as well as by the accelerated stress test at OCV conditions of Wu et al. [64] with an average degradation rate of 128 $\mu V/hr$. The effect of idling conditions was also confirmed by Franck-Lacaze et al. [65], who found degradation rates to be

eight times higher for the 20/540 mA/cm^2 cycle compared to the 120/540 mA/cm^2 cycle. Even though the authors all conclude that degradation at idling conditions is an important aspect of total fuel cell degradation, the reported degradation rates vary. The rate found by Pei et al. [51] is compensated for the degradation due to the start-stop cycle. The rate found by Wu et al. [49] is a rate for an accelerated stress test with variations in the testing conditions due to testing problems in the lab, while the findings from Franck-Lacaze et al. [65] merely indicate the difference between the two cycles and represent the degradation of the complete cycle, not the isolated effect of just the idling aspect.

The degradation due to dynamic loading in the fuel cell bus studies [51], [53] was found by applying a complex loading cycle and compensating for the start-stop procedure and idling time in the loading cycle, and the degradation is given as a voltage reduction per cycle between idling and rated power. In contrast, Fletcher et al. [36] report a degradation rate per unit of power change, but it is unclear how this value was calculated.

The values found for constant load operation differ between 1 and 6 µV/hr in the reviews by [9], [49] when the fuel cell is operated under the right conditions, whereas the manufacturer of the fuel cell used by Fletcher et al. [36] expects practically no degradation at constant load below 80% of full load, excluding the low-load regions. This expectation may be due to the way the fuel cell is operated. If the vehicle used by Fletcher et al. is operated in the same way as the bus used by Pei et al. and Chen et al., then it may be logical that there is no degradation expected in this condition: the vehicles simply do not operate in this way.

To conclude, it is suggested that the values of the study from Chen et al. [53], combined with a value for constant-load operation from [9], [49], will be considered for implementation in the modelling of the fuel cell hybrid system. The values are shown in table 3.1. The values reported by Pei et al. [51] are percentages, from which a voltage decrease can be inferred, whereas Chen et al. [53] report the actual values. These values are considered to be better than the calculated values, even though the differences are small. The values used by Fletcher et al. [36] can also be considered. However, due to the fact that the degradation rates are a combination of literature by Chen et al., and information supplied by the manufacturer, the logic behind the derived values is less clear. For some conditions, no definition is given altogether, reducing the credibility of these values.

In order to implement the values of table 3.1, the exact definitions of the various conditions will need to be coupled to the fuel cell system applied in the case study. This will be done in a later stage of this research.

Table 3.1: Suggested cell-level degradation rates to apply in fuel cell model

Condition	Definition	Degradation rate	Source
Start-stop	From offline to idling to offline again	13.79 µV/cycle	[53]
Idling	Constant operation in the low-current region	8.662 µV/hour	[53]
Dynamic loading	From idling to maximum power	0.419 µV/cycle	[53]
High power	Operating at limited voltage	10 µV/hour	[53]
Constant load	Operating between idling and high power region	1-6 µV/hour	[9], [49]

4

Problem formulation

A literature gap has been found and described in chapter 2. No applications of mixed-integer quadratically constrained programming (MIQCP) were found that model the performance of a fuel cell on board a ship. A fuel cell model based on its polarisation curve ($I-V$ curve) is proposed. An approach to modelling fuel cell degradation can be developed using the information gathered in chapter 3. Condition-dependent fuel cell degradation will be modelled. The polarisation curve is continuously influenced by the fuel cell's degradation status. As the fuel cell degrades, the voltage and power will decrease. Using an MIQCP to model the effect of the fuel cell's degradation on its performance in an energy management system is regarded as the main contribution of this thesis.

A general description of the proposed model is discussed first and is followed by a description of the mathematical model in section 4.2. The calculation of battery degradation, taking place outside of the optimisation, is discussed in section 4.3.

4.1. Problem description

The proposed model incorporates three main factors. First, the fuel cell's linearised polarisation curve is used to relate the fuel cell's operating current (I) to its voltage (V). The polarisation curve of a fuel cell can, in many cases, be linearised when looking at part of the operating region [7]. The beginning-of-life (BoL) current-voltage relation can be described using the open-circuit voltage V_{OC} and the ohmic resistance R_{ohm}:

$$V = V_{\text{OC}} - I \cdot R_{\text{ohm}} \tag{4.1}$$

This relation will be used to describe the fuel cell at beginning-of-life (BoL) conditions when no degradation has taken place.

Next, the fuel cell power (P) can be calculated as the product of voltage and current. As the voltage is linearly dependent on the current, modelling the fuel cell power as a function of voltage and current leads to a quadratic model. The relation between fuel cell power and current is then given by equation 4.2.

$$P = V_{\text{OC}} \cdot I - I^2 \cdot R_{\text{ohm}} \tag{4.2}$$

Finally, the polarisation curve is continuously influenced by the fuel cell's degradation status deg. The degradation status represents the fuel cell's voltage loss and is a measure of its state-of-health (SoH). In the proposed model, the fuel cell's voltage loss is implemented as a voltage drop over the complete polarisation curve as follows:

$$V = V_{\text{OC}} - I \cdot R_{\text{ohm}} - deg \tag{4.3}$$

A graphical overview of the degradation modelling proposed in this thesis is given in figure 4.1. The various operating regions of the fuel cell are coupled to a value for degradation. The two light-grey areas in figure 4.1a indicate the regions with enhanced degradation, while the dark-grey areas represent the areas in which the fuel cell cannot operate. The 'base region' indicates the operating region of the fuel cell where fuel cell degradation is low. Besides the three operating conditions given in figure 4.1a, starting procedures and load change will also contribute to the degradation of the fuel cell.

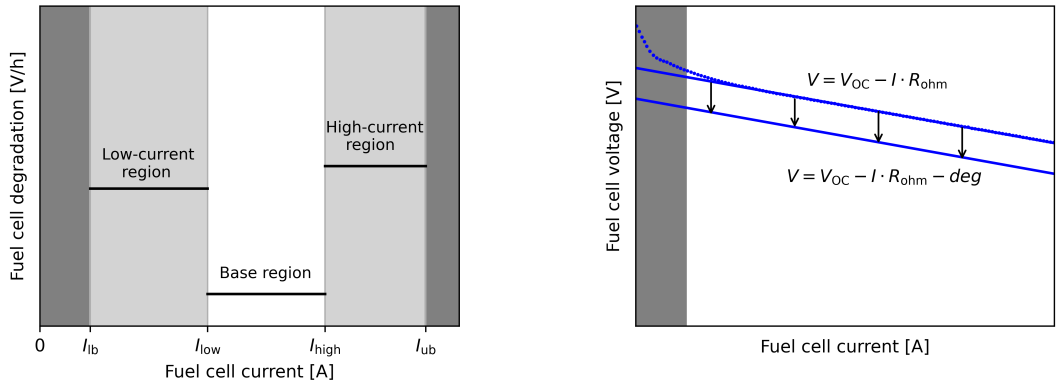

(a) Operating regions defined by I_{lb}, I_{low}, I_{high} and I_{ub}

(b) Effect of degradation on polarisation curve

Figure 4.1: Approach to modelling degradation, starts and load change excluded from overview

This approach allows us to model the fuel cell's power output using its polarisation curve, while continuously taking the influence of degradation on its performance into account.

An additional operational characteristic of the fuel cell model needs to be included. Not only is the fuel cell's operating range limited by an upper bound to its current (I_{ub}), there is also a lower bound for the operating current (I_{lb}). If the fuel cell turns on it will operate with at least this minimum fuel cell current, and the model should incorporate this.

Finally, by modelling the fuel cell using its current, voltage, and power, the hydrogen consumption can be determined. The operating current of a fuel cell is assumed to be proportional to its fuel flow $\dot{m}_{H_2}$ [18]. This allows us to calculate the fuel consumption for any simulated trip.

The fuel cell model will be implemented in the MIQCP model. Multiple fuel cells are modelled, and are described by the set of fuel cells. The proposed energy management system will also include a linear battery model, capable of describing the battery power and the battery's energy content. This type of model is widely used to model power system operation [67] and is regarded as suitable for this thesis. Together, all components of the hybrid model need to supply the required power. They do this at each time step for which the optimisation is run: the set of time steps includes all time steps considered during the optimisation. The energy management system then has the freedom to choose the distribution of power generation between these components, at each time step within the set. The resulting power distribution influences the battery's energy content, fuel consumption during the time step, and fuel cell degradation.

Two separate goals are defined: on the one hand, the model can be used to minimise the total fuel consumption, and on the other hand the total fuel cell degradation can be minimised. These goals are also combined by translating the two goals into one, by representing the fuel consumption and fuel cell degradation as costs and minimising the total costs.

4.2. Mathematical model

The mathematical model consists of sets, parameters, variables and constraints, and aims to minimise the objective function. The application of the big M method is explained in the first subsection, as this is used frequently throughout this model. This is followed by three subsections discussing the sets, parameters and variables which are used to define the mathematical model. The objective functions defined for this thesis, which the model aims to minimise, are discussed in section 4.2.5. The constraints are discussed in section 4.2.6. The constraints define the interaction between variables and ensure that the mathematical model describes the operation of the hybrid system. Finally, section 4.2.7 is used to describe the implementation process.

The mathematical model described by Dall'Armi et al. [17] formed the inspiration for this thesis. While the approach is different, as their problem is linear while the method proposed here is quadratic, it is important to stress that certain parts of the model are used from Dall'Armi's study. For example, the objective functions defined in section 4.2.5 were inspired by [17]. The modelling of the fuel cell degradation due to start cycles and load changes is also similar to the method by Dall'Armi et al. [17].

The approach to modelling the degradation due to the operating regions, as seen in figure 4.1a, is seen as a contribution to the literature. Continuously incorporating fuel cell degradation in the performance of the fuel cell by modelling it as a vertical shift in the polarisation curve (figure 4.1b) is seen as the main contribution to the literature.

4.2.1. Explanation of big M method

The big M method is applied several times throughout this thesis. It is used to model several on/off mechanisms, such as the status of the fuel cell, the (dis)charging of the battery and the starting procedures of the fuel cell. Additionally, the big M method is applied to describe if the fuel cell operates below or above a certain current. The method is explained extensively in this section to help understand the concept.

The big M method can be applied in different scenarios, but throughout this thesis, the big M method will be used to model the following logical statement: If $a > b \leftrightarrow \delta = 1$, and if $a \leq b \leftrightarrow \delta = 0$. Here δ is a binary variable. Either a or b can be a continuous variable, while the other is a constant parameter. This logical statement can be transformed into a formulation suitable for linear programming by using the following equation, where ϵ relates to a very small number and M relates to a large number.

$$b + \epsilon - M(1 - \delta) \leq a \leq b + M\delta \tag{4.4}$$

The logical statement can be explained by analysing the following scenarios: If $a > b$ then δ must be 1 to satisfy the upper bound of a. Conversely, if δ is 1 then a must be larger than or equal to $b + \epsilon$ to satisfy its lower bound.

Similarly, if $a < b + \epsilon$ then δ must be 0 to satisfy the lower bound of a. If δ is 0 then a must be smaller than or equal to b to stay within its upper bound.

When $\epsilon = 0$, this statement is related to $a \geq b$, and if ϵ has a small value (say 0.001), it is related to $a > b$. Both versions of the statement will be used. The value of M has to be large enough. If the variable's upper bound is known, the value for M can be chosen to be slightly larger than this upper bound. If M is too small, it may lead to unwanted constraints on the variable.

4.2.2. Sets

The model consists of two sets, containing a number of elements. The first set contains all fuel cell systems and represents the collection of all fuel cell systems. Each fuel cell system can be described as element f in set F, which can be written as $f \in F$. If the system configuration consists of k fuel cell systems, then the set can be described as:

$$F = \{1, 2, ..., k\} \tag{4.5}$$

The second set contains all the time steps for the optimisation: this is determined by the length of the load profile and the time step applied. All time steps are included in set T, this can be written as $t \in T$. If there are p time steps in the total range considered during the optimisation, then the set can similarly be described as:

$$T = \{1, 2, ..., p\} \tag{4.6}$$

Note that the numbering does not represent the time itself, the indices are unitless and merely relate to the element of the set.

4.2.3. Parameters

The parameters are constant values used in the formulation of the mathematical model. Most parameters can be split into three categories: parameters required for the formulation of the fuel cell model, fuel cell degradation, and the battery model. They are discussed in this order.

The origin of some parameters remains unclear in this section but this is explained in more detail in section 5.3. The values of all parameters are given in the same section.

There are also some parameters which are unrelated to any of the categories. P_{dem} is the power demand at each time step. dt is the length of the time steps. t_{end} represents the final time step of the considered load profile: it relates to the last element of set T. Finally, M represents a very large number and ϵ represents a very small number; they are both used to model if-else statements in the mathematical model using the big-M method discussed in section 4.2.1.

Fuel cell

The fuel cell's voltage is modelled using two parameters, the open-circuit voltage V_{OC} and the ohmic resistance R_{ohm}. A fuel cell's current during a time step of length dt is translated to hydrogen consumed during the time step (in grams) using the constant c. The auxiliary losses of the fuel cell are implemented using the auxiliary efficiency η_{aux}. The parameters I_{ub} and I_{lb} are used to limit the operating region of the fuel cell when it is on.

Fuel cell degradation

Five parameters for fuel cell degradation are used to relate all the defined operating conditions to a value for degradation. The parameters used to describe degradation due to the fuel cell's operating regions are ΔV_{low}, ΔV_{base} and ΔV_{high}. They represent an hourly voltage loss. ΔV_{start} is used to describe the voltage loss per starting procedure. ΔV_{dP} represents the voltage loss associated with a load change cycle. The fuel cell's load change is modelled as a fraction of its rated power, and so the model uses the parameter P_{rated}.

Besides the constants relating the operating conditions to a voltage loss, some parameters are required to model the operating conditions themselves. The parameter I_{low} describes the upper bound of the low-current region, while I_{high} describes the lower bound of the high-current region. Both regions can be seen in figure 4.1a. Together with the fuel cell's minimum (I_{lb}) and maximum (I_{ub}) operating current, they define the operating regions of the fuel cell.

The degradation status, or voltage loss, of the fuel cell may not exceed the value for the parameter $V_{\text{loss,ub}}$. Each optimisation starts with a certain initial degradation status deg_0, which for the beginning-of-life (BoL) optimisations is equal to $0\,\text{V}$.

Battery

E_{bat} is the total energy content of the battery. The available energy content is limited by the lower and upper bounds for its state-of-energy (SoE), represented by SoE_{lb} and SoE_{ub}: these are fractions of the total energy content, between 0 and 1. The battery has an initial state-of-energy SoE_0. Its maximum power is P_{max}. The battery has separate charge and discharge efficiencies, η_{c} and η_{d} respectively. Finally, the battery's degradation is evaluated outside of the optimisation using its maximum energy throughput $E_{\text{tp,max}}$.

4.2.4. Variables

The variables of a mathematical model can also be described as decision variables. Its values are adjusted based on the goals of the optimisation: this is described by the objective function of the mathematical model. To what extent the value of the variables can be adjusted is based on the constraints imposed on them. The constraints imposed on only the variables themselves are discussed in this section: these are the lower and upper bounds of the variables. The interplay between the various variables is described using more complex constraints in the next section.

The variables of the mathematical model are defined in this subsection. In a similar style to the previous section, the variables can be split into three categories: variables used to model the fuel cell, degradation, and battery respectively.

Fuel cell

The fuel cell's current, voltage and power can be described using continuous variables. Variables $I_f(t)$ represent the operating current of fuel cell f at time step t for each $f \in F$ and for each $t \in T$. Similarly, the variables $V_f(t)$ and $P_f(t)$ represent the voltage and power of fuel cell f at time step t for each $f \in F$ and for each $t \in T$, respectively. The variable for the fuel cell's power includes the auxiliary losses: the delivered power is less. All three variables are non-negative, as defined by constraint 4.7. The variable for the fuel cell current is constrained to have an upper bound of I_{ub} via constraint 4.8. Please note that the fuel cell voltage and power are constrained as a result of the fuel cell current's limit.

Additionally, a binary variable is used to represent the on-off status of the fuel cell. The variable $\delta_f(t)$ is equal to 1 if fuel cell f generates power at time step t, and is 0 if it does not.

$$I_f(t), V_f(t), P_f(t) \in \mathbb{R}_{\geq 0} \qquad \forall t \in T, f \in F \tag{4.7}$$

$$I_f(t) \leq I_{\text{ub}} \qquad \forall t \in T, f \in F \tag{4.8}$$

$$\delta_f(t) \in (0, 1) \qquad \forall t \in T, f \in F \tag{4.9}$$

Fuel cell degradation

Additional variables are required to model fuel cell degradation. Three new binary variables are introduced using constraint 4.10. $z_{\text{start}_f}(t)$ is 1 if fuel cell f starts at time step t and 0 if it does not. $z_{\text{low}_f}(t)$ and $z_{\text{high}_f}(t)$ are binary variables. $z_{\text{low}_f}(t)$ is 1 if fuel cell f operates below I_{low} at time step t, and 0 if it does not. Similarly, $z_{\text{high}_f}(t)$ is 1 if fuel cell f operates above I_{high} if fuel cell f operates above I_{high} at time step t.

An auxiliary variable $diff_f(t)$ is introduced and represents the power change of fuel cell f from time step $t-1$ to time step t as a fraction of its rated power. This is a continuous variable which can take non-negative values (constraint 4.11). This auxiliary variable is used to define the non-negative continuous variable $dP_f(t)$, the absolute value of power change. $dP_f(t)$ can then be used to find the degradation due to load change.

The increase in degradation due to all five conditions at time step t is captured by the variable $\Delta deg_f(t)$, which represents the additional voltage loss originating at time step t. It influences the actual degradation status of the fuel cell at the next time step. The variable for degradation status is defined as $deg_f(t)$ and describes the total voltage loss of fuel cell f at time step t, influencing the fuel cell's performance. Both are continuous non-negative variables, just like $dP_f(t)$, as defined in constraint 4.12. Finally, the fuel cell's degradation is limited to the upper bound of its voltage loss, $V_{\text{loss,ub}}$.

$$z_{\text{low}_f}(t), z_{\text{high}_f}(t), z_{\text{start}_f}(t) \in (0,1) \qquad \forall t \in T, f \in F \tag{4.10}$$

$$diff_f(t) \in \mathbb{R} \qquad \forall t \in T, f \in F \tag{4.11}$$

$$dP_f(t), \Delta deg_f(t), deg_f(t) \in \mathbb{R}_{\geq 0} \qquad \forall t \in T, f \in F \tag{4.12}$$

$$deg_f(t) \leq V_{\text{loss,ub}} \qquad \forall t \in T, f \in F \tag{4.13}$$

Battery

A single battery system is modelled using two non-negative continuous variables for charging and discharging power, defined in constraint 4.14. Both variables are constrained to be lower than the maximum battery power P_{max}, using constraint 4.15. $P_{\text{c}}(t)$ represents the effective charging power of the battery: this is related to the energy entering the battery. This is less than what is supplied to the battery, with losses due to the charging efficiency. P_{d} represents the discharge power and is related to the energy leaving the battery. Due to losses, the effective delivered power is lower.

$dE(t)$ is a continuous variable and represents the change in energy content due to the battery's power at time step t. It influences the battery's energy content at the next time step. The variable can be negative and is defined in constraint 4.16. The energy content is defined using the non-negative continuous variable $E(t)$, and is constrained using its lower and upper bounds for the state-of-energy, SoE_{lb} and SoE_{ub}.

Finally, the battery cannot charge and discharge simultaneously. Two binary variables are introduced to prevent this. The variable $\delta_{\text{c}}(t)$ takes the value 1 if the battery is charging at time step t, and 0 if it is not. Likewise, $\delta_{\text{d}}(t)$ is 1 if the battery is delivering power at time step t, and 0 if it is not.

$$P_{\text{c}}(t), P_{\text{d}}(t), E(t) \in \mathbb{R}_{\geq 0} \qquad \forall t \in T \tag{4.14}$$

$$P_{\text{c}}(t), P_{\text{d}}(t) \leq P_{\text{max}} \qquad \forall t \in T \tag{4.15}$$

$$dE(t) \in \mathbb{R} \qquad \forall t \in T \tag{4.16}$$

$$SoE_{\text{lb}} \cdot E_{\text{bat}} \leq E(t) \leq SoE_{\text{ub}} \cdot E_{\text{bat}} \qquad \forall t \in T \tag{4.17}$$

$$\delta_{\text{c}}(t), \delta_{\text{d}}(t) \in (0,1) \qquad \forall t \in T \tag{4.18}$$

4.2.5. Objective functions

The mathematical model can be used for several goals. Two possible objective functions are defined: the minimisation of fuel consumption and the minimisation of fuel cell degradation. The comparison between the results for the two objective functions can give insight into how much fuel cell degradation can be prevented, and what this costs in terms of increased fuel consumption.

The two objective functions are also combined into a new objective function by translating fuel consumption and degradation into costs. This combination of the two can be used to find an optimal operating strategy when considering both aspects of fuel consumption and degradation, for various cost scenarios.

The fuel cell current during a time step of length dt is translated to hydrogen consumption using the constant c. The minimisation of fuel consumption during the load profile can then be described as the sum of the fuel consumption of all fuel cell systems $f \in F$ during all time steps $t \in T$, and results in a value for total hydrogen consumption (in grams). The minimisation of fuel consumption is described by the following objective function:

$$\min \sum_{t \in T} \sum_{f \in F} c \cdot I_f(t) \tag{4.19}$$

An alternative objective function is defined to minimise the total voltage loss during the simulated load profile. Minimising the total voltage loss generated during the load profile is achieved by applying equation 4.20 as the objective function for the optimisation:

$$\min \sum_{t \in T} \sum_{f \in F} \Delta deg_f(t) \tag{4.20}$$

Finally, a weighted-sum approach to multi-objective optimisation is carried out. The two single-objective optimisation problems are translated into a new single-objective optimisation problem by translating hydrogen consumption and fuel cell degradation into costs, using constants c_1 and c_2 respectively. How these constants are constructed is clarified in section 5.3. The relative importance of both objective functions is influenced by the hydrogen and fuel cell costs. A minimisation of the total costs is carried out using equation 4.21 as the objective function:

$$\min \sum_{t \in T} \sum_{f \in F} (c_1 \cdot I_f(t) + c_2 \cdot \Delta deg_f(t)) \tag{4.21}$$

4.2.6. Constraints

The constraints form the foundation of the mathematical model. They are used to ensure that the mathematical model accurately represents the components considered in the energy management system. The constraints for the fuel cell, fuel cell degradation, and battery will be introduced in this order. Please note that the general lower and upper bounds of the variables were introduced in section 4.2.4. Constraint 4.22 is the only general constraint, used to regulate the power balance.

$$\sum_{f \in F} P_f(t) \cdot \eta_{\mathsf{aux}} + P_{\mathsf{d}}(t) \cdot \eta_{\mathsf{d}} - \frac{P_{\mathsf{c}}(t)}{\eta_{\mathsf{c}}} = P_{\mathsf{dem}}(t) \qquad \forall t \in T \tag{4.22}$$

Fuel cell

Constraint 4.23 ensures that the fuel cell voltage follows the linear relation between current and voltage while taking into account the fuel cell's voltage loss $deg_f(t)$. Constraint 4.24 is used to define the generated power and transform it into kilowatts. As mentioned in the problem description in section 4.1, the fuel cell needs to operate at a current higher than I_{lb} if it is turned on. The fuel cell also needs to be able to turn off, so a simple lower bound on the variable for the fuel cell current is not enough.

Constraints 4.25 and 4.26 are used to provide the possibility to turn the fuel cell off, while ensuring a minimum operating current I_{lb}. The first constraint is used to define the on/off status of the fuel cell, following the logical statement: $P_f(t) > 0 \leftrightarrow \delta_f(t) = 1$, and $P_f(t) = 0 \leftrightarrow \delta_f(t) = 0$. This ensures that the binary variable is equal to 1 if the fuel cell is on, and is 0 when it is off. The constraint is used to set a lower bound to the operating current when it is turned on, following the logical statement: $\delta_f(t) = 1 \leftrightarrow I_f(t) \geq I_{\mathsf{lb}}$, and $\delta_f(t) = 0 \leftrightarrow I_f(t) = 0$. If the fuel cell is on the fuel cell current must be at least equal to the lower bound, and the fuel cell is off when the current is equal to 0.

$$V_f(t) = V_{\mathsf{OC}} - R_{\mathsf{ohm}} \cdot I_f(t) - deg_f(t) \qquad \forall t \in T, f \in F \tag{4.23}$$

$$P_f(t) = \frac{V_f(t) \cdot I_f(t)}{1000} \qquad \forall t \in T, f \in F \tag{4.24}$$

$$0 + \epsilon - M(1 - \delta_f(t)) \leq P_f(t) \leq 0 + M \cdot \delta_f(t) \qquad \forall t \in T, f \in F \tag{4.25}$$

$$I_{\mathsf{lb}} - M(1 - \delta_f(t)) \leq I_f(t) \leq 0 + M \cdot \delta_f(t) \qquad \forall t \in T, f \in F \tag{4.26}$$

Fuel cell degradation

Five fuel cell operating conditions and their related degradation rates (per cell) were discussed in the literature review. The set of constraints below is used to model all operating conditions and relate them to its condition-specific voltage loss ΔV. Three degradation mechanisms are related to the region in which the fuel cell is operated: the low, medium, and high-current regions. The degradation due to the fuel cell's operating region is constructed as follows: when the fuel cell is on, it will always experience a base degradation of $2\,\mu V/h$ per cell. Additionally, when the fuel cell is operating in the low- or high-current region, the difference between the base degradation and the region-specific degradation is added, so $6.7\,\mu V/h$ and $8\,\mu V/h$ per cell respectively. An overview of this modelling method can be seen in figure 4.2.

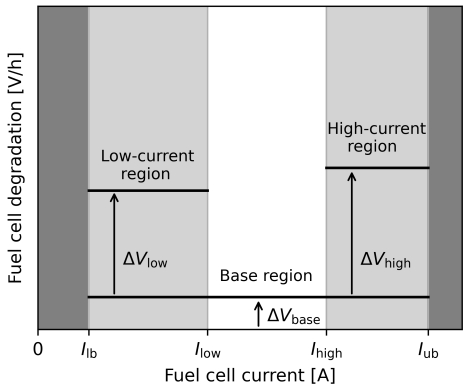

Figure 4.2: Modelling method of fuel cell degradation in three operating regions

Two new binary variables are introduced to indicate if a fuel cell system is operating in the low-current or high-current region, $z_{\text{low}\,f}(t)$ and $z_{\text{high}\,f}(t)$ respectively. They are implemented using the big M method in constraints 4.27 and 4.28. They have a value of 1 if the fuel cell is operating in the relevant region, and are equal to 0 if it is not operating in that region. The first constraint is used to implement the logical statement: $I_f(t) \leq I_{\text{low}} \leftrightarrow z_{\text{low}\,f}(t) = 1$, and $I_f(t) \geq I_{\text{low}} \leftrightarrow z_{\text{low}\,f}(t) = 0$. The following constraint is used to implement the statement: $I_f(t) \geq I_{\text{high}} \leftrightarrow z_{\text{high}\,f}(t) = 1$, and $I_f(t) \leq I_{\text{high}} \leftrightarrow z_{\text{high}\,f}(t) = 0$.

An additional binary variable $z_{\text{start}\,f}(t)$ is used to indicate if fuel cell f initiates a starting procedure during time step t. Constraint 4.30 is used to model $\delta_f(t) > \delta_f(t-1) \leftrightarrow z_{\text{start}\,f}(t) = 1$, and $\delta_f(t) \leq \delta_f(t-1) \leftrightarrow z_{\text{high}\,f}(t) = 0$. This approach does not work for the first time step, so a separate constraint is required. If the fuel cell delivers power at the first time step, it is assumed that the fuel cell starts at that time step (constraint 4.29).

The continuous variable $diff_f(t)$, which can be negative, is equal to the normalised power change of system f from time step $t-1$ to t. It is expressed as a fraction of rated power to prevent numerical issues due to extremely small numbers. The continuous variable $diff_f(t)$ is transformed into the non-negative continuous variable $dP_f(t)$. $diff_f(t)$ can be seen as an auxiliary variable required to take the absolute value of the power change, as this cannot be done directly.

$$I_f(t) - M(1 - z_{\text{low}\,f}(t)) \leq I_{\text{low}} \leq I_f(t) + M \cdot z_{\text{low}\,f}(t) \qquad \forall t \in T, f \in F \qquad (4.27)$$

$$I_{\text{high}} - M(1 - z_{\text{high}\,f}(t)) \leq I_f(t) \leq I_{\text{high}} + M \cdot z_{\text{high}\,f}(t) \qquad \forall t \in T, f \in F \qquad (4.28)$$

$$z_{\text{start}\,f}(1) = \delta_f(1) \qquad \forall f \in F \qquad (4.29)$$

$$\delta_f(t-1) + \epsilon - M(1 - z_{\text{start}\,f}(t)) \leq \delta_f(t) \leq \delta_f(t-1) + M \cdot z_{\text{start}\,f}(t) \qquad \forall t \in T \setminus \{1\}, f \in F \qquad (4.30)$$

$$diff_f(1) = \frac{1}{P_{\text{rated}}} P_f(1) \qquad \forall f \in F \qquad (4.31)$$

$$diff_f(t) = \frac{1}{P_{\text{rated}}} (P_f(t) - P_f(t-1)) \qquad \forall t \in T \setminus \{1\}, f \in F \qquad (4.32)$$

$$dP_f(t) = \mid diff_f(t) \mid \qquad \forall t \in T, f \in F \qquad (4.33)$$

The five variables for the degradation mechanisms occurring during time step t are summed and translated to a voltage loss at time step t using the continuous variable $\Delta deg_f(t)$. The value of this variable

is the additional voltage loss originating at time step t. It influences the actual degradation status of the fuel cell at the next time step, $deg_f(t)$. This variable can be interpreted as equal to the sum of all $\Delta deg_f(t)$ but is implemented slightly differently. The degradation status $deg_f(t)$ influences the effectively generated voltage $V_f(t)$ through constraint 4.23.

$$\Delta deg_f(t) = \Delta V_{\text{base}} \cdot \delta_f(t) + \Delta V_{\text{low}} \cdot z_{\text{low}\,f}(t) \cdot \delta_f(t) + \Delta V_{\text{high}} \cdot z_{\text{high}\,f}(t) + \Delta V_{\text{start}} \cdot z_{\text{start}\,f}(t) + \Delta V_{\text{dP}} \cdot dP_f(t) \qquad \forall t \in T, f \in F \tag{4.34}$$

$$deg_f(t) = deg_f(t-1) + \Delta deg_f(t-1) \qquad \forall t \in T \setminus \{1\}, f \in F \tag{4.35}$$

$$deg_f(1) = deg_{0,\,f} \qquad \forall f \in F \tag{4.36}$$

Battery

Constraint 4.37 is used to define the charging status of the battery: if $P_{\text{c}}(t) > 0$ then $\delta_{\text{c}}(t) = 1$, and if $P_{\text{c}}(t) = 0$ then $\delta_{\text{c}}(t) = 0$. The following constraint ensures the same for the discharging status of the battery. Constraint 4.39 prevents simultaneous charging and discharging: at any time step, the battery can be off completely, it can charge, or it can discharge, but it can't both charge and discharge at the same time.

Constraints 4.40 until 4.43 are used to define the energy content of the battery. Constraint 4.40 defines the battery's initial energy content. Constraint 4.41 relates the battery power during time step t with length dt to a change in energy during this time step, $dE(t)$. The change in energy at time step t affects the energy content of the battery at the next time step: this is implemented using constraint 4.42. Constraint 4.43 is added to prevent the battery's energy content from surpassing the lower or upper bound due to the power at the final time step. The effect of the power output at the final time step was not yet accounted for in constraint 4.17 for the energy content $E(t)$.

$$0 + \epsilon - M(1 - \delta_{\text{c}}(t)) \leq P_{\text{c}}(t) \leq 0 + M \cdot \delta_{\text{c}}(t) \qquad \forall t \in T \tag{4.37}$$

$$0 + \epsilon - M(1 - \delta_{\text{d}}(t)) \leq P_{\text{d}}(t) \leq 0 + M \cdot \delta_{\text{d}}(t) \qquad \forall t \in T \tag{4.38}$$

$$\delta_{\text{c}}(t) + \delta_{\text{d}}(t) \leq 1 \qquad \forall t \in T \tag{4.39}$$

$$E(1) = SoE_0 \cdot E_{\text{bat}} \tag{4.40}$$

$$dt \cdot (P_{\text{c}}(t) - P_{\text{d}}(t)) = dE(t) \qquad \forall t \in T \tag{4.41}$$

$$E(t) = E(t-1) + dE(t-1) \qquad \forall t \in T \setminus \{1\} \tag{4.42}$$

$$SoE_{\text{lb}} \cdot E_{\text{bat}} \leq E(t_{\text{end}}) + dE(t_{\text{end}}) \leq SoE_{\text{ub}} \cdot E_{\text{bat}} \tag{4.43}$$

4.2.7. Implementation of the model

The mathematical model is transformed into Python code, using Spyder software. The model is solved using Gurobi, a suitable solver for mixed-integer quadratically constrained programming. Four of the five papers which used MIQP, cited in the literature review, used Gurobi to solve their quadratic models [44]-[47]. An HP ZBook Power G7 Mobile Workstation with an Intel(R) Core(TM) i7-10750H CPU @ 2.60GHz and 16 GB of RAM is used as hardware to run the model.

4.3. Battery degradation

To keep the computational complexity of the model limited, battery degradation is not incorporated in the optimisation. Instead, battery degradation is evaluated after the optimisation, using the total amount of energy spent on battery charging. The method applied by Pivetta et al. [13], which in turn is based on the research by Terlouw and Bauer [68], is used to determine the battery's degradation.

An energy capacity loss of 20% is used as the EoL definition [13]. In this approach, we assume that the battery degrades linearly over its lifetime, and the average battery energy capacity E_{av} during its lifetime is then 90% of its initial energy capacity E_{bat}. A limited depth-of-discharge (DoD) is used for the battery to limit degradation effects [24], from $SoE = 0.2$ until $SoE = 0.8$: the resulting DoD is 60%. Toshiba's data sheet states that the number of lifecycles N_{cycles} is more than 20000 [69]. The maximum energy throughput can then be calculated using:

$$E_{\text{tp,max}} = N_{\text{cycles}} \cdot E_{\text{av}} \cdot DoD \tag{4.44}$$

This value is used to evaluate the state-of-health of the battery by looking at the total energy spent on battery charging during any simulated load profile.

5

Case study

The case study used for this thesis is an existing general cargo vessel, the MV Ankie. Measurements of the engine's power output have been made available for the purpose of this thesis and are used as the power demand of the ship. The power requirement of the vessel is used to choose a commercially available fuel cell system to model.

The vessel's characteristics are given in section 5.1. Two figures are included that show the ship's power demand during a trip, one for a long operational profile and one for a shorter but more power-intensive operational profile. This is followed by a section describing the process of selecting and modelling a fuel cell system. Lastly, an overview and explanation of all input to the mathematical model is given in section 5.3.

5.1. The vessel used in the case study

The MV Ankie, a general cargo vessel, is selected as a case study for the purpose of this thesis. The ship is currently in operation and it has one main diesel engine and a controllable pitch propeller. Some of the ship's specifications are given in table 5.1.

Table 5.1: Case vessel specifications, from [70]

Characteristic	Value
Length	88.9 m
Width	12.5 m
DWT	3638 t
Year built	2007
Engine	Wärtsilä 9L20

Measurements taken on board the general cargo vessel MV Ankie have been used before in research from the SH2IPDRIVE project. Some of these measurements were made available for the purpose of this thesis. Mylonopoulos et al. [70] used the measured diesel engine's power output as the load requirement of the vessel. The ship does not have a fixed route, and thus the power measurements do not show a single clearly defined operational profile. The maximum recorded power output of the diesel engine is just above 1200 kW.

Mylonopoulos et al. [70] developed several possible system configurations for a conceptual retrofit of this cargo vessel to a fuel cell/battery hybrid vessel. They state that the fuel cells must be able to supply the maximum power demand of 1200 kW. In collaboration with the vessel's operators and industry experts, Mylonopoulos et al. [70] determined that the battery packs should have a total energy capacity of 550 kWh and a total power of 800 kW. These requirements will be used in this thesis. Specifically, the required installed fuel cell power of 1200 kW is used to select a fuel cell system in the coming section.

Two different load profiles were defined using the available measurement data and can be seen in figure 5.1. The long load profile, seen in figure 5.1a, includes both a long time at constant operation as

well as a period of load fluctuations. From now on, this load profile is referred to as the 'energy-intensive profile' or 'E-intensive profile'.

The shorter profile, seen in figure 5.1b, has a sustained high-power operation with two peaks near the maximum power demand of the vessel. This load profile is from now on referred to as the 'power-intensive profile', or 'P-intensive profile'. These load profiles will be used separately as input to the model.

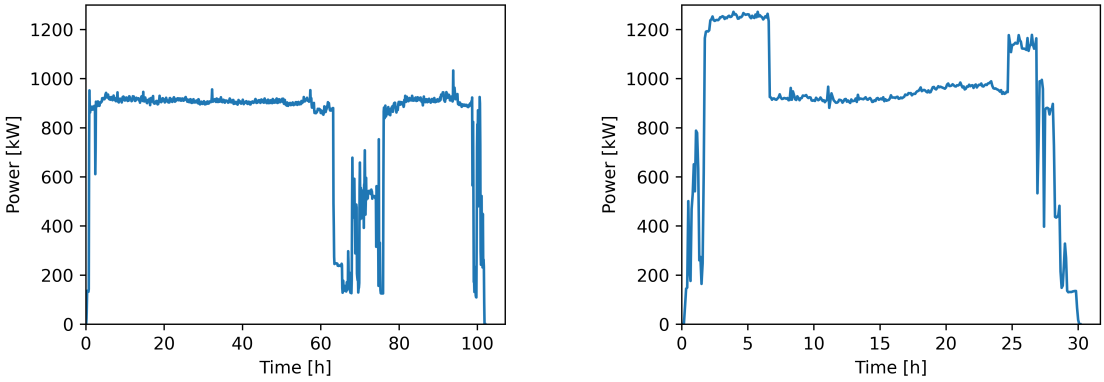

(a) Energy-intensive load profile

(b) Power-intensive load profile

Figure 5.1: Two different operational profiles applied in this thesis

The measurements were taken at a fixed interval of five minutes. While fuel cell voltage is important for the management of the DC grid at very small time scales, the energy balance in a hybrid system has a long timescale [71]. For the purpose of this study, a longer timescale is regarded as suitable while acknowledging that the short-term effects of voltage fluctuations are not represented.

5.2. Fuel cell selection and modelling

The fuel cell selection and subsequent modelling are discussed in this section. First, a commercially available fuel cell system suitable for maritime application is chosen based on the available data. The Nedstack maritime systems are chosen and the following sections are used to describe the process of modelling the chosen fuel cell system. First, the stack performance is described in section 5.2.2. The stack performance is translated to the system performance using auxiliary losses, and this process is described in section 5.2.3. Finally, the final models describing the performance of the two maritime fuel cell systems are presented in section 5.2.4.

5.2.1. Selecting a fuel cell system

Commercially available fuel cell systems which are marketed as suitable for maritime purposes are assessed in this section. Two maritime fuel cell systems from Nedstack are analysed, as well as all the fuel cell systems covered by Mylonopoulos et al. [70]. Factors such as weight, volume and costs were important considerations for selecting the fuel cell system in the research by Mylonopoulos et al. [70]. For the purpose of this thesis, the available data on the fuel cell's operational characteristics has a large impact on the possibility of modelling the system. An overview of the relevant fuel cell systems is given in table 5.2. The table includes the systems' rated power as well as some remarks on the available data.

The large amount of data supplied in Nedstack's data sheet [72], including a polarisation curve which extends past the nominal operating point, is seen as a large advantage. The extension of the polarisation curve past its rated operating point at beginning-of-life conditions allows us to model the system until end-of-life conditions using the extensive polarisation curve. The stack specifications and operating conditions are described in great detail in the data sheet, and multiple operating points are described for both the $13\,\text{kW}$ fuel cell stack and the maritime fuel cell systems. Besides that, the availability of the $600\,\text{kW}$ system provides the possibility of modelling only two separate systems. For these reasons, the Nedstack systems are selected for further analysis.

Table 5.2: Review of commercial maritime fuel cell systems

Fuel cell system	Power [kW]	Remarks
zepp.Y50 [73] by zepp.solutions	50	Efficiency and fuel consumption as function of output power, no polarisation curve
HyPM HD90 [74] by Hydrogenics	90	Production halted, extensive polarisation curve
MT-FCPI-120 [75] by Nedstack	120	Extensive polarisation curve stack and fuel consumption data
zepp.X150-M [73] by zepp.solutions	150	Marinised version is mentioned, no information found
HyPM HD180 [76] by Hydrogenics	180	Production halted, extensive polarisation curve
Marine System 200 [77] by Powercell Group	200	Limited data available, no polarisation curve
FCWave [78] by Ballard	200	Limited data available, no polarisation curve
MT-FCPI-600 [79] by Nedstack	600	Extensive polarisation curve for stack, two systems can provide required power

5.2.2. Fuel cell stack model

Nedstack's fuel cell stack is first modelled as it forms the basis of both maritime fuel cell systems. The rated power of 13.6 kW is delivered at 230 A [72]. An open-source web-based tool developed by Rohatgi [80] is used to extract data points from the polarisation curve and power curve supplied in the data sheet [72]. The two separate data sets are used to construct a linear current-voltage relation and a quadratic current-power relation, as suggested in the problem description in section 4.1. The constants V_{OC} and R_{ohm}, used in equations 4.1 and 4.2, must be equal in both relations. Trend line equations have been constructed by minimising the mean absolute percentage error (MAPE) between the points generated by the trend line and the points extracted from the data. This is achieved by using the Excel solver add-in to vary the constant values V_{OC} and R_{ohm} to minimise the MAPE. The final values for V_{OC} and R_{ohm} were found by minimising the average MAPE of the voltage trend and the power trend, while only looking at the data for $I > 30$ A. This value for the fuel cell's minimum operating current I_{lb} was confirmed in a meeting with Wouter Balk, test engineer at Nedstack (private communication, Oct. 25, 2023). $V_{\text{OC}} = 80.64$ V and $R_{\text{ohm}} = 0.0939\,\Omega$ were found to best describe the stack's performance curves for $I > 30$ A.

The resulting trend lines, as well as the data points extracted from the polarisation curve, can be seen in figure 5.2. The voltage trend line has a visible variation in the region below 30 A, underestimating its voltage. However, the trend lines are considered suitable for the purpose of this thesis, as the fuel cell won't be operated in the region below 30 A, indicated by the dark grey region in the figure.

Besides the trend lines for voltage and power, the stack's fuel consumption is included in the figure as a second horizontal axis. The fuel consumption is found as follows. For a single cell running at stoichiometric operation, the relation between its current and its hydrogen consumption can be described by equation 5.1 [18]:

$$I = zF\nu \tag{5.1}$$

Here z is the number of electrons transferred per hydrogen molecule (2), F is the Faraday constant in C/mol and ν is the hydrogen consumption in mol/s. The cell's molar flow can be translated into a mass flow by using the molar mass of hydrogen, M_{H_2} (in g/mol). The stack's mass flow is found by multiplying the cell's hydrogen consumption with the number of cells in the stack n. The equation is

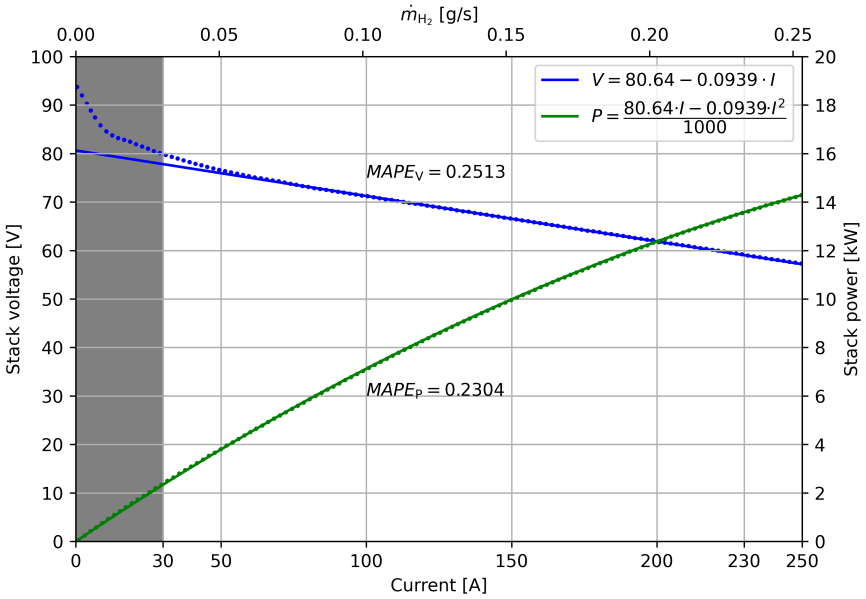

Figure 5.2: Fuel cell stack trend lines through data points from [72] for $I > 30$ A

further refined by dividing by the hydrogen utilisation factor η_{fuel}, which compensates for the fact that part of the hydrogen is not used to generate current [18]. The stack's hydrogen consumption, in grams per second, can then be found using equation 5.2

$$\dot{m}_{\text{H}_2,\text{stack}} = \frac{M_{\text{H}_2} \cdot I \cdot n}{zF \cdot \eta_{\text{fuel}}} \tag{5.2}$$

The hydrogen utilisation factor is "commonly set at 99%-100%" [81]. This matches with the estimate of 1% hydrogen loss due to anode purging in the Nedstack system which was mentioned by Wouter Balk (private communication, Oct. 25, 2023).

The stack's maximum hydrogen consumption was given as 154 normal litres per minute [72]. The definition of the normal flow used by Nedstack was confirmed to be at conditions of 0°C and atmospheric pressure by Wouter Balk (private communication, Oct. 25, 2023). Using the density of hydrogen at these conditions the maximum hydrogen consumption can be calculated to be $0.228\,\text{g/s}$. The hydrogen consumption at 230 A, calculated with equation 5.2, results in a 2% overestimation at $0.233\,\text{g/s}$, corresponding well to the reported value.

Finally, the fuel cell efficiency can be described by equation 5.3, with the fuel cell power in kW and the lower heating value (LHV) in kJ/g [18].

$$\eta_{\text{fc}} = \frac{P_{\text{fc}}}{\dot{m}_{\text{H}_2} \cdot LHV} \tag{5.3}$$

The stack's efficiency is given in the appendix in figure A.2. The figure also includes the linear relation between fuel cell current and fuel consumption.

5.2.3. Determining auxiliary losses in the maritime fuel cell systems

Auxiliary losses occur when scaling from one stack to the larger systems. The available data on fuel consumption and power output of the 600 kW system are exactly five times larger than for the 120 kW system, so the 120 kW system is used to determine the losses, and specifically the version consisting of twelve stacks connected in series ($N_{\text{s}} = 12$). Its current is limited to 200 A, and its reported performance is summarised in table 5.3. For convenience, the fuel consumption is calculated to grams per second as well.

When a graph is constructed by simply multiplying the stack's trend lines by the number of series-connected stacks ($N_{\text{s}} = 12$), the nominal power of 120 kW is produced near 150 A and the peak power of 148 kW is produced near 200 A. These points are represented by points 1 and 2 respectively in

Table 5.3: Overview of 120 kW system conditions reported in Nedstack's data sheet [75]

	Power	Reported hydrogen consumption	Rewritten hydrogen consumption	Current
Nominal	120 kW	59 kg/MWh	1.966 g/s	Undefined
Rated/max	148 kW	8 kg/h	2.22 g/s	200 A

figure 5.3. While this does seem like the perfect definition of nominal and rated conditions, this would suggest no additional losses are generated in the twelve-stack system. Furthermore, it does not match the available data on hydrogen consumption.

The nominal hydrogen consumption, given as a specific consumption, can be translated into grams per second by using its nominal power. At 120 kW the system produces one MWh in eight hours and twenty minutes, so the nominal hydrogen consumption refers to a mass flow of 1.966 g/s. The reported maximum hydrogen consumption is equal to 2.22 g/s. After dividing the hydrogen consumption by the number of stacks, equation 5.2 can be used to determine the operating current based on the fuel consumption. The nominal consumption would be related to a current of 162 A and the maximum hydrogen consumption would be related to a current of only 183 A. This would suggest that the reported maximum consumption is recorded below the maximum operating current, which does not seem realistic. Besides, the nominal current based on hydrogen consumption is higher than expected based on the simple relation between stack power and system power. This deviation may be explained by the presence of additional auxiliary losses in the fuel cell system.

An auxiliary loss is added to the trend line for twelve stacks to match the system's reported nominal fuel consumption to its nominal power. A linear profile of the system's losses was suggested by Wouter Balk (private communication, Oct. 25, 2023). The losses mainly consist of the air blower in the system and were suggested to be around $5 - 7$% of the total generated power. A linear power loss is added with the intent of shifting point 1 in figure 5.3, the nominal power (120 kW), from 150 A to 162 A. This is achieved by applying a 5.57% power loss to the system, in line with the suggested power loss. The reported nominal fuel consumption is now matched with the nominal power using the relation between current and fuel consumption. The results are given in figure 5.3.

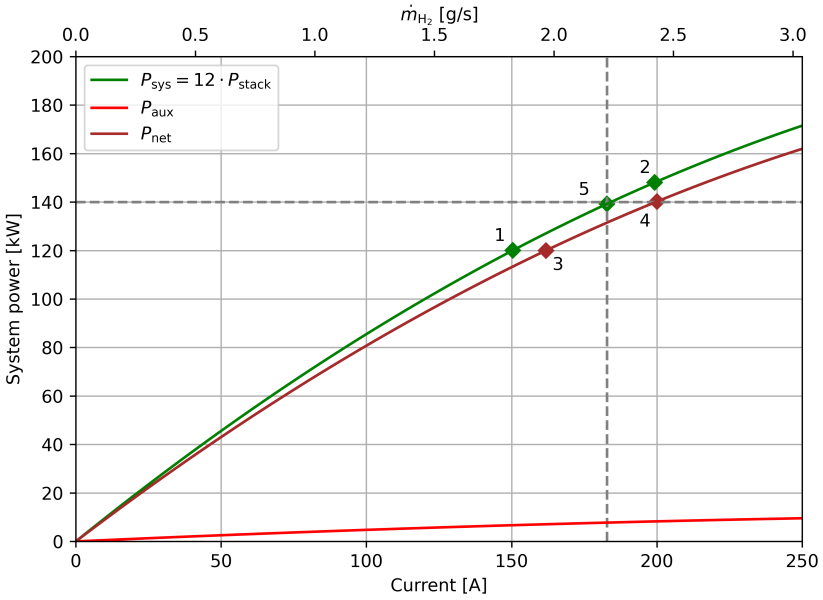

Figure 5.3: A 5.57% loss shifts the nominal operating point from 1 to 3, matching the reported consumption to power

In the figure, points 1 and 2 are the nominal and peak power on the simple system power curve. Point 3 represents the nominal operating point of the fuel cell after compensating for auxiliary losses,

with a 120 kW production at 162 A. At this point, the fuel cell operates at its nominal operating power and fuel consumption as reported in table 5.3. The addition of losses led to a reduction of the system's peak power from 148 kW near 200 A (point 3) to 140 kW at 200 A (point 4). The maximum hydrogen consumption is now higher than the reported maximum consumption rate of 8 kg/h. Interestingly, a power of 140 kW on the simple power curve relates to the maximum hydrogen consumption reported on the data sheet, which might explain the discrepancy (point 5).

To conclude, there are some discrepancies in the data sheet, which hinder the reproducibility of the model developed in this thesis. From now on, it is assumed that 5.57% of the stack power is lost to auxiliary components in the system ($\eta_{\text{aux}} = 1 - 0.0557$). The peak power is reduced to 140 kW at 200 A while the nominal power is produced at 162 A. The maximum hydrogen consumption reported in the data sheet is an underestimation based on the peak power of 140 kW applied to the curve without losses.

5.2.4. Fuel cell systems with parallel connections

While the 120 kW system could be modelled using only series connections between stacks, a configuration with parallel connections is also described in the data sheet. Besides that, the 600 kW only has a configuration with parallel connections. The 600 kW system consists of sixty stacks. The system generates a voltage in the range of 500-1000 V and operates with a current of 0-1200 A. This is achieved by six parallel lines ($N_{\text{p}} = 6$) of ten stacks connected in series ($N_{\text{s}} = 10$). The fuel cell system voltage V_{sys} can be described by equation 5.4 for any combination of N_{s} and N_{p}:

$$V_{\text{sys}} = N_{\text{s}}(V_{\text{OC,stack}} - \frac{1}{N_{\text{p}}} R_{\text{ohm,stack}} \cdot I) \tag{5.4}$$

Here I relates to the system's total current, the sum of all current through parallel lines. Applying equation 5.4 to the 120 kW and 600 kW configurations leads to the operating characteristics in figure 5.4. Note that auxiliary power losses are applied to find the power curve. The minimum operating current of the system I_{lb} is represented in the figure using the dark grey region, and is found by multiplying the stacks's minimum operating current I_{lb} by N_{s}. The total fuel consumption of the system $\dot{m}_{\text{H}_2,\text{sys}}$ is found by multiplying the stack's fuel consumption (equation 5.2) with the number of series-connected stacks N_{s}:

$$\dot{m}_{\text{H}_2,\text{sys}} = N_{\text{s}} \cdot \frac{M_{\text{H}_2} \cdot I \cdot n}{zF \cdot \eta_{\text{fuel}}} \tag{5.5}$$

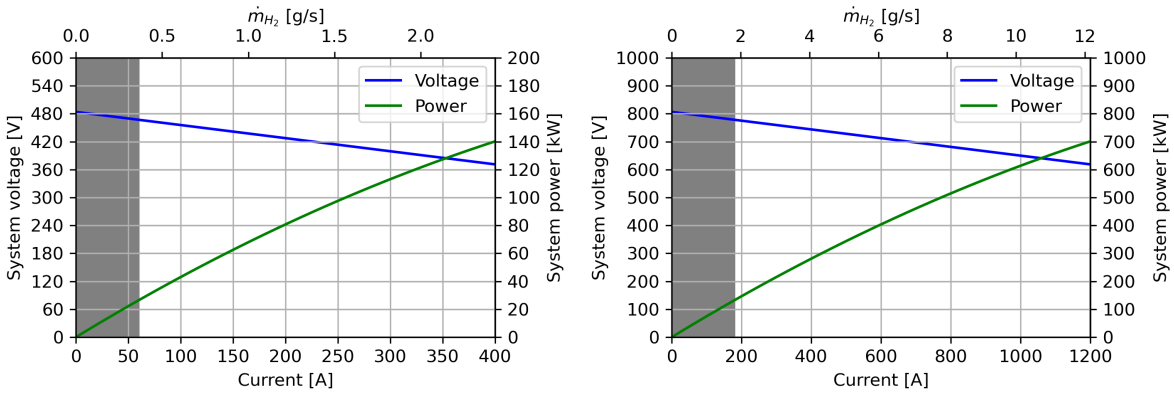

(a) 120 kW system, parallel layout

(b) 600 kW system

Figure 5.4: System characteristics for Nedstack's maritime systems, based on the stack trend lines

5.3. Input to the model

An overview of all fixed input parameters of the mathematical model is given below in table 5.4. To simplify, all parameters are given for the 600 kW system. The values which differ, such as the currents defining the operating regions, degradation rates, and rated power can be translated into values for the 120 kW system by taking into account the number of stacks, N_{p} and N_{s}.

Pei et al. suggested an end-of-life (EoL) definition of a voltage loss equal to 10% of the cell's voltage [51], presumably 10% from a voltage of 0.7 V. Dall'Armi et al. used an EoL definition of 20% of the cell's reference voltage [17] without specifying the value of the reference voltage. In this case, the fuel cell's EoL criteria is defined as a voltage loss of 0.1 V per cell, which is approximately 10% of the cell's V_{OC}. With $n = 96$ and $N_{\text{S}} = 10$ this results in $V_{\text{loss,ub}} = 96$V.

The fuel cell degradation rates for the five operation regions are based on the cell-level degradation rates found during the literature review, described in section 3.4. All cell-level degradation rates in table 3.1 are multiplied by the number of cells n and the number of series-connected stacks N_{s}. The degradation rates for the operating regions are hourly, while the voltage losses due to starts and load change are per cycle. The value for ΔV_{dP} is multiplied by the normalised absolute power change $dP_f(t)$ in the mathematical model, which represents load change as a fraction of the full cycle.

The charging and discharging efficiency of the battery are assumed based on a review of the literature. This led to the conclusion that the efficiencies used in similar studies were mostly based on assumptions as well. Some authors report values as low as 0.88 for both efficiencies [25], while others use values of 0.98 and 1 for charging and discharging respectively [82]. The values used in this thesis represent a middle ground between these reported values and consciously show a difference between the charging and discharging efficiency. This last aspect is incorporated in multiple papers modelling energy management systems and can be supported by an experimental battery study that shows a difference between charging and discharging efficiency [83].

The values for M and ϵ had to be chosen such that the big-M method works as expected: a small value for ϵ is required and is chosen rather arbitrarily. The value for M is chosen based on the upper bound of all variables in the applications of the big M method. It has to be larger than the fuel cell power due to constraint 4.25, larger than the fuel cell current due to constraint 4.26, and larger than the battery power due to constraint 4.37. The maximum value of these three variables is 1200 for the fuel cell current, so $M = 2000$ is large enough.

There are also input parameters that vary per optimisation run. The length of the time step dt is varied for both load profiles. The constant c, is used to determine the fuel consumption during a time step with length dt due to an operating current I. Its value can be calculated as follows:

$$c = \frac{M_{\text{H}_2} \cdot n \cdot N_{\text{s}}}{zF \cdot \eta_{\text{fuel}}} \cdot dt \tag{5.6}$$

Additionally, the hydrogen and fuel cell costs are varied to carry out the minimisation of total costs for different price scenarios. The two coefficients in the minimisation of total costs, c_1 and c_2, are calculated as follows:

$$c_1 = c \cdot c_{\text{H}_2} \tag{5.7}$$

$$c_2 = \frac{c_{\text{PEM}} \cdot P_{\text{rated}}}{V_{\text{loss,ub}}} \tag{5.8}$$

At the time of writing, the cost of hydrogen (c_{H_2}) at fuel stations ranges between 18 to 25 €/kg in the Netherlands, while prices as low as 10 €/kg are reported at German fuel stations [86].

The costs of state-of-the-art maritime fuel cell systems c_{PEM} have been reported to be around 1000 to 2500 €/kW [87], with the Clean Hydrogen Joint Undertaking reporting a specific fuel cell cost of 2000 €/kW [88]. If the production of PEM fuel cell systems increases, a price of around 600 €/kW is projected near the end of this decade, with a long-term objective for heavy-duty systems of 80 €/kW in 2050 [87].

Table 5.4: Input parameters of the mathematical model, for the 600 kW system

Parameters	Value	Unit	Source
E_{bat}	550	kWh	Chosen based on [70]
$E_{\text{tp,max}}$	7.28	GWh	Based on [13], described in section 4.3
F	96485	C/mol	[18]
I_{lb}	180	A	Assumed
I_{low}	600	A	Assumed
I_{high}	1020	A	Assumed
I_{ub}	1200	A	[75]
LHV	120	kJ/g	[84]
M	2000	-	Chosen
M_{H_2}	2.01568	g/mol	[85]
n	96	-	[72]
$N_{\text{cycle,max}}$	20000	-	[69]
N_{p}	6	-	Deduced from [79]
N_{s}	10	-	Deduced from [79]
P_{rated}	600	kW	[79]
R_{ohm}	0.0939	Ω	Determined in section 5.2
SoE_0	0.8	-	Chosen
SoE_{lb}	0.2	-	[17], [24]
SoE_{ub}	0.8	-	[24]
$V_{\text{loss,ub}}$	96	V	[51]
$V_{\text{OC,stack}}$	80.64	V	Determined in section 5.2
z	2	-	[18]
ΔV_{base}	0.00192	V/h	Assumed based on [9], [49]
ΔV_{dP}	0.000216	V	[53]
ΔV_{high}	0.00768	V/h	[53]
ΔV_{low}	0.006432	V/h	[53]
ΔV_{start}	0.013248	V	[53]
ϵ	0.01	-	Chosen
η_{aux}	0.9443	-	Determined in section 5.2
η_{c}	0.95	-	Assumed
η_{d}	0.98	-	Assumed
η_{fuel}	0.99	-	[81]

6

Verification of the model

The implementation of the mathematical model is executed in steps. The model is verified by using various tests. For each test, a hypothesis is defined that should describe the expectation of how the model should behave. If the results do not match the hypothesis, first the hypothesis is checked to see if the assumptions were correct. If the assumptions look correct, the model is checked for any errors in the formulation. If no errors are found in the formulation, the implementation of the model in the code is checked to see if there are any programming errors. If any changes are made after failing a check, the verification is restarted from scratch.

Verification tests are carried out by changing parameters in three categories. The objective function can be changed by varying parameters in the existing objective function, which adjusts the goal of the optimisation. Changing functional parameters impacts the model by changing the 'external' characteristics imposed on the mathematical model, such as the power demand or the efficiencies. Finally, right-hand side (RHS) parameters are related to the constant value in a constraint and change the lower or upper bounds of a variable.

The verification process is carried out as the model is developed. The verification of the fuel cell model (without degradation) is described in section 6.1. This is followed by the verification of a stand-alone battery model. The verification of the hybrid model is described in section 6.3. The model for fuel cell degradation is verified by only looking at the fuel cell, and this process is described in section 6.4. Ultimately, verification tests are carried out on the hybrid model which includes fuel cell degradation.

The step size used during the verification process increases as the model becomes more complex, as is described in the sections on the verification process. Separate from the model verification, the time step selection and its implications are discussed in section 6.6.

6.1. Verification of the fuel cell model

The fuel cell model, without degradation, is tested using the 102-hour-long operational profile. This immediately leads to the conclusion that applying ten separate fuel cell systems is not realistic with respect to computational complexity. Iterating between the numbers of fuel cells which can provide the required 1200 kW by simply varying the number of series-connected stacks in a system, leads to the following run times for imaginary systems: 7 seconds for two 600 kW systems, 163 seconds for three 400 kW systems, 265 seconds for four 300 kW systems, and 408 seconds for six 200 kW systems. It was not possible to find an accurate (below 2.5% gap) solution within one hour for the ten 120 kW systems. As the model will only increase in complexity, the two 600 kW systems are used to model the hybrid propulsion system. This choice will lead to a decrease in operational flexibility and may result in higher fuel consumption and/or fuel cell degradation when compared to the optimal power allocation using ten systems.

The fuel cell model is verified using the energy-intensive operational profile with time steps of 5 minutes. While testing only the fuel cell systems, I_{lb} is set to 0 to ensure that low power demand can be provided by the fuel cell system as well. The model is solved while minimising total fuel consumption, which led to a total fuel consumption of 4.56 t. This is the optimal solution of the objective function and will be represented by the symbol Z in this verification process. The power supplied by the two fuel cell

systems is practically identical at each time step, and the same goes for the systems' fuel consumption. This can be explained by the simple fact that the system's efficiency decreases as the current increases; the most beneficial strategy is to run both systems at equal, low power. The total energy generated by the fuel cell, $dt \cdot \sum_{t \in T} P_f(t)$, is equal to 43.3 MWh for both systems. This value is used in the verification process, as it indicates the share of energy delivered by both fuel cell systems. For the purpose of the verification process, E_1 represents the energy delivered by system 1, and E_2 the energy delivered by system 2.

Table 6.1: Verification tests for fuel cell model

Type of test	Description	Expected	Result	OK?
Objective function	Change to maximisation	$Z > 4.56$, I_f maximised for one system while minimised for other	$Z = 4.94$, difference between operating current is maximised at each time step	OK
Objective function	Decrease η_{fuel} from 0.99 to 0.95 for system 1	$Z > 4.56$, $E_1 < 43.3$, $E_2 > 43.3$	$Z = 4.65$, $E_1 = 41.4$, $E_2 = 46.5$	OK
Functional	Decrease η_{aux} to 0.9	$Z > 4.56$	$Z = 4.83$	OK
Functional	Reduce $P_{\text{dem}}(t)$ to zero for all time steps	$Z = 0$, $E_1 = E_2 = 0$	$Z = 0$, $E_1 = E_2 = 0$	OK
Right-hand side	Increase V_{OC} to 90	$Z < 4.56$	$Z = 3.95$	OK
Right-hand side	Decrease I_{ub} to 500 A for system 1	$Z > 4.56$, $E_1 < 43295$, $E_2 > 43295$	$Z = 4.62$, $E_1 = 34.1$, $E_1 = 53.8$	OK

6.2. Verification of the battery model

The battery model is tested to ensure that the model works as expected. As none of the objective functions suggested in section 4.2.5 can be applied to the battery-only model, the following objective function is used to verify the battery model:

$$\min \sum_{t \in T} (P_{\text{c}}(t) + P_{\text{d}}(t)) \tag{6.1}$$

In contrast to the fuel cell model, the battery model consists of only one system. The optimisation consists of following the power demand only, and there are no ways in which the model can find an optimum strategy, it merely has to follow the power demand. Even though the results are not interesting, the process allows us to verify the battery model. Several tests are carried out, among which:

- Using a power demand that ensures the battery is empty at the time step before the final time step: if the power at the final time step is too high, the model is infeasible, which shows that constraint 4.43 works.
- Using a power demand consisting of negative values (power supply): the battery model works fine and shows the charging of the battery.
- Decreasing the efficiencies η_{c} and η_{d} results in reduced effective charging power P_{c} and increased required discharging power P_{d} for a constant power demand.
- A power demand of 0 results in both δ_{c} and δ_{d} being 0 as well.
- Reducing ϵ to 0 with a power demand of 0's and changing the objective function to the maximization of $\sum_{t \in T} (\delta_{\text{c}}(t) + \delta_{\text{d}}(t))$ leads to both δ's being 1 at all time steps, even though P_{c} and P_{d} are 0. This should not be allowed and does not occur when $\epsilon = 0.001$, highlighting the importance of including ϵ in constraints 4.37 and 4.38.
- Reducing M to 400 leads to an infeasible model, showing the importance of choosing the right value for M.

6.3. Verification of the hybrid model

The hybrid model is verified using a reduced load profile to limit the computational time. The objective function is the minimisation of fuel consumption. The model is tested by using hourly data for power demand to limit the number of time steps from 1225 to 103. The optimisation led to a hydrogen consumption of 4.58 t, which will be the objective value to which the results of the verification will be compared. Besides that, the value for the total energy discharged by and supplied to the battery relates to the extent of the battery usage. These can be expressed as $dt \cdot \sum_{t \in T}(P_{\mathsf{d}}(t)) = 0.96$ MWh and $dt \cdot \sum_{t \in T}(P_{\mathsf{c}}(t)) = 0.55$ MWh, and are represented by E_1 and E_2 in the table, respectively.

Table 6.2: Verification tests for the hybrid model

Type of test	Description	Expected	Result	OK?
Objective function	Change to maximisation	$Z > 4.58$, $E_1 > 0.96$	$Z = 5.20$, $E_1 = 12$	OK
Objective function	Change to min $\sum_{t \in T} P_{\mathsf{c}}(t)$	$Z > 4.58$, $E_1 < 0.96$, $E_2 = 0$	$Z = 4.88$, $E_1 = 0.40$, $E_2 = 0$	OK
Functional	Increase battery efficiencies to 1	$Z < 4.58$, $E_1 > 0.96$, $E_2 > 0.55$	$Z = 4.57$, $E_1 = 1.34$, $E_2 = 0.92$	OK
RHS	Reduce SoE_{ub} and SoE_0 to 0.5	$Z > 4.58$, $E_1 < 0.96$, $E_2 < 0.55$	$Z = 4.59$, $E_1 = 0.54$, $E_2 = 0.33$	OK

6.4. Verification of model for fuel cell degradation

The fuel cell degradation model is carefully verified by checking if the output values of the newly introduced variables match the expectation based on the operating current. This has been done for a very simplified demand profile and showed that the constraints work as expected. In addition, the fuel cell model with the included degradation has been run for the hourly load profile, and some generic tests have been carried out. Minimising fuel consumption leads to a fuel consumption of $Z = 4.61$ t, and a voltage loss of 311 and 285 mV for system 1 and 2 respectively (combined 0.60 V). For easy comparison, the total fuel consumption is referred to as $Z_1 = 4.61$ while the combined voltage loss of the two systems is referred to as $Z_2 = 0.60$ in the table describing the verification tests, table 6.3.

Table 6.3: Verification tests for fuel cell degradation

Type of test	Description	Expected	Result	OK?
Objective function	Change to min deg (4.20)	$Z_1 > 4608.15$, $Z_2 < 596.6$	$Z_1 = 4635.65$, $Z_2 = 466.96$	OK
Functional	Reduce I_{low} from 600 to 400 A	$Z_2 < 596.6$, less time spent operating in low-current region	$Z_2 = 544$, yes	OK
Functional	Double ΔV_{base}	$Z_1 > 4608.15$, $Z_2 > 596.6$	$Z_1 > 4608.83$, $Z_2 > 969.32$	OK
Functional	Remove $deg_f(t)$ from the voltage relation (4.23)	$Z_1 < 4608.15$	$Z_1 = 4607.18$	OK
Functional	Increase power demand by 400 kW	$Z_1 > 4608.15$, $Z_2 > 596.6$	$Z_1 = 7510.44$, $Z_2 = 1777.80$, mostly due to deg at high current	OK
RHS	Set starting deg to $deg_f(1) = 20$ V for both systems	$Z_1 > 4608.15$	$Z_1 = 4768.66$	OK

6.5. Verification of final model with degradation

Due to the model's increasing complexity, the verification of the complete model is executed using the hourly data for the power-intensive load profile. The benchmark result during the verification process is determined for the minimisation of hydrogen consumption. This resulted in a total fuel consumption of 1.54 t, with a total combined voltage loss of 0.18 V. These will be represented as $Z_1 = 1540.2$ and $Z_2 = 177.5$ respectively in table 6.4.

Table 6.4: Verification of the complete model

Type of test	Description	Expected	Result	OK?
Objective function	Change to min deg (4.20)	$Z_1 > 1540.2$, $Z_2 < 177.5$	$Z_1 = 1577.8$, $Z_2 = 131.1$	OK
Objective function	Change η_{fuel} to 0.8 only for system 2	$Z_1 > 1540.2$, system 1 is used more than system 2	$Z_1 = 1698$, system 1 supplies 61% of total fuel cell power	OK
Functional	Reduce I_{high} from 1020 to 800 A	$Z_1 > 1540.2$, $Z_2 > 177.5$	$Z_1 = 1540.3$, $Z_2 = 269.7$	OK
Functional	Reduce SoE_0 to 0.2	$Z_1 > 1540.2$, $Z_2 > 177.5$	$Z_1 = 1562.3$, $Z_2 = 194.2$	OK
RHS	Increase deg_0 to 48 V, which is a starting SoH of 50%	$Z_1 > 1540.2$, $Z_2 > 177.5$	$Z_1 = 1686.2$, $Z_2 = 192.9$	OK
RHS	Increase $P_{\text{dem}}(t)$ by 200 kW	$Z_1 > 1540.2$, $Z_2 > 177.5$	$Z_1 = 1972.2$, $Z_2 = 288.9$	OK

In the first functional test, the reduction of the lower-bound for the high-current region was expected to lead to an increase in fuel cell degradation, as more time would be spent operating in the high-current region. This was clearly the case, with an increase in degradation of around 50%. The increase in degradation led to a limited increase in fuel consumption.

In the first RHS test, the increase in degradation is due to the occurrence of operating in the high-current region. Due to the starting degradation of $deg_0 = 48$ V, the highest output power recorded during the load profile now relates to a fuel cell current in the high-current region, which did not occur for $deg_0 = 0$ V.

6.6. Time step selection

Increasingly large time steps were used during the verification tests as the model became more complex. While choosing the time step size dt to use for generating the final results, a trade-off between accuracy and computational complexity has to be carried out. The power-intensive load profile is used to investigate the sensitivity of the model results to the time step size. The energy-intensive load profile is approximately four times longer, and a time step of four times longer will be chosen as well.

Time step sizes of one hour, thirty minutes, fifteen minutes and five minutes have been used to carry out the optimisation. This required 3 seconds, 71 seconds, and almost one hour to reach the standard solution gap of 0.01% for the first three time-step sizes. The solution gap was stranded at 0.012% for the final run, which took 8 hours. The resulting voltage losses, for minimisation of fuel consumption and minimisation of degradation, are included in figure 6.1.

While the degradation is significantly higher for small step sizes while minimising hydrogen consumption, the voltage loss when minimising degradation is quite constant. The degradation actually increases as the step size gets larger, as there are fewer options to minimise the degradation.

Assuming the fuel consumption resulting from the smallest time step is most accurate, the fuel consumption is consistently overestimated when using the larger time step. In ascending length of dt the fuel consumption is overestimated by 0.6, 0.2 and 0.6%, respectively, for both objective functions applied. The battery usage is underestimated by 6% for the 15 minute time step but overestimated

by 5% for $dt = 30$m, while minimising degradation. The battery usage is consistently underestimated when minimising fuel consumption.

A time step of 15 minutes is chosen to apply to the power-intensive load profile. It is deemed as the best trade-off between computational complexity and accuracy. The total degradation can be accurately determined while including degradation in the minimisation problem. The quality of the solution is higher compared to the time step of five minutes; it takes less time to find, and an initial near-optimal solution is found faster. At the same time, the suggested time step size for the extensive load profile is 1 hour.

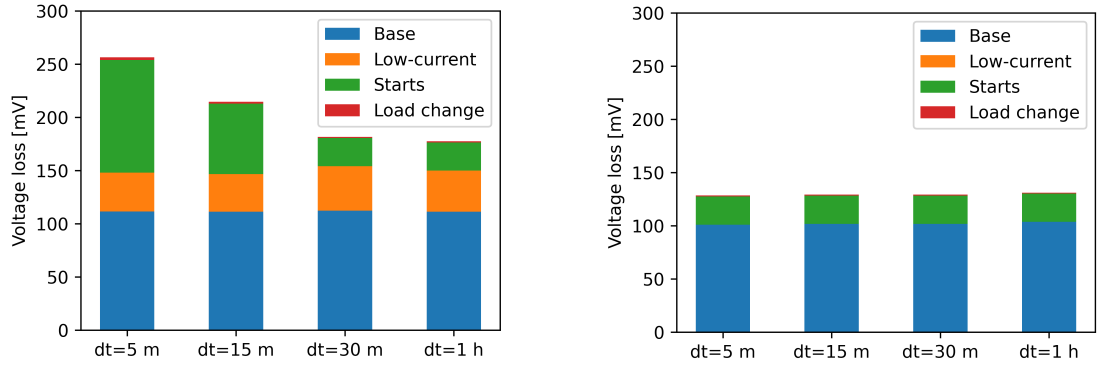

(a) Results degradation for min(m_{H_2})

(b) Results degradation for min(deg)

Figure 6.1: Comparison of voltage loss during the power-intensive load profile, for various time step sizes

The choice of a larger time step size can be explained with the assumption that the battery will compensate for all the intermediate load changes. While the comparison between the results of the power-intensive load profile did not lead to a clear reduction in battery usage for the various dt while minimising degradation, the effects were clearer when minimising fuel consumption. This led to an underestimation of battery usage by 15% for the two intermediate step sizes, and by 45% for the largest step size of one hour.

Additional measurements are available at an interval of 200 ms. These are used to compare battery usage and fuel cell degradation by looking at various increases in dt. A fuel cell operating at constant power is compared with a fuel cell operating by load-following. If the fuel cell is operating at constant power, then the battery is absorbing all fluctuations. With a large time step size, this is not included in the model. The increase in dt from one second to ten seconds was the most impactful on battery usage, with a 30% reduction due to the large step size. This can be seen in figure 6.2. The results for the increases in dt from 200 ms to 1 s, from 10 s to 1 m and from 1 m to 5 m are given in the appendix in figure B.1. The underestimation of battery usage compounds as the time steps get larger, and results in an underestimation of battery usage by about 30%, with a related increase in fuel consumption of only 0.6%.

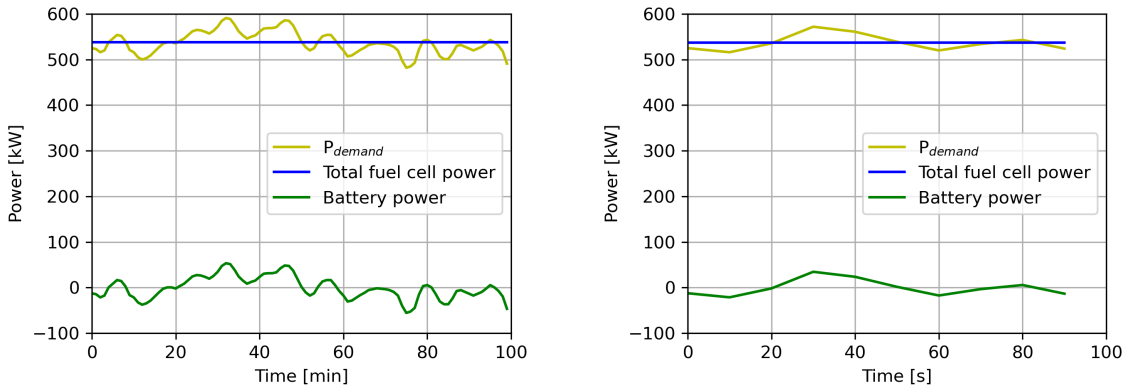

(a) 100 seconds at $dt = 1$ s

(b) 100 seconds at $dt = 10$ s

Figure 6.2: Reduction in power fluctuations by changing dt from 1 s to 10 s

Besides the underestimation of battery usage, the comparison of results between minimising fuel consumption and minimising degradation will show a smaller effect. For time step sizes of 200 ms and one second, the degradation is portrayed accurately by the larger step size. A larger difference in degradation is found when comparing $dt = 1$ to $dt = 10$ seconds. For $dt = 1$s, load-following leads to an increase in degradation by 500% compared to the degradation when operating at a constant load, while the degradation is only doubled for the larger time step size. This effect diminishes again for larger time step sizes, but this may lead to a significant underestimation of the fuel cell degradation when minimising fuel consumption.

Table 6.5: Degradation for constant fuel cell power and for fuel cell load-following for different dt

Profile	**Degradation at constant power [mV]**	**Degradation for load-following [mV]**	
		Small dt	Large dt
Twenty seconds at 200 ms & 1 s	10.7	60.8	60.1
Hundred seconds at 1 s & 10 s	53.3	320	110
Fifteen minutes at 10 s & 1 m	480	837	582
One hour at 1 m & 5 m	1920	2240	1979

7 Results

The two load profiles introduced in section 5.1 are used in the proposed model. Due to the model's complexity, a time step size of $dt = 1$ hour is used for the 102-hour-long energy-extensive load profile, and the power profile is simulated with time steps of $dt = 15$ minutes. As a result of these large step sizes, the battery usage will be underestimated. This also leads to an underestimation of fuel consumption.

The results of the two single-objective optimisations are discussed in section 7.1. The weighted-sum approach is used to minimise the total costs, and results of the sensitivity analysis are given in 7.2. The results of the long-term simulation of the vessel are discussed in the final paragraph.

Figures for the power balance are given throughout this chapter. The curves describing the battery and fuel cell power are compensated for the losses. The charging power of the battery (negative values) represents the power supplied to the battery, i.e. the surplus in the power balance, not what is effectively charging the battery, which is less. Similarly, the battery discharge power and fuel cell power represent the power delivered to the grid, excluding losses.

7.1. Comparing single objective optimisation runs

The energy-intensive and the power-intensive load profiles are used to run the model. Both objective functions are used: the minimisation of fuel consumption (min($m_{\mathrm{H_2}}$)) and degradation (min(deg)). The resulting power balance and battery energy content are given below, in addition to some key results such as fuel consumption, degradation and battery usage. The degradation is further analysed by looking at the degradation per operating condition.

7.1.1. Single-objective optimisations using the energy-intensive load profile

The two single-objective optimisations, defined in section 4.2.5, are applied to the 102 hour load profile. Some of the key results are summarised in table 7.1. The total degradation can be reduced by 35% by minimising degradation only. The battery usage increases by a factor 3.5, resulting in a limited increase in hydrogen consumption by only 2%.

Table 7.1: Key results of the single-objective optimisations using the energy-intensive profile

Objective	Fuel consumption [kg]	Total fuel cell degradation [mV]	Energy spent on battery charging [kWh]
Minimising fuel consumption	4576	613.3	566.9
Minimising degradation	4659	396.9	2034

An overview of the degradation per operating condition is given in figure 7.1. Operating in the low-current region can be effectively reduced using the minimisation of degradation.

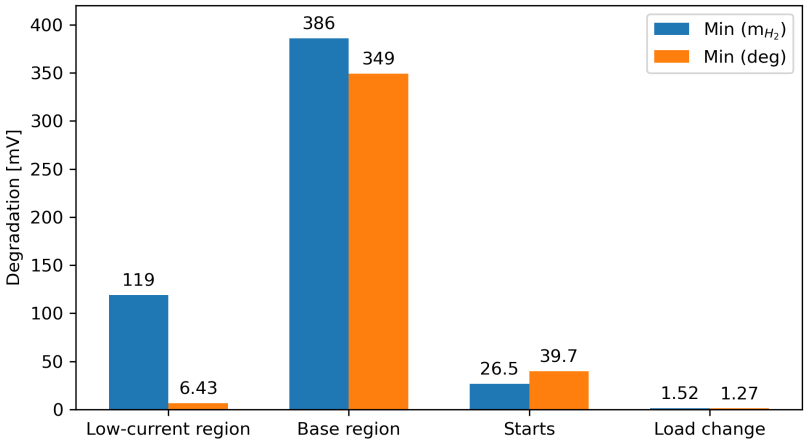

Figure 7.1: Degradation per operating condition during the energy-extensive load profile for both objectives

Finally, the resulting power balance and battery state of energy are given in figure 7.2.

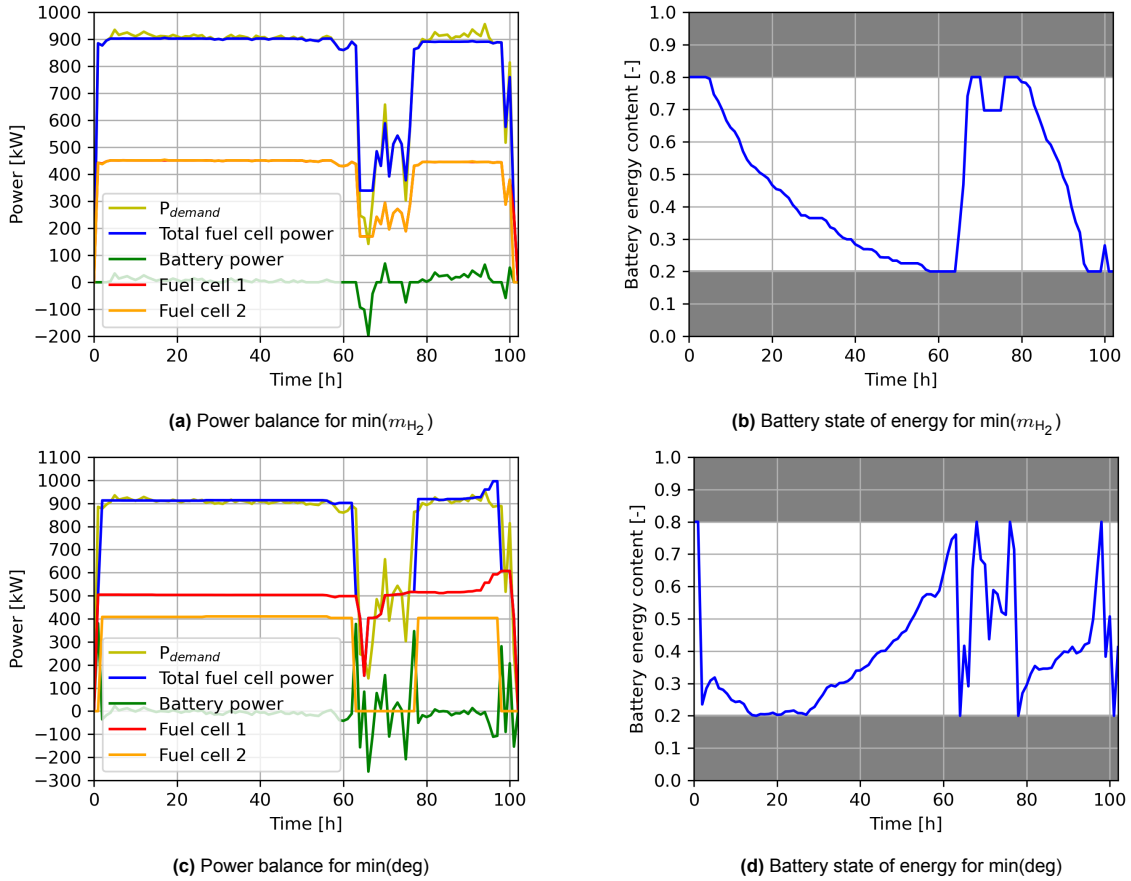

(a) Power balance for min(m_{H_2})

(b) Battery state of energy for min(m_{H_2})

(c) Power balance for min(deg)

(d) Battery state of energy for min(deg)

Figure 7.2: Results for the single-objective optimisations using the E-intensive profile

A clear difference can be seen between the top figures and the bottom figures, which, among others, indicates the role of the battery in the operational strategy. For the minimisation of fuel consumption, the battery is used to keep the fuel cell systems at efficient operating conditions: in the first sixty hours, the fuel cell systems provide power at a near-constant output just below the power demand. When the power drops the battery is recharged. This happens while operating at lower loads, and thus at

relatively efficient operating conditions.

When minimising degradation, the battery is used to keep the fuel cell power nearly constant for the first sixty hours. One system is kept offline for the first hour while the battery supplies the remainder of the required power. Most of the decrease in degradation is due to a different strategy between the two fuel cell systems themselves: by turning off one fuel cell system when it is possible, the system which is turned off experiences less degradation. When minimising hydrogen consumption, the two systems are operating at low power with high efficiencies. Both systems are experiencing degradation due to the fact that they are turned on, as well as the fact that they are operating in the low-current region. In the second strategy, only one system is on, and this system does not operate in the low-current region but in the base region, which means that the system experiences significantly less degradation. The other system is turned off and thus does not experience degradation at all.

7.1.2. Single-objective optimisations using the power-intensive load profile

The difference between the two optimal operational strategies for the minimisation of fuel consumption and degradation, respectively, can be seen in figure 7.3.

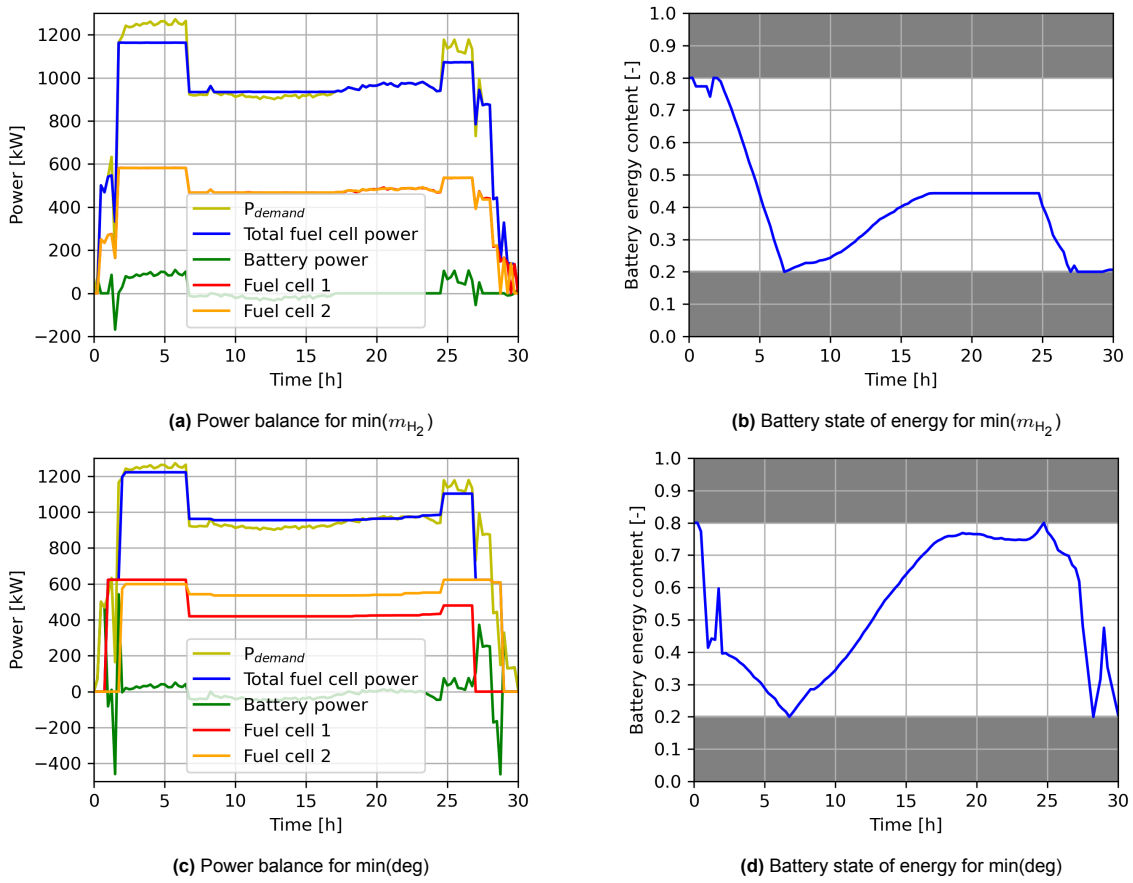

(a) Power balance for min(m_{H_2})

(b) Battery state of energy for min(m_{H_2})

(c) Power balance for min(deg)

(d) Battery state of energy for min(deg)

Figure 7.3: Overview of the results for the single-objective optimisation of the power profile at BoL

Again, the resulting strategy is shown using the power balance and the battery's energy content to support the understanding of the operational strategy. In the broad sense, the different optimisations show similar behaviour as discussed in the previous section. Minimisation of fuel consumption results in the battery being used for peak-shaving, while the fuel cell systems mostly operate at similar output levels. Minimisation of degradation results in less operating time in the low-current region and a fuel cell system is turned off if it is possible.

In the final time steps of the minimisation of fuel consumption, in the bottom-right corner of figure 7.3a, various start-stop cycles can be seen which could easily be prevented. This shows the downside of the optimisation model as it is: when minimising fuel consumption there is very limited reason to take degradation into account.

An overview of some key results is given in table 7.2. Minimisation of degradation leads to 40% less degradation compared to the voltage loss occurring while minimising fuel consumption.

Table 7.2: Key results of the single-objective optimisations for the power-intensive load profile

Objective	Fuel consumption [kg]	Total fuel cell degradation [mV]	Energy spent on battery charging [kWh]
Minimising fuel consumption	1539	214.6	236.1
Minimising degradation	1569	129.2	788

Finally, the degradation per origin is given for both objectives. Even for the power-intensive operational profile, the fuel cell is not operated in the high-current region.

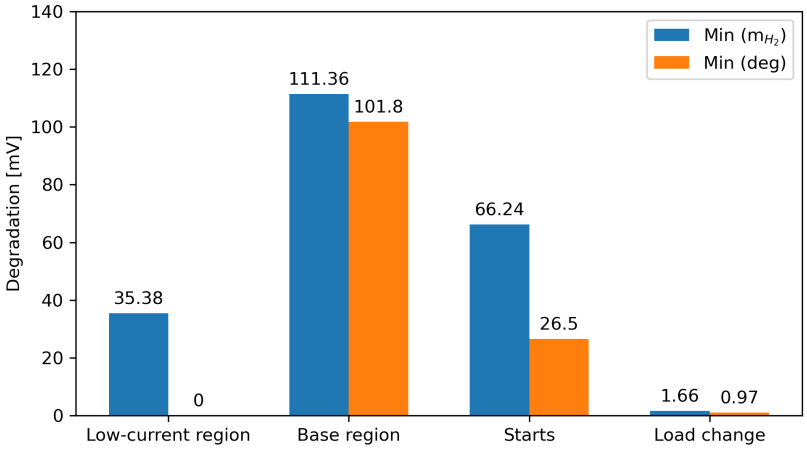

Figure 7.4: Degradation per operating condition during the power profile for both objectives

7.2. Sensitivity analysis using price scenarios

A weighted-sum approach to multi-objective optimisation is carried out using a combination of the two previously used objectives, transforming both the fuel consumption and fuel cell degradation into cost, as described in section 4.2.5.

A sensitivity analysis of the multi-objective optimisation model is carried out on the two previously introduced load profiles. This is done by running the model for various combinations of fuel cell system costs c_{PEM} and hydrogen costs c_{H_2}. Projections for the fuel cell costs, as well as a discussion of the current hydrogen costs, can be found in section 5.3.

The sensitivity analysis is carried out by varying the hydrogen costs (in €/kg) between 1 and 20 with steps of 1, and between 20 and 200 with steps of 10, with an additional test at 0.1 €/kg. This is done for three scenarios of fuel cell costs: the costs at the time of writing of around 2000 €/kW, the mid-term projected costs of 600 €/kW and a long-term goal of 200 €/kW. For each optimisation, the model takes into account the hydrogen and fuel cell costs while trying to find the optimal operational strategy, in terms of costs. This will lead to different considerations between hydrogen consumption, fuel cell degradation and the extent to which the battery is used.

The effect of the varying costs on the resulting performance of the system is analysed using three main performance indicators: the resulting hydrogen consumption, fuel cell degradation and battery usage throughout each optimisation. The sensitivity analysis is performed on both load profiles, for realistic costs of hydrogen and for the extended price range. In each part of the sensitivity analysis, the results from the single-objective optimisations are included for comparison's sake. The results of the

sensitivity analysis using the energy-intensive load profile are given below and are accompanied by an extensive analysis of the resulting changes in the power balance. The results of the extended price range, as well as the results for the power-intensive load profile, can be seen in the appendix. They are given in figures C.1, C.2 and C.3 respectively.

An overview of the results for the realistic hydrogen price range is given in figure 7.5.

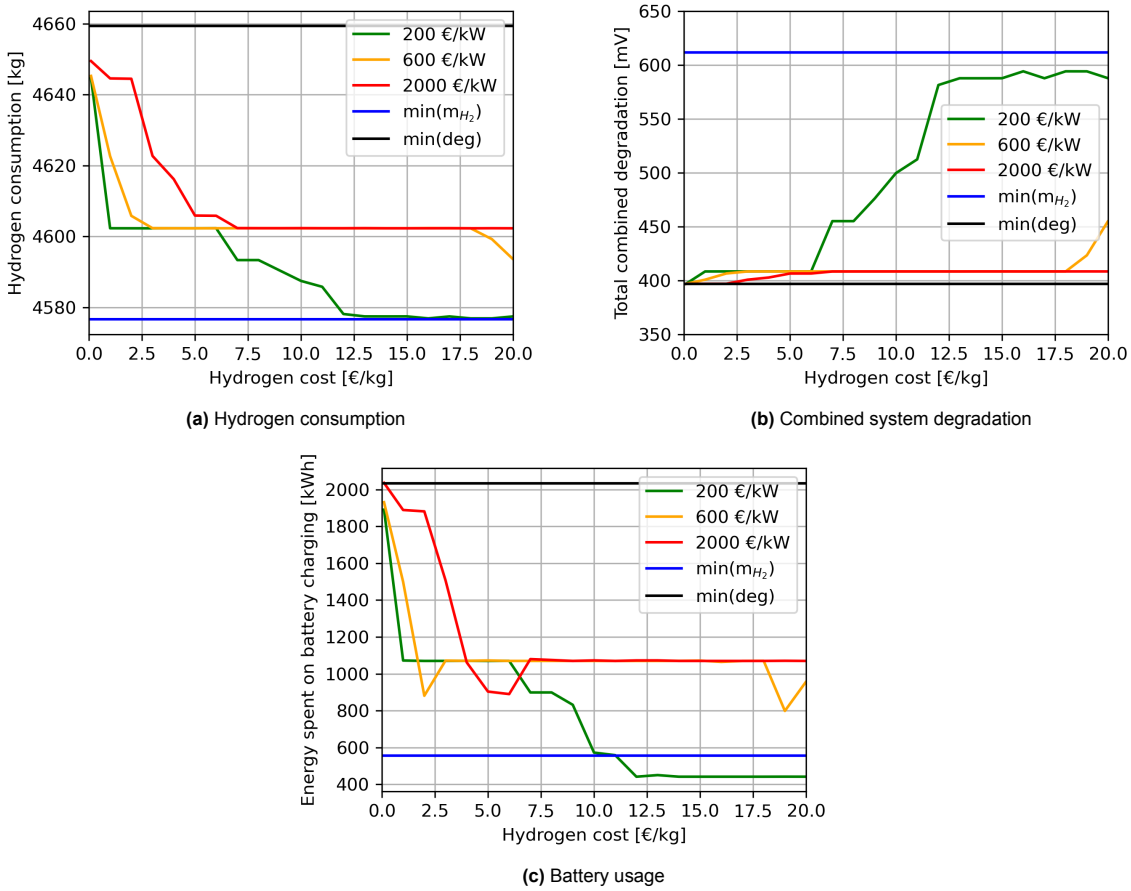

(a) Hydrogen consumption

(b) Combined system degradation

(c) Battery usage

Figure 7.5: Model sensitivity to various PEM system and H_2 costs for the energy-intensive load profile

The resulting hydrogen consumption for the various combinations of hydrogen and fuel cell costs can be seen in figure 7.5a. For each of the results, the fuel consumption is well below the result for the single-objective optimisation of minimising degradation. As can be expected, hydrogen consumption is higher when the fuel cell system costs are higher, and vice versa. The 200 and 600 €/kW scenarios show similar results for the low hydrogen cost region, where a steep decline in hydrogen consumption can be seen and only a slight increase in fuel cell degradation occurs. For the high fuel cell cost scenario, the decline in hydrogen consumption occurs more slowly and the voltage degradation stays near the lower limit for the most part.

At higher hydrogen costs, the current and mid-term fuel cell costs scenarios now lead to the same operational strategy, as seen by the flat lines in all three figures, indicating that it is not worth it to decrease fuel consumption as the resulting increase in degradation is more costly. Conversely, the results for the low fuel cell cost scenario show a deviation from this strategy at 6 €/kg, when the costs associated with hydrogen consumption start to outweigh the costs associated with fuel cell degradation. A large increase in fuel cell degradation can be seen in figure 7.5b while the fuel consumption reaches similar values as the single-objective fuel consumption minimisation run.

The results for the extended price range, seen in the appendix in figure C.1, show that the hydrogen consumption converges to the consumption found in the single object optimisation as the hydrogen cost increases. On the other hand, the inclusion of degradation in the multi-objective optimisation leads to slightly lower degradation than what results from the single-objective optimisation of fuel consumption, even if the hydrogen consumption is very similar to the result for the single-objective optimisation.

Finally, there are some cases for which it may be interesting to compare the operational strategy by looking at the power output of all components in the hybrid energy system. For each of the considered cases, the strategy at the first 60 hours is fairly similar, and the battery is empty at $t = 60$ for all scenarios as well. Most of the difference in strategy is observed after the first sixty hours, so the following plots will start there.

For low fuel cell costs and high hydrogen costs, it can be seen that the battery is used even less when including degradation, compared to the single-objective optimisation of minimising fuel consumption (bottom-right corner of figure 7.5c). The results for the minimisation of fuel consumption can be seen in figure 7.6, for the final 42 hours of operation, and the results for low fuel cell costs are given in figure 7.7.

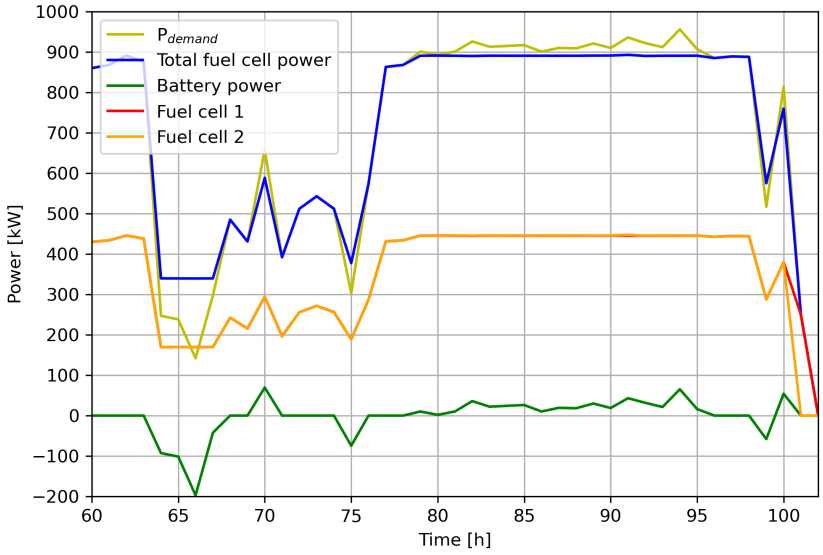

Figure 7.6: Power balance while minimising fuel consumption for $t > 60$h

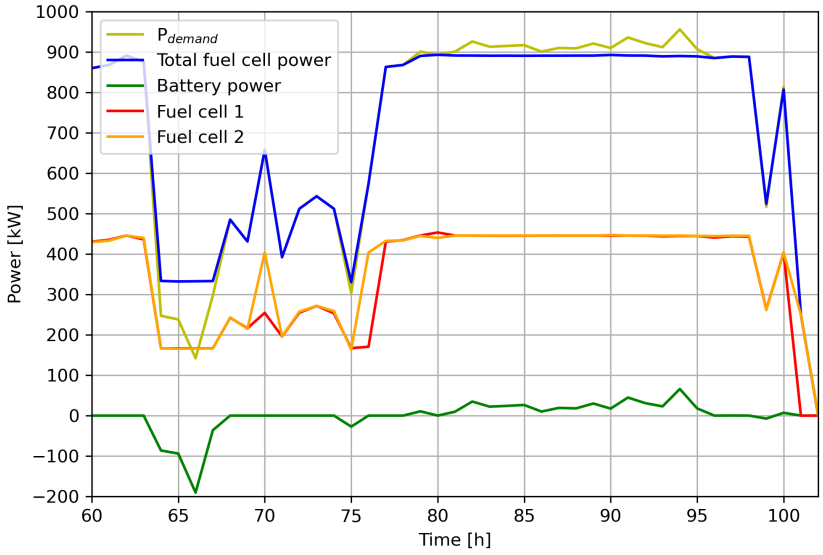

Figure 7.7: Power balance for low FC costs (200 €/kW) and high H_2 costs (15 €/kg), $t > 60$h

In the single-objective optimisation, the battery is used for peak-shaving and is charged when the power demand is low. Additionally, the single-objective optimisation leads to mostly identical fuel cell

power output, even when the demand is low, resulting in degradation in the low-power region. This occurs between $t = 64$ and $t = 76$, as well as $t = 99$ and $t = 100$, as seen in figure 7.6.

In the multi-objective optimisation with low fuel cell costs (200 €/kW) and high hydrogen costs (15 €/kg), seen in figure 7.7, the operational strategy is almost completely similar to the strategy for minimising fuel consumption. The fuel consumption is practically equal as well, yet the degradation is still a bit lower, as can be seen in figure 7.5b. This decrease in degradation is only related to preventing operating in the low-current region, which occurs at $t = 70$ and $t = 76$. At these points, one of both systems are operated just above the cut-off for the low-current region, which relates to a power output of about 400 kW at BoL. Additionally, the two fuel cell systems deliver the total requested power at $t = 100$ and stay inside the low-degradation zone. This leads to reduced use of the battery (the battery is used for peak-shaving at $t = 100$ in figure 7.6) and only a slight increase in fuel consumption.

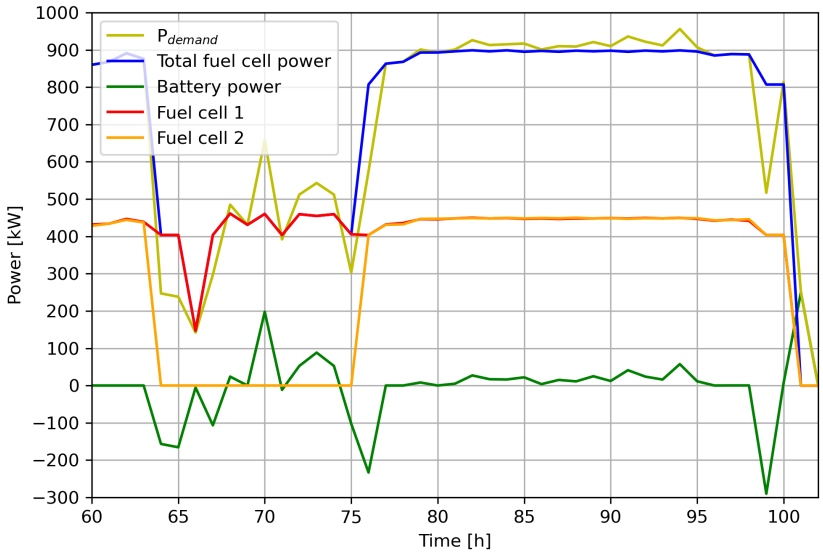

Figure 7.8: Power balance for medium FC costs (600 €/kW) and high H_2 costs (15 €/kg)

A larger difference can be noted when comparing to the results for the mid-term fuel cell cost scenario of 600 €/kW, as seen in figure 7.8.

For this scenario, the degradation remains very low, see figure 7.5b. Until $t = 60$h the power balance is again similar, but a fuel cell system is turned off as soon as it is possible. At this point, the remaining fuel cell operates just above the lower bound of the low-degradation region while charging the battery ($t = 64, 65$). This extra battery power is then used to keep the fuel cell in efficient operating conditions until $t = 75$. When the second fuel cell system starts to operate again, the battery is recharged and is finally used to keep the fuel cells at near-constant power at high efficiencies. Finally, the last point where the degradation is reduced compared to the previous figures is the fact that the fuel cells are both turned off for the final hour of operating, while the battery supplies all the required power at the final hour. This scenario uses the battery more and has a higher hydrogen consumption compared to the low-cost fuel cell/high-cost hydrogen scenario.

7.3. Long-term simulation of the system's performance

A long-term simulation of the operation of the vessel is carried out using the method proposed by Dall'Armi et al. [17]. The long-term operation of the hybrid system is simulated by linearly extrapolating the degradation during the operational profile to a value for degradation during the complete month. The resulting voltage loss is used to update the starting degradation for the next month. This method can be described as a set of sequential optimisations of the load profile. It is performed using the minimisation of costs with a hydrogen price of 8 €/kg and a fuel cell price of 600 €/kW.

The long load profile and power profile are analysed separately. For each of the load profiles, it is assumed that this load profile is representative of the ship's load profile for the entire duration of the fuel

cell's life. The model is run starting with BoL conditions, and the fuel cells' degradation during the first run is linearly extrapolated to a single month of operation. An updated degradation status is used as a starting value for the next month of operation. The effect of degradation on the long-term operation of the system is quantified by looking at KPIs such as the evolution of fuel consumption, degradation and operating costs over time.

The difference in results of the long-term simulation when using the two load profiles is given in section 7.3.1. The change in optimal operation during the system's lifetime is analysed in section 7.3.2 for the energy-intensive load profile, and in section 7.3.3 for the power-intensive load profile. Finally, an overview of the results for both load profiles is given in section 7.3.4, where the results for the weighted-sum approach are compared to results for the two single-objective optimisation strategies.

7.3.1. Comparing load profiles for minimising costs

An overview of the development of the state-of-health for the hybrid system, found separately for both load profiles, is given in figure 7.9. For the energy-intensive (E-intensive) load profile, the fuel cell systems need replacement during the 67th month of operation. The extrapolation of degradation during the 102 hour load profile to the monthly degradation leads to a negative starting SoH for month 68, and the following optimisation does not lead to any solution. Similarly, the fuel cell systems need to be replaced during the 54th month of operation for the power-intensive load profile, a lifetime decrease of almost 20% compared to the energy-intensive load profile.

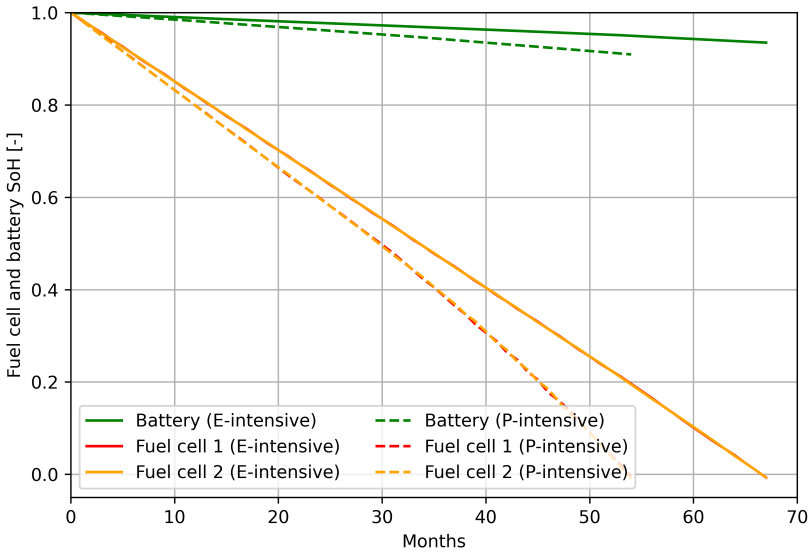

Figure 7.9: Lifetime estimation for both load profiles while minimising total costs

As expected, the power profile leads to faster degradation and increased battery usage compared to the longer load profile. Additionally, the curve describing the fuel cell's SoH is not linear in time for the power profile: the fuel cell system degrades faster near the end of its lifetime. The cause of this phenomenon is explained in more detail in section 7.3.3.

The evolution of the daily operating costs for both load profiles is given in figure 7.10, as well as how the costs are built up. The power profile leads to higher costs, mainly due to higher daily fuel consumption. However, even though the power profile leads to a similar daily degradation as the long load profile at the beginning of life, the fuel cell systems start to degrade faster for the power profile, leading to a fast increase in fuel costs during its shorter lifetime.

The energy-intensive load profile has a daily hydrogen consumption of 1083 kg per day at BoL and 1294 kg per day during its final month of operation, an increase of almost 20%. The consumption increases from 1235 kg per day to 1498 kg per day during its final month for the power-intensive profile, an increase of 21%.

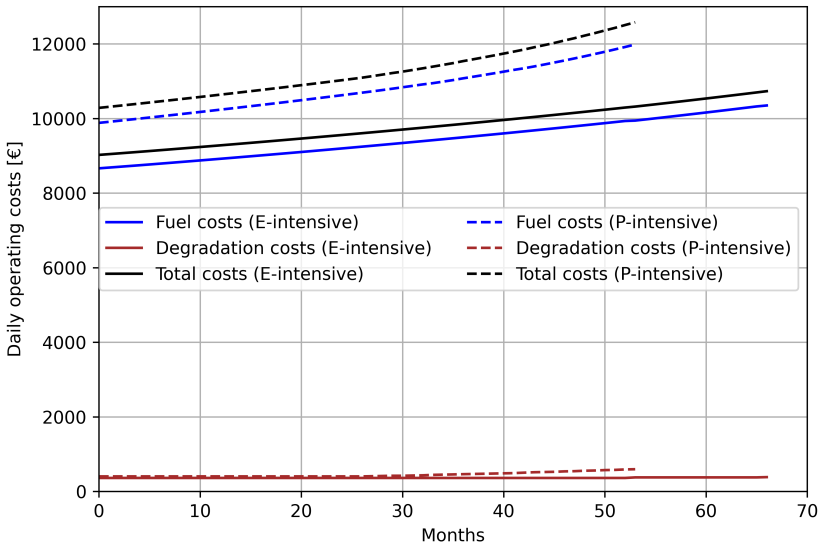

Figure 7.10: Daily costs for both load profiles until fuel cells' EoL

7.3.2. Optimal operation during lifetime for the energy-intensive profile

The degradation of the fuel cells leads to an increasing daily fuel consumption during the system's lifetime, as seen in figure 7.10. As the system gets older, a higher operating current is required for the same power output. The power output of both fuel cell systems, as well as the average current of the systems, are given for BoL, halfway and near EoL conditions. This can be seen in figure 7.11.

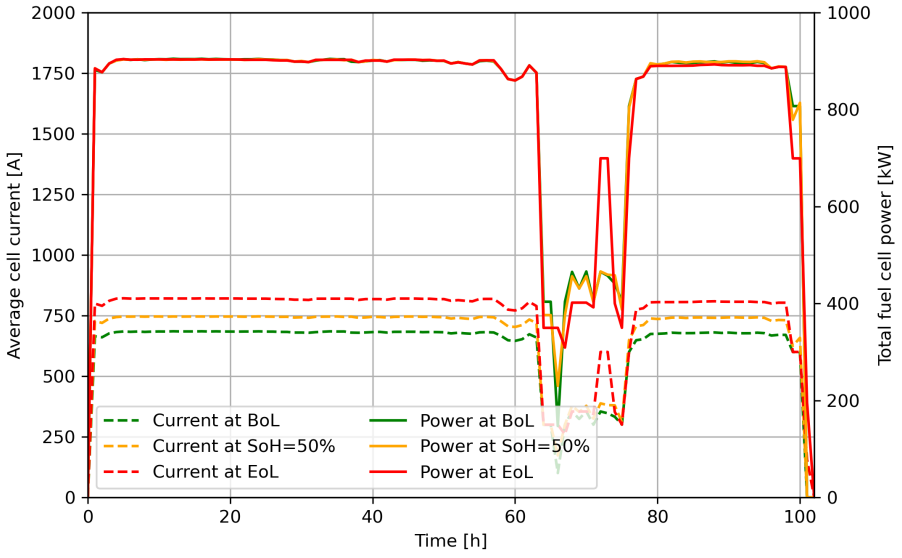

Figure 7.11: Evolution of average fuel cell current and total fuel cell power over time for the E-intensive load profile

The operational strategy remains very similar during the system's lifetime, except for the large peak at the EoL conditions during the hours $t = 72$ and $t = 73$. Investigation of individual power outputs of the fuel cell systems shows that similar to the power balance in figure 7.8, one of the two fuel cell systems is turned off for a long period between $t = 64$ and $t = 75$. As the fuel cell system ages, the upper bound of the low-current region ($600\,\text{A}$) is related to an increasingly lower fuel cell power. The observable power peak starts to occur when both systems have a total voltage loss of around $75\,\text{V}$. At this point, the boundary of the low-current region has changed from just above $400\,\text{kW}$ to $360\,\text{kW}$. The

second fuel cell is turned on during these two hours to fill up the battery, after which it is turned off again. Besides this, the pattern for delivered power remains mostly the same, with a steady increase in current and fuel consumption.

7.3.3. Optimal operation during lifetime for power-intensive load profile

The long-term consecutive optimisation using the power profile leads to a system lifetime of 54 months, experiencing higher degradation compared to the long profile. An overview of the average fuel cell current and total fuel cell power is given in figure 7.12 for the first month, the 30th month and the final month of operating.

Similar to the long load profile, an increase in fuel consumption can be noted during the system's lifetime, as seen in figure 7.10. In contrast to the results for the energy-intensive load profile, the increase in fuel consumption is not linear for the power-intensive load profile, caused by the high power demand. The increased voltage loss of the fuel cells leads to unavoidable hours spent operating in the high-current region for this load profile, starting from the 27th month. The systems experience a combined voltage loss per trip of $134\,\mathrm{mV}$ until the 27th month, whereas this increases to $200\,\mathrm{mV}$ for the final months. The combined degradation per operating condition can be seen in figure 7.13, which shows that the increase in degradation over time is practically only due to the increased amount of time spent in the high-current region.

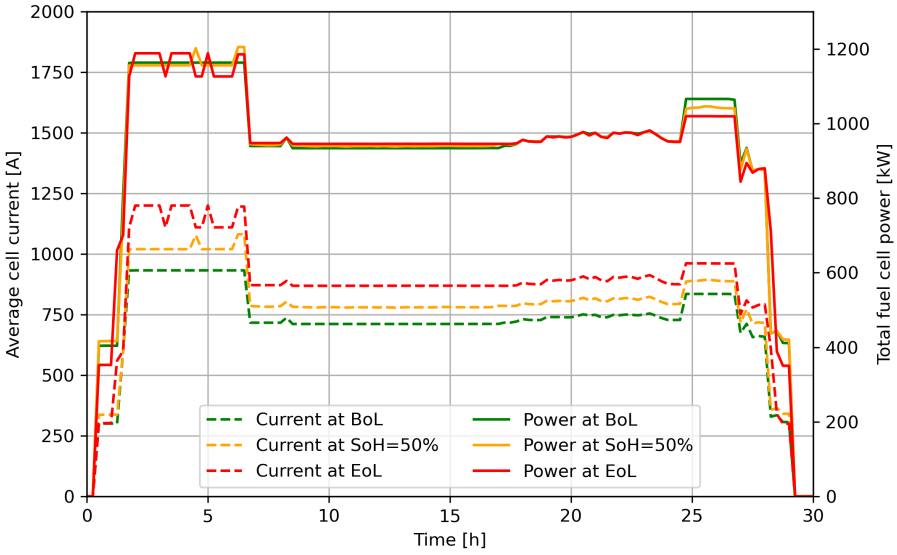

Figure 7.12: Evolution of average fuel cell current and total power over time for the P-intensive profile

7.3.4. Comparing results for all objective functions

Table 7.3 provides an overview of all results of the long-term simulations, quantifying the influence of the various objective functions. The results for the minimisation of fuel consumption only (min(m_{H_2})) and degradation only (min(deg)) are included in the table for both load profiles. Additionally, the results for the minimisation of total costs are given in the table. A fuel cell price of 600 €/kW and hydrogen costs of 8 €/kg are used.

When comparing the effect of minimising total costs to only minimising fuel consumption, a large (50 and 43%) increase in fuel cell lifetime can be observed as a result of a significant (33 and 31%) reduction in degradation (for the respective operating profiles). This is achieved with a limited (< 0.5%) increase in hydrogen consumption, but it does lead to a significant (~160%) decrease in final battery SoH for both load profiles. Even though the fuel consumption is higher when minimising total costs, the large decrease in fuel cell degradation leads to lower operating costs. The fuel cell's lifetime and the average operating costs are both positively influenced by including the costs related to fuel cell degradation in the objective function.

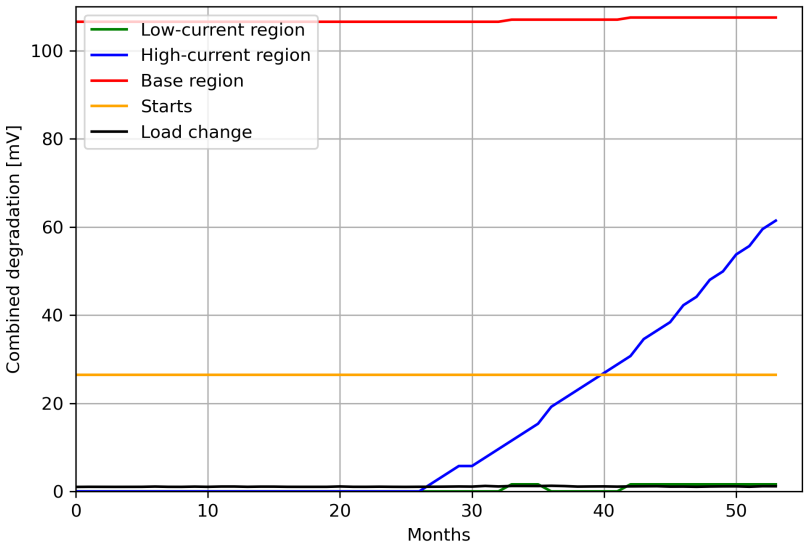

Figure 7.13: Combined degradation effects per operating condition during the lifetime of the system

The comparison between only minimising fuel cell degradation and minimising total costs shows that there is not much left to gain in terms of fuel cell degradation. Minimising only fuel cell degradation leads to a limited increase (2 months) in fuel cell lifetime, compared to minimising total costs. The battery is used substantially more when only minimising degradation, with an 84% and 59% increase in battery degradation for the respective load profiles. An increase in fuel consumption of around ~1.6% can be observed when only minimising degradation. This is partly related to the increase in battery usage and partly related to less efficient fuel cell usage. Besides fuel cell degradation, there is no reason to use the fuel cells in an efficient operating point. Minimisation of degradation leads to similar average operating costs as the minimisation of fuel consumption.

To conclude, the fuel cell lifetime can be significantly increased by including degradation in the minimisation of total operating costs, and the resulting operating strategy performs well in both objectives.

Table 7.3: Results of long-term simulation using various objectives and load profiles

	Energy-intensive operating profile			**Power-intensive operating profile**		
	min(m_{H_2})	min(deg)	min(costs)	min(m_{H_2})	min(deg)	min(costs)
Fuel cell lifetime (months)	44	68	66	37	55	53
Battery SoH in final month (%)	97.6	88.2	93.6	96.3	85.5	90.9
Average hydrogen consumption (kg/day)	1175	1201	1181	1344	1368	1348
Average fuel cell degradation (mV/day)	72.4	46.9	48.5	86.0	58.0	59.7
Average operating costs (€/day)	9941	9957	9811	11397	11376	11229

8

Discussion

The goal of this thesis was to investigate the effect of incorporating fuel cell degradation in an energy management system for a fuel cell/battery hybrid ship. This was achieved by using quadratic programming to model the fuel cell's performance based on its polarisation curve. The fuel cell's degradation is incorporated in the model as a downward shift of the polarisation curve.

For the case study applied in this thesis, the results for the single-objective optimisations show that fuel cell degradation can be limited by approximately 35% when minimising degradation, compared to minimising fuel consumption. The decrease in degradation is of similar size for both load profiles which were assessed. The weighted-sum approach, which is used to incorporate fuel consumption and fuel cell degradation in the objective function, leads to values for fuel consumption and degradation close to the results of their respective single-objective optimisations. The sensitivity analysis shows that decreasing fuel cell degradation at the cost of slightly increased fuel consumption is a cost-efficient choice, for a large range of hydrogen and fuel cell costs. Besides that, the minimisation of total costs results in decreased fuel cell degradation for all hydrogen costs. Finally, the long-term simulation of the vessel's performance shows that the lifetime can be extended by approximately 50% with the weighted-sum approach. The average degradation can be reduced by up to 33%, compared to the average degradation when only minimising fuel consumption. The average daily operating costs are reduced compared to either single-objective optimisation.

The reduction in degradation identified in this case study appears to fall somewhere between the results reported in various reviewed literature. It can be observed that the decrease in degradation found for this case study is somewhat in the middle of some of the reviewed literature. Dall'Armi et al. [17] and Fletcher et al. [36] both compare their results for minimising total costs (including fuel cell degradation) to their results for minimising fuel consumption only. The research by Dall'Armi et al. [17] shows a lifetime increase of 185%, related to a reduction of fuel cell degradation by 65%. The large degradation reduction is likely related to the highly fluctuating power demand. The fuel cell power heavily fluctuates when only minimising fuel consumption, resulting in large gains when minimising degradation. Conversely, the results of Fletcher et al. [36] show a decrease in degradation of only 15% for the operation of a hybrid car. The drive cycle was 37 minutes and the degradation due to the single start-stop cycle represented most of the degradation (75% and 89% in both optimisation methods). Degradation due to load changes has been reduced by 97% while the degradation due to low-current operation is reduced by 21%, but these operating conditions do not represent much of the total degradation. Their assessed load cycle does not allow a lot of improvement with regard to degradation.

Besides the relative reduction in degradation due to the new operating strategies, the resulting estimated lifetime of the hybrid systems is interesting as well. Dall'Armi et al. [17] extended the system lifetime to 22 months by including degradation, if the battery is replaced on time. This is significantly less than the estimated lifetime presented in this thesis. This may be partly explained by the large difference in load profile, but may also be caused by a different implementation of fuel cell degradation. While the degradation due to load transients and start cycles are modelled in a similar way, fuel cell degradation due to the operating regions is defined differently by Dall'Armi et al. [17]. They use a linear relation between fuel cell degradation and operating current. The related coefficients are not given, which makes the analysis of the fuel cell degradation quite hard. The lifetime estimation in the

research by Fletcher et al. [36] amounts to only 702 hours, approximately one month of continuous operation. With an average drive cycle of only 37 minutes and a higher voltage loss due to start-stop cycles ($24\,\mu V$), the start-stop cycles alone result in a voltage loss of almost $40\,\mu V$ per hour per cell. This is in sharp contrast to the fuel cell degradation experienced in this thesis. Operating in the base region results in a voltage loss of only $2\,\mu V$ per hour per cell. Combined with extended operation at constant loads, this provides an opportunity to run the fuel cell in very favourable operating conditions. The degradation rates used in this thesis, combined with the long time steps and relatively constant power output, may explain the large discrepancy in the lifetime estimates.

The results in this thesis give insight into the expected fuel cell lifetime for applications at long, constant loads, but the lifetime may be sensitive to the model's input. It is unclear if the degradation rates used in this thesis can be considered representative of a fuel cell operating onboard a ship. The applied degradation rates can easily be adjusted if more accurate fuel cell degradation rates are available, and may have a large influence on the estimated lifetime. Besides the (perhaps too) favourable definition of fuel cell degradation used in this thesis, there are some additional limitations of the developed model. For example, the value for the battery efficiency used in this thesis is based on a rough estimation using relevant literature. A difference in operating strategy is expected when less favourable battery efficiencies are applied in the minimisation of total operating costs. Decreasing fuel cell degradation requires more battery usage, leading to more fuel consumption. If the battery efficiency is lower, the increase in fuel consumption is larger, so the model may be quite sensitive to the battery efficiency. Finally, the application of mixed-integer quadratically constrained programming allows us to accurately model the fuel cell's performance using an important characteristic of the fuel cell but the approach strongly limits the number of time steps that can be simulated. Applying the load profiles and time step sizes used by Dall'Armi et al. and Fletcher et al. would likely be impossible without simplifying the model in some way.

Opportunities for further research include new thorough research in condition-dependent degradation rates, to increase the robustness of the input data. The fuel cell bus studies by Pei et al. [51] and Chen et al. [53] are often used to incorporate fuel cell degradation in energy management strategies, but this highlights the dependence on one main set of results. Besides that, the operating conditions of the fuel cell inside the bus are undoubtedly different than those in a ship. Furthermore, the operating regions defined to model fuel cell degradation can be refined by reviewing the literature and using commonly applied definitions of idling and high-current operation to determine the operating regions. Additionally, while the degradation in the operating region is now visualised as a step function (figure 4.1), a more gradual relation between degradation and operating current may be more realistic. This could be implemented by applying piecewise linear constraints for the fuel cell degradation. The effects of fuel cell degradation are now incorporated as a vertical shift of the polarisation curve, but the slope of the polarisation curve may also be affected by fuel cell degradation, as suggested by the findings in [89]. In other words, not only is the open-circuit voltage affected by increased activation losses, but the fuel cell's resistance also increases as the fuel cell degrades. These are some starting points for future research that would strengthen the developed model and expand on the idea of modelling the fuel cell's performance using the interplay between its polarisation curve and its degradation.

9

Conclusion

The goal of this thesis was to investigate the impact of incorporating fuel cell degradation in an energy management system while minimising total costs. Applications of linear programming as an energy management system were found in the literature, but these required a linearisation of the fuel cell model. The application of quadratic programming to model the fuel cell and its degradation was identified as a literature gap.

The model developed in this thesis consists of a fuel cell model using a linear current-voltage relation and resulting quadratic current-power relation. Five operating conditions of the fuel cell are linked to fuel cell degradation using the literature. The fuel cell's $I-V$ curve is continuously influenced by the voltage loss incurred due to its various operating conditions. A simple battery model was used to complete the model of the hybrid system. The model was used to simulate the performance of an ocean-going vessel. Two distinct operational profiles of the vessel were determined and used to determine the performance of a theoretical retrofit of the vessel. Two separate objective functions were defined: the minimisation of fuel consumption and the minimisation of fuel cell degradation. These objectives were also combined in a weighted-sum approach using the costs of hydrogen and the fuel cell system.

The results for minimising degradation show an average decrease in fuel cell degradation of about 37%, compared to the voltage loss when only minimising fuel consumption. These results were found for beginning-of-life conditions, and are an average for both operational profiles.

The sensitivity analysis showed that a small increase in fuel consumption (0.5%) to significantly reduce (35%) fuel cell degradation is cost-optimal for current (2000 €/kW) and mid-term (600 €/kW) fuel cell cost scenarios.

A long-term simulation of the vessel's performance was executed using sequential optimisation of the load profile at the start of each month. The voltage loss resulting from the load profile was extrapolated to one month of operation and added to the starting degradation of the following month. The results show that the fuel cell system's lifetime can be extended by up to 50% by incorporating fuel cell degradation in the objective function. The fuel cell's lifetime estimates are 53 months for the power-intensive profile and 66 months for the energy-intensive profile, indicating the influence of the power demand. The ageing of the fuel cell systems occurs linearly for the energy-intensive but non-linearly for the power-intensive load profile. The difference is mainly caused by the increase in time spent in the high-current region as the system ages, due to the high power demand of the load profile.

Finally, the fuel consumption increases from 1083 kg per day to 1294 kg per day for the energy-intensive load profile, and from 1235 kg per day to 1498 kg per day for the power-intensive load profile. The degradation is relatively constant over time for the energy-intensive profile but increases for the power-intensive profile. The total costs, consisting of both fuel consumption and degradation, mainly increase due to the increase in fuel consumption.

To conclude, this thesis provides a possibility to model the operational characteristics of a fuel cell/battery hybrid vessel, while taking into account degradation. The model can be applied to a different use case by changing the model input and can be refined to include new insights on fuel cell degradation. With the increasingly stringent emission regulations, this thesis is highly relevant. It provides a clear and intuitive method of fuel cell modelling for its readers, providing a small step towards more fuel cell-friendly operating of hybrid systems.

References

[1] International Maritime Organization, *Resolution MEPC.304(72): Initial IMO Strategy on Reduction of GHG Emissions from Ships*, 2018.

[2] E. A. Bouman, H. Lindstad, A. Rialland, and A. H. Strømman, "State-of-the-art technologies, measures, and potential for reducing GHG emissions from shipping – A review," *Transportation Research Part D-transport and Environment*, vol. 52, pp. 408–421, May 2017. DOI: 10.1016/j.trd.2017.03.022.

[3] International Maritime Organization, *Resolution MEPC.377(80) - 2023 IMO Strategy on Reduction of GHG Emissions from Ships*, 2023.

[4] European Parliament. "Fit for 55: deal on new EU rules for cleaner maritime fuels." (Mar. 23, 2023), [Online]. Available: https://www.europarl.europa.eu/news/en/press-room/20230320IPR77909/fit-for-55-deal-on-new-eu-rules-for-cleaner-maritime-fuels.

[5] European Commission. "Proposal for a REGULATION OF THE EUROPEAN PARLIAMENT AND OF THE COUNCIL on the use of renewable and low-carbon fuels in maritime transport and amending Directive 2009/16/EC." (Jul. 14, 2021), [Online]. Available: https://eur-lex.europa.eu/legal-content/EN/TXT/?uri=COM:2021:562:FIN.

[6] European Commission. "ANNEXES to the Proposal for a REGULATION OF THE EUROPEAN PARLIAMENT AND OF THE COUNCIL on the use of renewable and low-carbon fuels in maritime transport and amending Directive 2009/16/EC." (Jul. 14, 2021), [Online]. Available: https://eur-lex.europa.eu/legal-content/EN/TXT/?uri=COM:2021:562:FIN.

[7] L. van Biert and K. Visser, "Fuel cells systems for sustainable ships," in *Sustainable Energy Systems on Ships*, 1st ed., Elsevier, 2022, pp. 81–121.

[8] J. Wang, "Barriers of scaling-up fuel cells: Cost, durability and reliability," *Energy*, vol. 80, pp. 509–521, Feb. 2015. DOI: 10.1016/j.energy.2014.12.007.

[9] F. A. de Bruijn, V. A. T. Dam, and G. J. M. Janssen, "Review: Durability and Degradation Issues of PEM Fuel Cell Components," *Fuel Cells*, vol. 8, no. 1, pp. 3–22, Feb. 2008. DOI: 10.1002/fuce.200700053.

[10] P. Ren, P. Pei, Y. Li, W. Ziyao, C. Dongfang, and S. Huang, "Degradation mechanisms of proton exchange membrane fuel cell under typical automotive operating conditions," *Progress in Energy and Combustion Science*, vol. 80, no. 100859, Sep. 2020. DOI: 10.1016/j.pecs.2020.100859.

[11] M. A. Smit, "Towards 40 000 hours of operation for Nedstack's FCS XXL PEM fuel cell stacks," *Fuel Cells Bulletin*, vol. 2014, no. 8, pp. 12–15, Aug. 2014. DOI: 10.1016/s1464-2859(14)70238-x.

[12] L. Eudy and M. B. Post, "Fuel cell buses in us transit fleets: Current status 2017," National Renewable Energy Lab.(NREL), Golden, CO (United States), Tech. Rep., 2017.

[13] D. Pivetta, C. Dall'Armi, and R. Taccani, "Multi-objective optimization of hybrid PEMFC/Li-ion battery propulsion systems for small and medium size ferries," *International Journal of Hydrogen Energy*, vol. 46, no. 72, pp. 35 949–35 960, Oct. 2021. DOI: 10.1016/j.ijhydene.2021.02.124.

[14] R. Geertsma, R. R. Negenborn, K. Visser, and H. Hopman, "Design and control of hybrid power and propulsion systems for smart ships: A review of developments," *Applied Energy*, vol. 194, pp. 30–54, May 2017. DOI: 10.1016/j.apenergy.2017.02.060.

[15] L. van Biert, M. Godjevac, K. Visser, and P. Aravind, "A review of fuel cell systems for maritime applications," *Journal of Power Sources*, vol. 327, pp. 345–364, Sep. 2016. DOI: 10.1016/j.jpowsour.2016.07.007.

[16] H. S. Chen, Z. Zhang, C. Guan, and H. Gao, “Optimization of sizing and frequency control in battery/supercapacitor hybrid energy storage system for fuel cell ship,” *Energy*, vol. 197, no. 117285, Apr. 2020. DOI: 10.1016/j.energy.2020.117285.

[17] C. Dall’Armi, D. Pivetta, and R. Taccani, “Health-Conscious optimization of Long-Term operation for hybrid PEMFC ship propulsion systems,” *Energies*, vol. 14, no. 13, p. 3813, Jun. 2021. DOI: 10.3390/en14133813.

[18] R. O’Hayre, S. Cha, W. Colella, and F. B. Prinz, *Fuel Cell Fundamentals*, 3rd ed. John Wiley & Sons, 2016.

[19] F. Mylonopoulos, H. Polinder, and A. Coraddu, “A Comprehensive Review of Modeling and Optimization Methods for Ship Energy Systems,” *IEEE Access*, vol. 11, pp. 32 697–32 707, 2023. DOI: 10.1109/ACCESS.2023.3263719.

[20] N. Yousfi-Steiner, P. Moçotéguy, D. Candusso, D. Hissel, A. C. Hernandez, and A. Aslanides, “A review on PEM voltage degradation associated with water management: Impacts, influent factors and characterization,” *Journal of Power Sources*, vol. 183, no. 1, pp. 260–274, Aug. 2008. DOI: 10.1016/j.jpowsour.2008.04.037.

[21] U. Chakraborty, “Fuel crossover and internal current in proton exchange membrane fuel cell modeling,” *Applied Energy*, vol. 163, pp. 60–62, Feb. 2016. DOI: 10.1016/j.apenergy.2015.11.012.

[22] K. M. Bagherabadi, S. Skjong, J. Bruinsma, and E. Pedersen, “System-level modeling of marine power plant with PEMFC system and battery,” *International Journal of Naval Architecture and Ocean Engineering*, vol. 14, p. 100 487, Jan. 2022. DOI: 10.1016/j.ijnaoe.2022.100487.

[23] S. N. M, O. Tremblay, and L. Dessaint, “A generic fuel cell model for the simulation of fuel cell vehicles,” in *2009 IEEE Vehicle Power and Propulsion Conference*, IEEE, 2009, pp. 1722–1729. DOI: 10.1109/VPPC.2009.5289692.

[24] L. Balestra and I. Schjølberg, “Modelling and simulation of a zero-emission hybrid power plant for a domestic ferry,” *International Journal of Hydrogen Energy*, vol. 46, no. 18, pp. 10 924–10 938, Mar. 2021. DOI: 10.1016/j.ijhydene.2020.12.187.

[25] A. M. Bassam, A. W. Phillips, S. R. Turnock, and P. Wilson, “Development of a multi-scheme energy management strategy for a hybrid fuel cell driven passenger ship,” *International Journal of Hydrogen Energy*, vol. 42, no. 1, pp. 623–635, Jan. 2017. DOI: 10.1016/j.ijhydene.2016.08.209.

[26] J. Han, J. F. Charpentier, and T. Tang, “An Energy Management System of a Fuel Cell/Battery Hybrid Boat,” *Energies*, vol. 7, no. 5, pp. 2799–2820, Apr. 2014. DOI: 10.3390/en7052799.

[27] K. Priya, K. Sathishkumar, and N. Rajasekar, “A comprehensive review on parameter estimation techniques for Proton Exchange Membrane fuel cell modelling,” *Renewable & Sustainable Energy Reviews*, vol. 93, pp. 121–144, Oct. 2018. DOI: 10.1016/j.rser.2018.05.017.

[28] D. D. Boettner, G. Paganelli, Y. Guezennec, G. Rizzoni, and M. Moran, “Proton Exchange Membrane Fuel Cell System Model for Automotive Vehicle Simulation and Control,” *Journal of Energy Resources Technology-transactions of The Asme*, vol. 124, no. 1, pp. 20–27, Mar. 2002. DOI: 10.1115/1.1447927.

[29] G. Zhang and S. G. Kandlikar, “A critical review of cooling techniques in proton exchange membrane fuel cell stacks,” *International Journal of Hydrogen Energy*, vol. 37, no. 3, pp. 2412–2429, Feb. 2012. DOI: 10.1016/j.ijhydene.2011.11.010.

[30] H. R. Schmidt, P. Buchner, A. Datz, K. Dennerlein, S. Lang, and M. F. Waidhas, “Low-cost air-cooled PEFC stacks,” *Journal of Power Sources*, vol. 105, no. 2, pp. 243–249, Mar. 2002. DOI: 10.1016/s0378-7753(01)00947-8.

[31] Y. Sohn *et al.*, “Operating characteristics of an air-cooling PEMFC for portable applications,” *Journal of Power Sources*, vol. 145, no. 2, pp. 604–609, Aug. 2005. DOI: 10.1016/j.jpowsour.2005.02.062.

[32] P. Rodatz, G. Paganelli, A. Sciarretta, and L. Guzzella, “Optimal power management of an experimental fuel cell/supercapacitor-powered hybrid vehicle,” *Control Engineering Practice*, vol. 13, no. 1, pp. 41–53, Jan. 2005. DOI: 10.1016/j.conengprac.2003.12.016.

[33] J. Bernard, S. Delprat, T. M. Guerra, and F. N. Büchi, “Fuel efficient power management strategy for fuel cell hybrid powertrains,” *Control Engineering Practice*, vol. 18, no. 4, pp. 408–417, Apr. 2010. DOI: 10.1016/j.conengprac.2009.12.009.

[34] P. Wu and R. Bucknall, “Hybrid fuel cell and battery propulsion system modelling and multi-objective optimisation for a coastal ferry,” *International Journal of Hydrogen Energy*, vol. 45, no. 4, pp. 3193–3208, Jan. 2020. DOI: 10.1016/j.ijhydene.2019.11.152.

[35] Q. Li, W. Chen, Z. Liu, M. Li, and L. Ma, “Development of energy management system based on a power sharing strategy for a fuel cell-battery-supercapacitor hybrid tramway,” *Journal of Power Sources*, vol. 279, pp. 267–280, Apr. 2015. DOI: 10.1016/j.jpowsour.2014.12.042.

[36] T. H. Fletcher, R. H. Thring, and M. Watkinson, “An Energy Management Strategy to concurrently optimise fuel consumption & PEM fuel cell lifetime in a hybrid vehicle,” *International Journal of Hydrogen Energy*, vol. 41, no. 46, pp. 21 503–21 515, Dec. 2016. DOI: 10.1016/j.ijhydene.2016.08.157.

[37] C. Li and S. Liu, “Optimal fuzzy power control and management of fuel cell/battery hybrid vehicles,” *Journal of Power Sources*, vol. 192, no. 2, pp. 525–533, Jul. 2009. DOI: 10.1016/j.jpowsour.2009.03.007.

[38] L. Xu, J. Li, M. Ouyang, J. Hua, and Y. Geng, “Multi-mode control strategy for fuel cell electric vehicles regarding fuel economy and durability,” *International Journal of Hydrogen Energy*, vol. 39, no. 5, pp. 2374–2389, Feb. 2014. DOI: 10.1016/j.ijhydene.2013.11.133.

[39] K. S. Simmons, Y. Guezennec, and S. Onori, “Modeling and energy management control design for a fuel cell hybrid passenger bus,” *Journal of Power Sources*, vol. 246, pp. 736–746, Jan. 2014. DOI: 10.1016/j.jpowsour.2013.08.019.

[40] C. Zheng, N. Kim, and S. Cha, “Optimal control in the power management of fuel cell hybrid vehicles,” *International Journal of Hydrogen Energy*, vol. 37, no. 1, pp. 655–663, Jan. 2012. DOI: 10.1016/j.ijhydene.2011.09.091.

[41] J. P. Torreglosa, P. L. García, L. M. S. Fernández, and F. Jurado, “Hierarchical energy management system for stand-alone hybrid system based on generation costs and cascade control,” *Energy Conversion and Management*, vol. 77, pp. 514–526, Jan. 2014. DOI: 10.1016/j.enconman.2013.10.031.

[42] P. García-Triviño, F. Llorens-Iborra, C. A. García-Vázquez, A. J. G. Mena, L. M. Fernández-Ramírez, and F. Jurado, “Long-term optimization based on PSO of a grid-connected renewable energy/battery/hydrogen hybrid system,” *International Journal of Hydrogen Energy*, vol. 39, no. 21, pp. 10 805–10 816, Jul. 2014. DOI: 10.1016/j.ijhydene.2014.05.064.

[43] Y. Wang, S. J. Moura, S. G. Advani, and A. K. Prasad, “Power management system for a fuel cell/battery hybrid vehicle incorporating fuel cell and battery degradation,” *International Journal of Hydrogen Energy*, vol. 44, no. 16, pp. 8479–8492, Mar. 2019. DOI: 10.1016/j.ijhydene.2019.02.003.

[44] U. R. Nair and R. Costa-Castelló, “A model predictive Control-Based Energy Management Scheme for hybrid storage system in islanded microgrids,” *IEEE Access*, vol. 8, pp. 97 809–97 822, May 2020. DOI: 10.1109/access.2020.2996434.

[45] S. Sharma, Y. Xu, A. Verma, and B. K. Panigrahi, “Time-Coordinated multienergy management of smart buildings under uncertainties,” *IEEE Transactions on Industrial Informatics*, vol. 15, no. 8, pp. 4788–4798, Aug. 2019. DOI: 10.1109/tii.2019.2901120.

[46] S. Fang, Y. Xu, Z. Li, T. Zhao, and H. Wang, “Two-Step Multi-Objective management of hybrid energy storage system in All-Electric ship microgrids,” *IEEE Transactions on Vehicular Technology*, vol. 68, no. 4, pp. 3361–3373, Apr. 2019. DOI: 10.1109/tvt.2019.2898461.

[47] Y. Luo, S. Fang, I. Khan, T. Niu, and R. Liao, “Hierarchical robust shipboard hybrid energy storage sizing with three-layer power allocation,” *IET electrical systems in transportation*, vol. 13, no. 2, Apr. 2023. DOI: 10.1049/els2.12077.

[48] Á. Serna, I. Yahyaoui, J. E. Normey-Rico, C. De Prada, and F. Tadeo, "Predictive control for hydrogen production by electrolysis in an offshore platform using renewable energies," *International Journal of Hydrogen Energy*, vol. 42, no. 17, pp. 12 865–12 876, Apr. 2017. DOI: 10.1016/j.ijhydene.2016.11.077.

[49] J. Wu *et al.*, "A review of PEM fuel cell durability: Degradation mechanisms and mitigation strategies," *Journal of Power Sources*, vol. 184, no. 1, pp. 104–119, Sep. 2008. DOI: 10.1016/j.jpowsour.2008.06.006.

[50] S. J. C. Cleghorn *et al.*, "A polymer electrolyte fuel cell life test: 3 years of continuous operation," *Journal of Power Sources*, vol. 158, no. 1, pp. 446–454, Jul. 2006. DOI: 10.1016/j.jpowsour.2005.09.062.

[51] P. Pei, Q. Chang, and T. Tang, "A quick evaluating method for automotive fuel cell lifetime," *International Journal of Hydrogen Energy*, vol. 33, no. 14, pp. 3829–3836, Jul. 2008. DOI: 10.1016/j.ijhydene.2008.04.048.

[52] M. Marrony, R. Barrera, S. Quenet, S. Ginocchio, L. Montelatici, and A. Aslanides, "Durability study and lifetime prediction of baseline proton exchange membrane fuel cell under severe operating conditions," *Journal of Power Sources*, vol. 182, no. 2, pp. 469–475, Aug. 2008. DOI: 10.1016/j.jpowsour.2008.02.096.

[53] H. Chen, P. Pei, and M. Song, "Lifetime prediction and the economic lifetime of Proton Exchange Membrane fuel cells," *Applied Energy*, vol. 142, pp. 154–163, Mar. 2015. DOI: 10.1016/j.apenergy.2014.12.062.

[54] Y. Shao, G. Yin, and Y. Gao, "Understanding and approaches for the durability issues of Pt-based catalysts for PEM fuel cell," *Journal of Power Sources*, vol. 171, no. 2, pp. 558–566, Sep. 2007. DOI: 10.1016/j.jpowsour.2007.07.004.

[55] S. Zhang, X. Yuan, J. N. C. Hin, H. Wang, K. A. Friedrich, and M. Schulze, "A review of platinum-based catalyst layer degradation in proton exchange membrane fuel cells," *Journal of Power Sources*, vol. 194, no. 2, pp. 588–600, Dec. 2009. DOI: 10.1016/j.jpowsour.2009.06.073.

[56] L. Du, Y. Shao, J. Sun, G. Yin, J. Liu, and Y. Wang, "Advanced catalyst supports for PEM fuel cell cathodes," *Nano Energy*, vol. 29, pp. 314–322, Nov. 2016. DOI: 10.1016/j.nanoen.2016.03.016.

[57] L. Cindrella *et al.*, "Gas diffusion layer for proton exchange membrane fuel cells—A review," *Journal of Power Sources*, vol. 194, no. 1, pp. 146–160, Oct. 2009. DOI: 10.1016/j.jpowsour.2009.04.005.

[58] X. Yuan, H. Li, S. Zhang, J. W. Martin, and H. Wang, "A review of polymer electrolyte membrane fuel cell durability test protocols," *Journal of Power Sources*, vol. 196, no. 22, pp. 9107–9116, Nov. 2011. DOI: 10.1016/j.jpowsour.2011.07.082.

[59] M. Jouin, R. Gouriveau, D. Hissel, M. Péra, and N. Zerhouni, "Degradations analysis and aging modeling for health assessment and prognostics of PEMFC," *Reliability Engineering & System Safety*, vol. 148, pp. 78–95, Apr. 2016. DOI: 10.1016/j.ress.2015.12.003.

[60] R. Shimoi, T. Aoyama, and A. Iiyama, "Development of fuel cell stack durability based on actual vehicle test data: Current status and future work," *SAE International Journal of Engines*, vol. 2, no. 1, pp. 960–970, 2009.

[61] J. Zhao, Z. Tu, and S. H. Chan, "Carbon corrosion mechanism and mitigation strategies in a proton exchange membrane fuel cell (PEMFC): A review," *Journal of Power Sources*, vol. 488, p. 229 434, Mar. 2021. DOI: 10.1016/j.jpowsour.2020.229434.

[62] Y. Yang, W. Li, R. Lin, S. Xia, and Z. Jiang, "Impact of dummy load shut-down strategy on performance and durability of proton exchange membrane fuel cell stack," *Journal of Power Sources*, vol. 404, pp. 126–134, Nov. 2018. DOI: 10.1016/j.jpowsour.2018.10.003.

[63] C. Takei, K. Kakinuma, K. Kawashima, K. Tashiro, M. Watanabe, and M. Uchida, "Load cycle durability of a graphitized carbon black-supported platinum catalyst in polymer electrolyte fuel cell cathodes," *Journal of Power Sources*, vol. 324, pp. 729–737, Aug. 2016. DOI: 10.1016/j.jpowsour.2016.05.117.

[64] J. Wu *et al.*, “Proton exchange membrane fuel cell degradation under close to open-circuit conditions,” *Journal of Power Sources*, vol. 195, no. 4, pp. 1171–1176, Feb. 2010. DOI: 10.1016/j.jpowsour.2009.08.095.

[65] L. Franck-Lacaze *et al.*, “Ageing of PEMFC’s due to operation at low current density: Investigation of oxidative degradation,” *International Journal of Hydrogen Energy*, vol. 35, no. 19, pp. 10 472–10 481, Oct. 2010. DOI: 10.1016/j.ijhydene.2010.07.180.

[66] R. P. Lin, B. Li, Y. Hou, and J. Ma, “Investigation of dynamic driving cycle effect on performance degradation and micro-structure change of PEM fuel cell,” *International Journal of Hydrogen Energy*, vol. 34, no. 5, pp. 2369–2376, Mar. 2009. DOI: 10.1016/j.ijhydene.2008.10.054.

[67] D. Pozo, “Linear battery models for power systems analysis,” *Electric Power Systems Research*, vol. 212, p. 108 565, Nov. 2022. DOI: 10.1016/j.epsr.2022.108565.

[68] T. Terlouw and C. Bauer, “Multi-objective optimization of energy arbitrage in community energy storage systems using different battery technologies,” *Applied Energy*, vol. 239, pp. 356–372, Apr. 2019. DOI: 10.1016/j.apenergy.2019.01.227.

[69] Toshiba. “2P12S modules.” (), [Online]. Available: https://www.global.toshiba/ww/products-solutions/battery/scib/product/module/2p12s.html (visited on Oct. 31, 2023).

[70] F. Mylonopoulos, T. Kopka, A. Coraddu, and H. Polinder, “A model-based parametric study for comparison of system configurations and control of a hydrogen hybrid cargo vessel,” Jan. 2024. DOI: 10.59490/moses.2023.671.

[71] N. Shakeri, M. Zadeh, and J. Bruinsma, “Dynamic Modeling and Validation of a Fuel Cell-Based Hybrid Power System for Zero-Emission Marine Propulsion; an Equivalent Circuit Model Approach,” *IEEE Journal of Emerging and Selected Topics in Industrial Electronics*, pp. 1–16, 2023. DOI: 10.1109/JESTIE.2023.3288475.

[72] “FCS 13-XXL.” (Jul. 5, 2022), [Online]. Available: https://nedstack.com/en/pem-fcs-stack-technology/fcs-13-xxl.

[73] “Products & services - zepp.solutions hydrogen fuel cell systems.” (Sep. 21, 2023), [Online]. Available: https://zepp.solutions/en/services/.

[74] “HYPM HD 90.” (Apr. 16, 2012), [Online]. Available: https://pdf.directindustry.com/pdf/hydrogenics/hypm-hd-90/33492-420317.html.

[75] “Maritime Fuel cell system | MT-FCPI-120 | Nedstack.” (), [Online]. Available: https://nedstack.com/en/pemgen-solutions/maritime-power-installations/pemgen-mt-fcpi-120 (visited on Oct. 16, 2023).

[76] “HYPM HD 180.” (Apr. 16, 2012), [Online]. Available: https://pdf.directindustry.com/pdf/hydrogenics/hypm-hd-180/33492-420321.html.

[77] “Marine System 200.” (), [Online]. Available: https://powercellgroup.com/product/marine-system-200/ (visited on Oct. 16, 2023).

[78] “FCWave spec sheet.” (Jun. 2021), [Online]. Available: https://www.ballard.com/about-ballard/publication_library/product-specification-sheets/fcwave-spec-sheet.

[79] “Maritime Fuel cell system | MT-FCPI-600 | Nedstack.” (), [Online]. Available: https://nedstack.com/en/pemgen-solutions/maritime-power-installations/pemgen-mt-fcpi-600 (visited on Oct. 16, 2023).

[80] A. Rohatgi, *Webplotdigitizer: Version 4.6*, 2022. [Online]. Available: https://automeris.io/WebPlotDigitizer.

[81] Z. Hong, Q. Li, Y. Han, W. Shang, Y. Zhu, and W. Chen, “An energy management strategy based on dynamic power factor for fuel cell/battery hybrid locomotive,” *International Journal of Hydrogen Energy*, vol. 43, no. 6, pp. 3261–3272, Feb. 2018. DOI: 10.1016/j.ijhydene.2017.12.117.

[82] T. Wang *et al.*, “An optimized energy management strategy for fuel cell hybrid power system based on maximum efficiency range identification,” *Journal of Power Sources*, vol. 445, p. 227 333, Jan. 2020. DOI: 10.1016/j.jpowsour.2019.227333.

[83] H. He, R. Xiong, and J. Fan, “Evaluation of Lithium-Ion battery equivalent circuit models for state of charge estimation by an experimental approach,” *Energies*, vol. 4, no. 4, pp. 582–598, Mar. 2011. DOI: 10.3390/en4040582.

[84] The Engineering Toolbox. “Fuels - Higher and Lower Calorific Values.” (2003), [Online]. Available: https://www.engineeringtoolbox.com/fuels-higher-calorific-values-d_169.html.

[85] Horizon Educational. “What’s the molar mass of hydrogen?” (), [Online]. Available: https://www.horizoneducational.com/what-s-the-molar-mass-of-hydrogen/t1496 (visited on Oct. 16, 2023).

[86] “Refueling hydrogen in Germany & Europa - H2.LIVE.” (), [Online]. Available: https://h2.live/en/tankstellen/ (visited on Dec. 29, 2023).

[87] L. van Biert, K. Mrozewski, and P. ’t Hart, “Public final report: Inventory of the application of Fuel Cells in the MARitime sector (FCMAR),” Feb. 2021.

[88] Clean Hydrogen Joint Undertaking, “Strategic Research and Innovation Agenda 2021 – 2027,” Feb. 2022.

[89] D. Bezmalinović, B. Šimić, and F. Barbir, “Characterization of PEM fuel cell degradation by polarization change curves,” *Journal of Power Sources*, vol. 294, pp. 82–87, Oct. 2015. DOI: 10.1016/j.jpowsour.2015.06.047.

A

Fuel cell stack plots

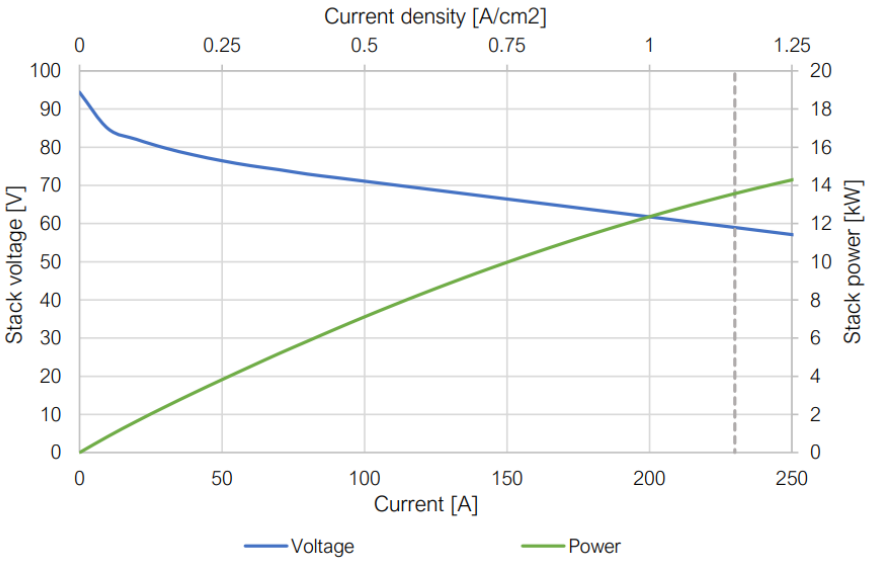

Figure A.1: Nedstack's 13-XXL stack performance, from [72]

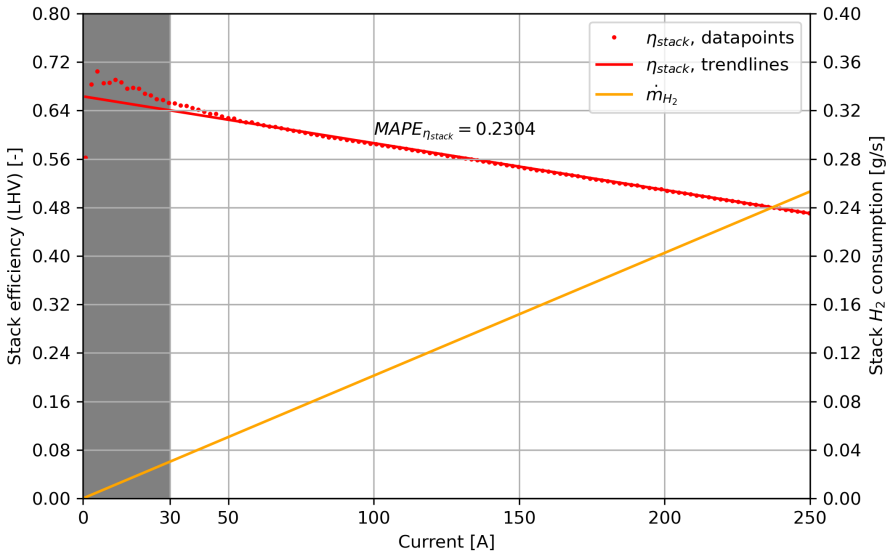

Figure A.2: Trend lines for stack efficiency and hydrogen consumption, using datapoints from [72]

B

Effect of increasing time step size dt

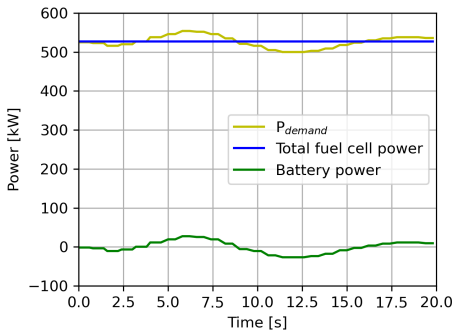

(a) Twenty seconds at 200ms

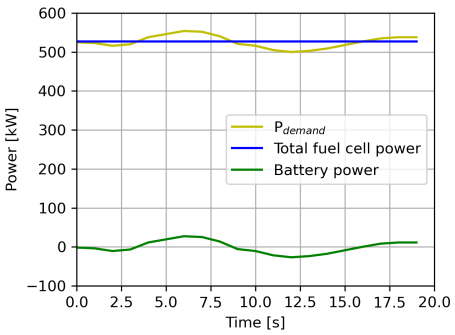

(b) Twenty seconds at 1s time step

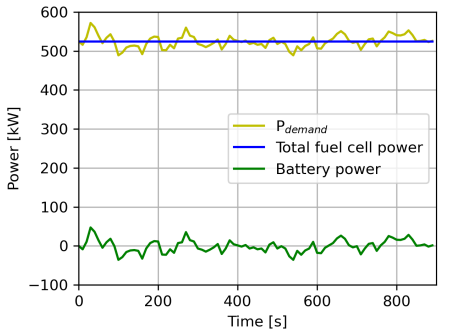

(c) 15 minutes at $10\,\mathrm{s}$

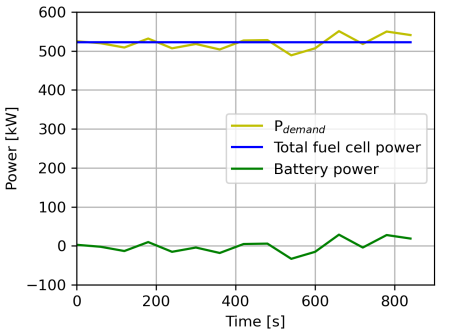

(d) 15 minutes at 1 min

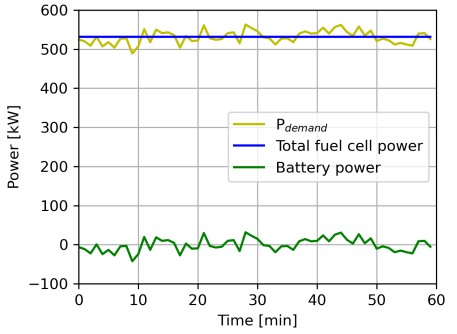

(e) 1 hour at 1 min

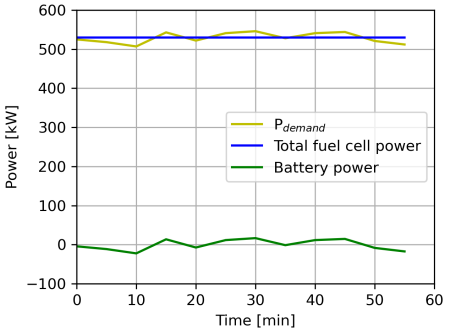

(f) 1 hour at 5 min

Figure B.1: Effect of increasing time step size on power fluctuations

C

Plots sensitivity analysis

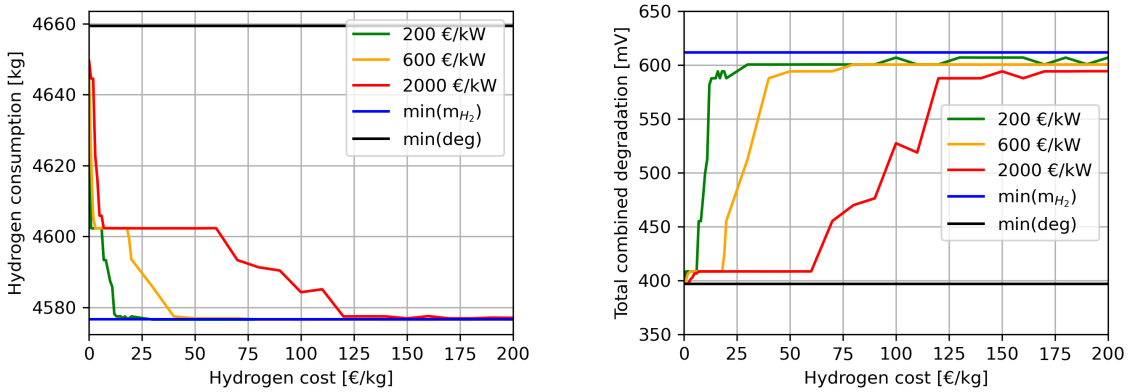

(a) Hydrogen consumption

(b) Combined system degradation

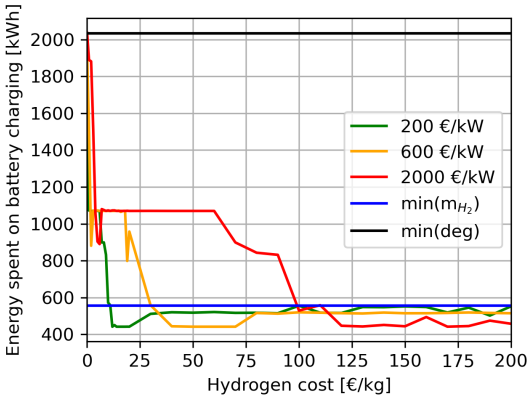

(c) Battery usage

Figure C.1: Model sensitivity to various PEM system and H_2 costs in extended price range for the E-intensive load profile

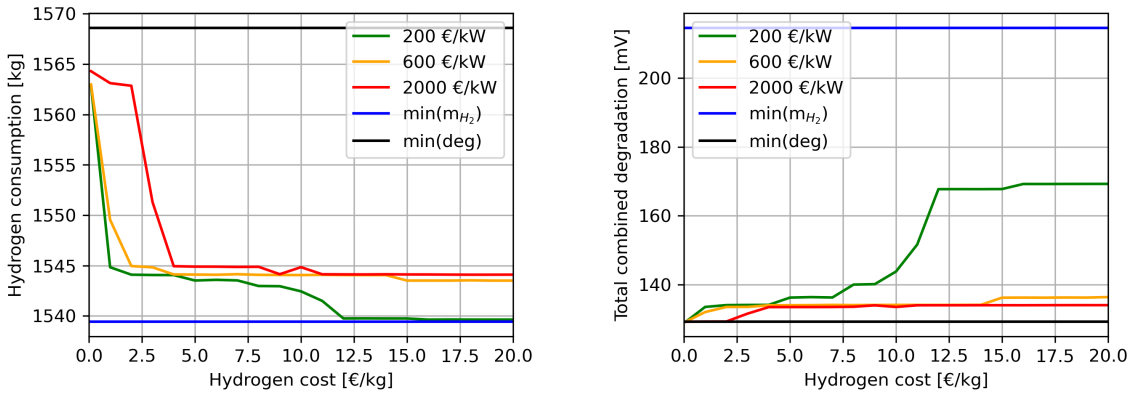

(a) Hydrogen consumption

(b) Combined system degradation

(c) Battery usage

Figure C.2: Model sensitivity to various PEM system and H_2 costs in realistic price range for the P-intensive load profile

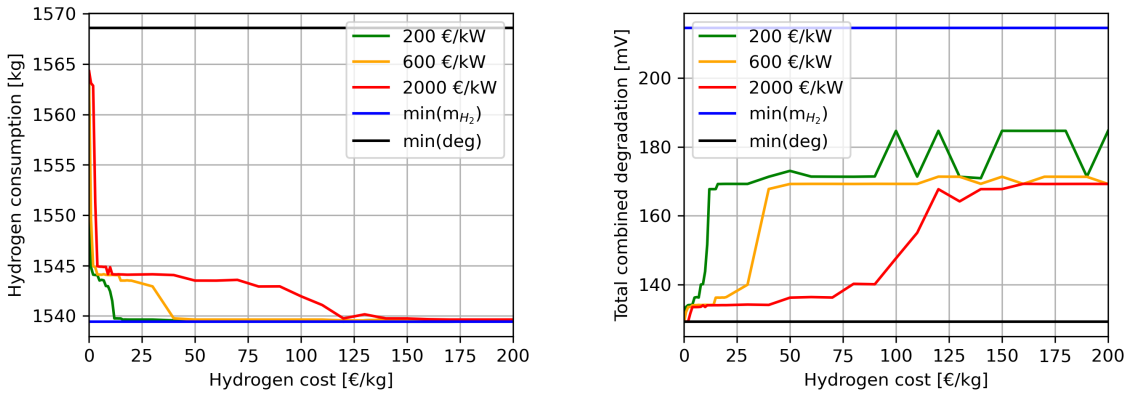

(a) Hydrogen consumption

(b) Combined system degradation

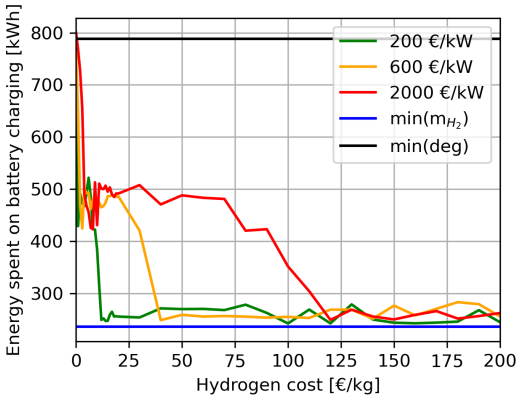

(c) Battery usage

Figure C.3: Model sensitivity to various PEM system and H_2 costs in extended price range for the P-intensive load profile